UNIVERSITÀ
POLITECNICA
DELLE MARCHE

Università Politecnica delle Marche
Corso di Dottorato in Ingegneria Civile, Ambientale, Edile ed Architettura

---

The Importance of Calibration and Modelling Non-Structural Elements in the Evaluation of Seismic Vulnerability Index of Strategic Buildings Before and After Retrofitting

Ph.D. Dissertation of:

Elisa Speranza

Advisor:

Prof. Ing. Fabrizio Gara

Co-Advisor:

Dott. Ing. Sandro Carbonari

Curriculum Supervisor:

Prof. Ing. Francesco Fatone

XXXII ciclo

Università Politecnica delle Marche
Facoltà di Ingegneria
Dipartimento di Ingegneria Civile, Edile ed Architettura

Via Brecce Bianche – 60131 – Ancona, Italia

Contents

List of Figures

List of Tables

Abstract

The conventional modelling of structures, used by engineers in common practice, are affected by considerable approximations such as those relevant to the foundation modelling, soil-structure interaction, modelling of non-structural elements. In particular, as for the modelling of non-structural elements, in engineering practice, non-structural components as infill walls can be considered in different ways: only in terms of weight, completely neglecting the stiffening contribution, or by modelling the infill walls through two-dimensional elements (shell) or one-dimensional elements (equivalent strut). The former which is the most commonly used, represents the lowest level of detail in the finite element structural modelling, characterized by a high level of approximation; on the contrary, the latter approach of modelling strongly depends on the elastic modulus of the infill walls. The contribution offered by these elements to the stiffness and strength of the building is affected by numerous uncertainties, due to the choice of appropriate constitutive models sufficiently representative of the multiple infill walls types present in a building. Therefore, many authors are working to find appropriate values for the mechanical properties and constitutive laws of infills but most of the studies in the literature refer to seismic problems for which a nonlinear behaviour are expected. Thus, stiffness of infills in the small or very small range of deformations has not been fully studied yet. However, a seismic design based on a high performance level for severe earthquakes may foresee that non-structural elements, including infills, do not suffer damage. In this case the actual elastic modulus of infills should be considered in a finite element model to reproduce the real behaviour of the building. This is the typical situation of retrofitting projects that include the introduction of dissipation devices that need to be effectively calibrated with the real stiffness of the building.

A possible method currently used to obtain an estimate of the elastic modulus of the infill walls for small vibrations (pre-cracked state), consists in the experimental dynamic identification of the building. Notoriously, the experimental dynamic identification allows to obtain the modal parameters of the structure object of study, such as the frequencies and the modal shapes of vibration. Once these values are known, the finite element model of the structure is updated by varying the elastic modulus of material until the modal parameters of the f.e.m. model converge with those obtained from in-situ dynamic identification tests.

With reference to strategic buildings, this thesis aims to investigate on the modelling of the non-structural elements related to internal and external infill walls, trying to quantify the difference induced by different modelling strategies on the value of the seismic vulnerability index. To this purpose, two case studies are analysed: the Benedetto Croce high school in Avezzano and the Varano high school in Camerino, which are r.c. frame buildings retrofitted with external steel towers equipped with viscous dampers at the base. For both case studies, three models are implemented, before and after the retrofitting; all the models foresee an increasing level of detail: i) a model only including structural components, ii) a model with external infill panels modelled as equivalent connecting struts according to literature, and iii) a model with external and internal infill walls calibrated through results of in-situ dynamic tests. Regarding the pre-retrofitting phase, the calculation of the seismic vulnerability index was carried out by means of nonlinear static analysis (pushover). As for the post-retrofitting

phase, the calculation of the seismic vulnerability index was carried out by means of non-linear dynamic analysis (I.D.A).

The results are shown in terms of comparison between the capacity curves obtained with push over analyses (pre-retrofitting) and with incremental dynamic analyses for the different model. In addition, the outcomes are shown also in terms of intensity level of the seismic action necessary to reach a predetermined limit state for the different models.

Keywords: infilled r.c. frame buildings, infill wall modelling, building dynamic identification, Operational and Experimental Modal Analysis.

Introduction

I.1. Research Motivation

In common engineer practice, the modelling of non-structural infills can be considered in different ways:

1. in terms of weight, completely neglecting the stiffening contribution;
2. through two-dimensional elements (shell) or one-dimensional elements (equivalent strut), using suggestions of the NTC 2018 technical standard (table C8.5.1) for the definition of elastic modules of the panel, or using literature values;
3. through two-dimensional elements (shell) or one-dimensional elements (equivalent strut), using results of dynamic identification tests (small vibrations), on the whole building and/or on the single infill wall, to define the elastic modules of the panel.

The first methodology, which is the most used, represents the lowest level of detail in the finite element structural modelling, is characterized by a high level of approximation, essentially due to the fact that non-structural elements are excluded from the modelling. In common practice, the high degree of approximation in the computation of the actual dynamic structural response is somehow covered through the introduction of safety coefficients in limit state checks, as required by the standard. This way may be appropriate when severe damage to the structure is expected for high seismic events, which justify the hypothesis of the absence of a stiffening contribution from infill walls. However, this assumption is not acceptable if a high performance level for the structure is required for severe earthquakes, including the absence of damage to infills to assure the fully operational condition (almost total absence of damage to the non-structures – safety critical objective) after the seismic event (Figure 1-1).

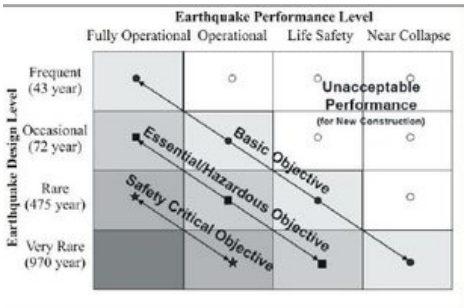

Figure 1-1: Earthquake performance level

If infills have to be modelled, methodologies 2 and 3 can be used. In both cases, however, the estimation of the elastic modulus of the infill walls plays a fundamental role in finite element modelling. The contribution offered by these elements to the stiffness and strength of the building is affected by many uncertainties, due to the choice of appropriate constitutive models sufficiently representative of the multiple infill walls types present in a building (for example, the different types of "non-structural" masonry, the simultaneous presence of infill adherent and non-adherent to the reinforced concrete frame, the difficulty of modelling panels with openings arranged in different positions and of different sizes). Moreover, the infill stiffness depends on the materials as well as on its discrete nature. Depending on the geographic region, dimensions and material type of the brick unit, and mortar characteristics are different as well as the construction practice. Also, the mentioned items have local quality and technical specification. Therefore, many authors are working to find values for the mechanical properties of infills.

Morandi et al. performed static tests on three real dimension infill masonry walls built with different types of hollow clay bricks and thicknesses. They obtained that for the wall with thickness of 8 cm the elastic modulus E_h relevant to the horizontal direction is equal to 991 MPa while the elastic modulus E_v for the vertical direction is equal 1873 MPa; for the 30 cm thick wall, E_h is equal to 1050 MPa while E_v is 3240 MPa. Finally, the wall composed by two side by side layers of 12 cm thick bricks gives E_h equal to 991 MPa and E_v equal to 1873 MPa.

Biondi et al. in 2016 presented the results of the mechanical parameters of two types of infill walls subjected to static tests; 12 made with hollow bricks ($80 \times 160 \times 330$ mm^3) having dimensions $1010 \times 1010 \times 800$ mm^3, and 12 with half-filled bricks ($120 \times 120 \times 250$ mm^3) having dimensions $770 \times 770 \times 120$ mm^3. The values of the normal modulus of elasticity have been calculated referring to the load branch between a stress equal to about ¼ and ½ of the ultimate load. Compression tests on hollow bricks panels with load parallel to the holes provided an elastic modulus of 610 MPa, while compression tests on panels with load orthogonal to the holes revealed an elastic modulus of 948 MPa. Compression tests on half-filled panels with load parallel to the holes revealed an elastic modulus of 1722.6 MPa, and compression tests on half-filled panels with load orthogonal to the holes revealed an elastic modulus of 835.0 MPa.

Other important authors have correlated the value of the elastic modulus of the masonry to the value of compressive stress. The main authors and their correlations are listed below:

- Sahlin (1971) $E_m = 750\, f_m$
- Paulay and Priestley (1992) $E_m = 750\, f_m$
- Sanbartolome (1990) $E_m = 500\, f_m$
- Sinha & Pedreschi (1983) $E_m = 1180\, f_m$
- Hendry (1990) $E_m = 2116\, f_m$
- Some others $E_m = 1000\, f_m$

Studies available in the literature, such as those listed, refer to values of the elastic modulus of the infills determined from static load tests considering stresses ranging between the 10-40% or 10-60% of the ultimate load of the panels, for which the earlier cracks in the panels have already developed. However, the seismic design of structures characterised by a high performance level (e.g. operational condition for severe earthquakes), must refer to values of the elastic modulus of infills, representative of the uncracked condition, which comply with the requirement of operational condition. Typical situations are those in which protection systems are employed to dissipative the seismic energy. In these cases, the finite element

model used to design the protection system must reproduce the real behaviour of the building, including the contribution of infills at their uncracked conditions.

Starting from above considerations, it can be concluded that there is no exact or univocal information to quantify the value of the elastic modulus of the infill walls, despite this parameter has a decisive influence on the overall stiffness of the buildings at operational conditions. Mechanical characteristics of the masonry suggested by the Italian standards in (table C.8.5.1) are defined on the basis of a qualitative description of the masonry or the wall Although the standard does not specify how the tabulated values have been obtained, they are average values, usually measured on the elastic branch of experimental stress - deformation curves, normally between 10-40% of the ultimate load.

A possible method currently used to obtain an estimate of the elastic modulus of the infill walls for small vibrations (corresponding to the uncracked condition) consists in the experimental dynamic identification of buildings. Notoriously, the experimental dynamic identification allows to obtain the modal parameters of the building, such as frequencies of vibration and mode shapes. Once these values are known, the finite element model can be completed with non-structural elements and updated by varying the elastic modulus of the infills until the modal parameters of the numerical model converge with those obtained from the dynamic identification. However, considering that the overall model is calibrated from results of experimental tests, the iterative calibration procedure is characterized by many variables, not least the friction that cannot be quantified. Therefore, the calibration procedure can lead to values of the elastic modules of the infill walls even far from real ones.

Recently, Nicoletti et. al have tested a new method for estimating the elastic modulus of the walls through experimental dynamic identification tests performed on the single panel (small vibrations). This thesis aims to evaluate effects of the different modelling strategies of infill walls, as well as the effects of different assumptions for their elastic modulus, on the calculation of the seismic vulnerability index before and after retrofitting of some buildings, proposed as case studies.

I.2. Thesis objectives

This thesis aims to quantify the difference, in terms of seismic vulnerability index, between a traditional modelling of the structures including only the structural components, and more accurate models, also including non-structural infill walls, calibrated using results of dynamic experimental identifications, carried out on in-situ experimental tests at operating conditions.

In order to get the thesis objectives, two case studies are analysed before and after retrofitting intervention: the High School Benedetto Croce in Avezzano and the High School Varano in Camerino. For each case study, three finite-element models have been implemented, characterized by a growing level of accuracy in the modelling of infills.

For what concerns the High School Benedetto Croce, three models are implemented before and after retrofitting works: model with only structural components (model A), a model with infill panels modelled as equivalent struts (model B), defined according to literature suggestions, and a model with external and internal infill walls modelled as equivalent struts and stiffness calibrated through the results of operational or experimental modal analysis (model C).

The seismic vulnerability index is calculated through non-linear static analysis (pushover) for model A, model B and model C before retrofitting works. After the building retrofit, for model A, model B and model C seismic vulnerability index is calculated through non-linear dynamic analysis (I.D.A), considering peculiarities and limits of the protection system adopted for the building retrofit.

For what concerns the High School Varano, three model are implemented before and after retrofitting works: a model with only structural components (model A), a model with external infill panels modelled as equivalent struts according to literature suggestions (model B), a model with external and internal infills modelled as non-linear shell element and stiffness calibrated through the results of operational modal analysis (model C). Even in this case, the seismic vulnerability index is calculated through non-linear static analysis (pushover) for model A, model B and model C before the building retrofit. After the retrofit, the seismic vulnerability index is calculated through non-linear dynamic analysis (I.D.A) from all the models.

The results are shown in terms of comparison between the capacity curves obtained with push over analyses (pre-retrofitting) and with incremental dynamic analyses (after-retrofitting) for the different models. In addition, the outcomes are shown also in terms of intensity level of the seismic action necessary to reach a predetermined limit state for the three models.

Both structures studied were not seismically acceptable according to current standards, therefore the seismic vulnerability assessment and a retrofit of the structure were necessary; the retrofitting project is based on the innovative system of dissipative towers patented by Ing. Alessandro Balducci. This innovative retrofitting system requires the construction of external steel towers, equipped with dissipative devices and dedicated to the seismic protection. The towers are supported by a central spherical hinge at the base and are connected at the perimeter at the foundation with viscous dampers. The towers have suitable in-plan arrangement, in order to regularize the modal response of the building, i.e. to limit possible torsional couplings; furthermore, they are useful to regularize the interstory drift of the building, which is fundamental for the damage limit state.

I.3. Thesis organization

Chapter 1 deals with the first case study of high school Benedetto Croce in Avezzano, in particular, the following topics are addressed: the mechanical and geometrical characteristics obtained through the in-situ tests, the modal parameters of the structure obtained through dynamic identification, the model calibration of the structure based on results of dynamic identification, and finally, the evaluation of seismic risk index before and after seismic retrofitting intervention, for the three models implemented.

Chapter 2 deals with the second case study of high school Varano in Camerino in particular, the following topics are addressed: the mechanical and geometrical characteristics obtained through the in-situ tests, the modal parameters of the structure obtained through dynamic identification, the model calibration of the structure based on results of dynamic identification, and finally, the evaluation of seismic risk index before and after seismic retrofitting intervention, for the models implemented. In this case, the high calculation burden

made it impossible to evaluate the post-intervention seismic risk index through I.D.A. within the established time interval. Work is still in progress to handle the model for this purpose.

Finally, Chapter 3 shows conclusion and future developments.

Chapter 1.

Case study: High School “Benedetto Croce” in Avezzano.

1.1. Description of the buildings

1.1.1. High School “Benedetto Croce” in Avezzano

The "Benedetto Croce" Institute is located in Via Cavalieri Vittorio Veneto, 9 in Avezzano (Figure 1-1 shows an image taken from Google Maps).

Figure 1-1: Territorial framework

The B. Croce school complex was built between the 1960s and the 1970s, it consists of 6 buildings, separated by seismic joints, named A, B, C, D, F, G according to the scheme of Figure 1-2. The total covered area is approximately 4200m^2 with a total built volume of approximately 41000 m^3.

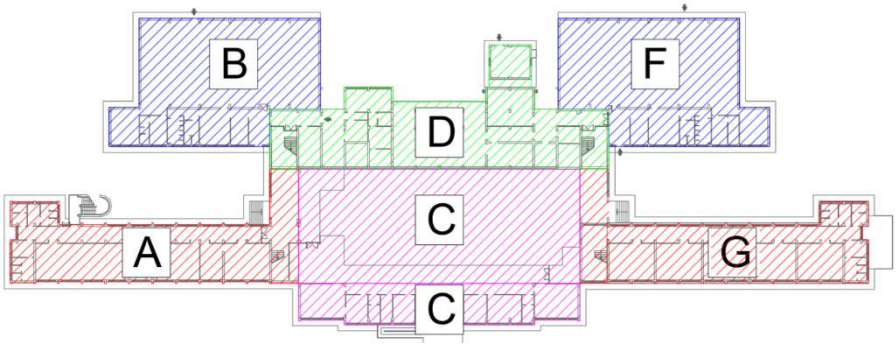

Figure 1-2: In-plane view of the Institute with indication of the buildings

Building A covers an area of approximately 506 m^2 and is intended for classrooms. The ground floor hosts the offices. The building G is symmetrical with respect to the bulding A and has the same intended use. The rooms on the ground floor are currently in use for a nursery school. The building D covers an area of approximately 640 m^2 and is also intended for classrooms. On the ground floor, all the technical rooms of the school are located. The building B and F are symmetrical with respect to the NNO-SSE axis and each one includes a gym and locker rooms. The gym has a surface area of 450m^2, while the locker rooms cover an area of about 170m^2. Building C includes the atrium, three rooms used as classrooms, three rooms for teaching and non-teaching staff, related services and the great hall. The great hall has a surface area of 318m^2, the other areas used as corridors and offices have a total area of 522m^2. The total area of building C is about 840m^2. The in-plane view of the entire complex is shown below. The structures of all the buildings consist of reinforced concrete frames. The foundations consist in surface T beams.

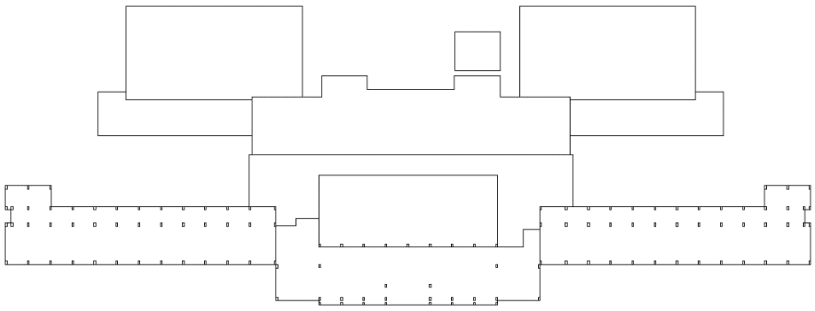

Figure 1-3: Ground floor plan

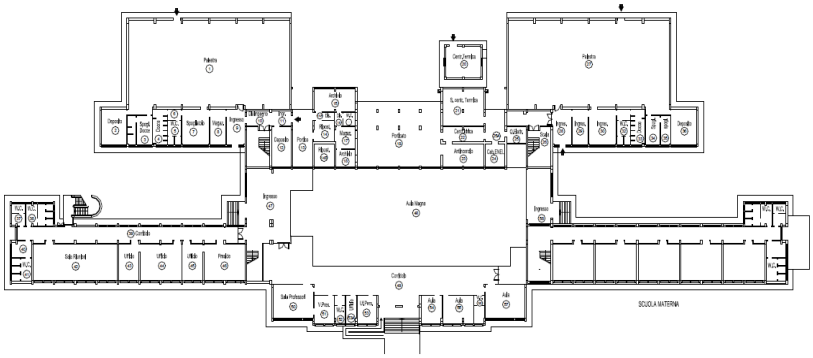

Figure 1-4: Ground floor plan

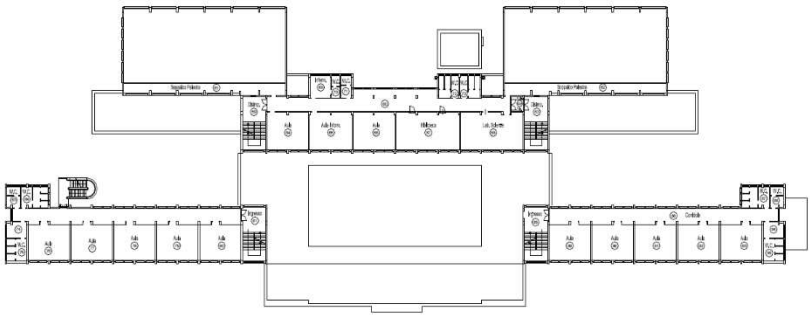

Figure 1-5: First floor plan

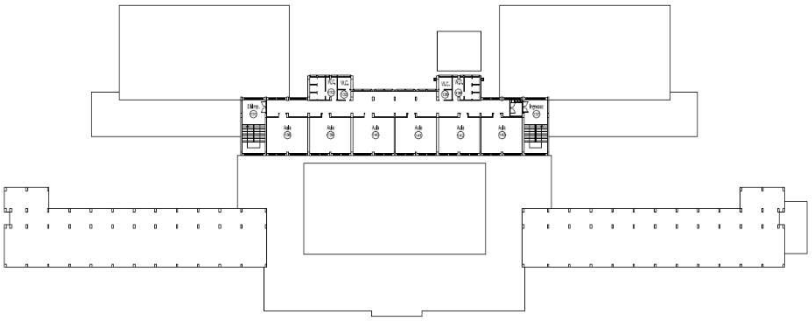

Figure 1-6: Second floor plan

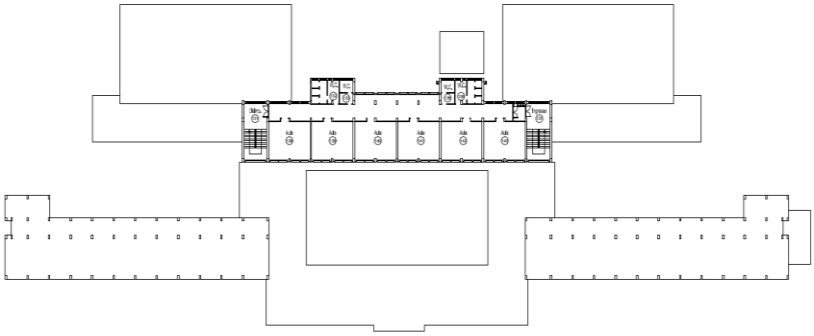

Figure 1-7: third floor plan

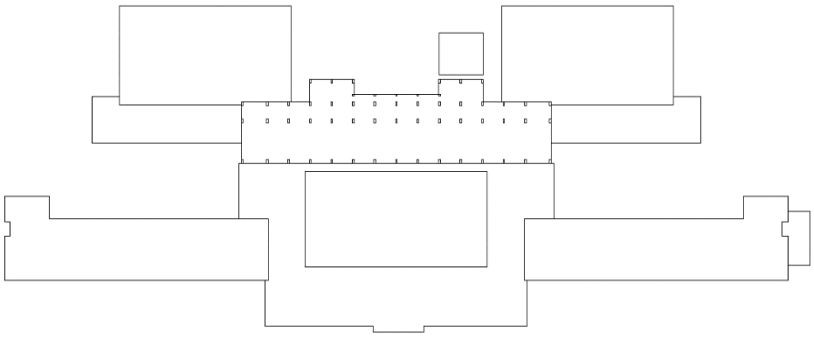

Figure 1-8: fourth floor plan

The present thesis work was carried out with reference to block "A".

The building A, as already mentioned, hosts the classrooms and offices. The in-plane standard carpentry is shown in the following figures.

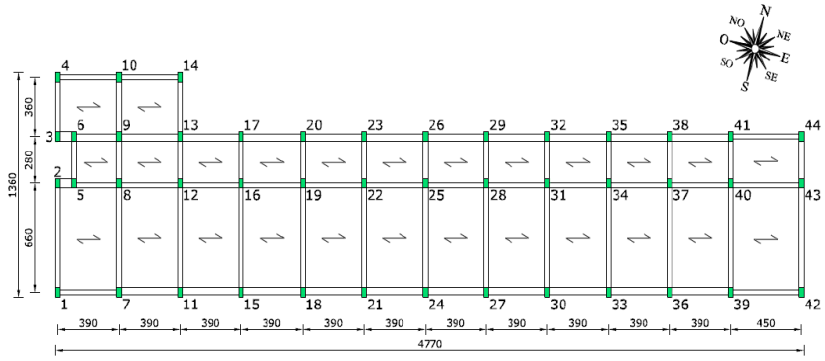

Figure 1-9: In-plan standard carpentry of Buildings A

Building A is a five-storey building (Figure 1-10), the foundations plan is about 1.25 m below street level. The structure presents short columns between the foundation and the ground floor (about 90 cm height), and on the attic floor (variable height). (Figure 1.11).

The columns have 30x60 cm dimensions and are arranged in greatest inertia direction. The beams of the structure in the NNO-SSE direction measuring 30x60 cm in size while in the ENE-OSO direction, dimensions are 30x45 cm or 45x16 cm.

Figure 1-10: External view of the building A

Figure 1-11: Coverage of the building: A view inside the body

Figure 1-12: Outside stairs. Building A

1.2. Investigation Campaign

The definition of the in-situ tests performed on the structures was aimed at achieving, when possible, an LC2 level of knowledge according to Italian Standards. The investigations concerned concretes, steels, joints, floors and infill walls and were carried out by TECNO IN of Napoli. The following paragraphs give the summary tables of the results obtained for the building A object study.

1.2.1. Investigation of the joints

The width of the joints was detected for all buildings. Table 1-1 shows the results obtained and highlights the seriousness of the problem deriving from the limited value of these quantities.

Table 1-1- Floor type carpentry of joints

Investigation	Building	Investigation site	Structural Elements	Amplitude [cm]
SG1	A: C	Ground floor	Column-Column	0,3
SG2	A: C	Ground floor	Beam-Beam	0,5
SG3	B: C	Ground floor	Beam-Beam	0,2
SG4	C: D	Ground floor	Column-Column	0,3
SG5	C: D	Ground floor	Column-Column	0,3
SG6	C: G	Ground floor	Beam-Beam	1,3
SG7	D: F	Ground floor	Beam-Beam	0,5

1.2.2. Slab/Floor

Stratigraphic characteristics of the floors of the building object study “A”.

Table 1-2- Stratigraphic characteristics of the slab

Element	Floor Building A: 2° floor
	Classroom Area
Structural characteristics	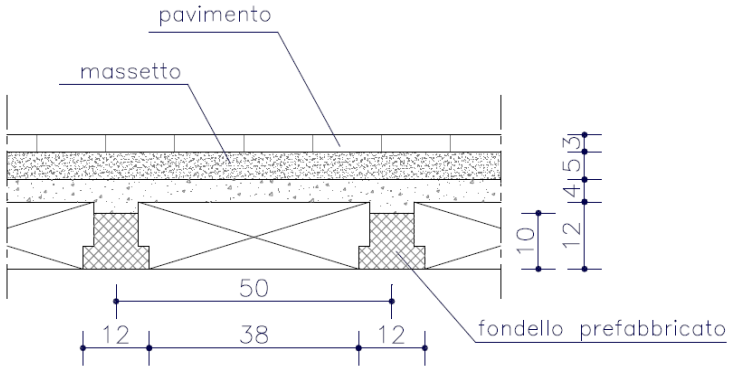

Element	Roof Floor Building A: Roof
	Roof
Structural characteristics	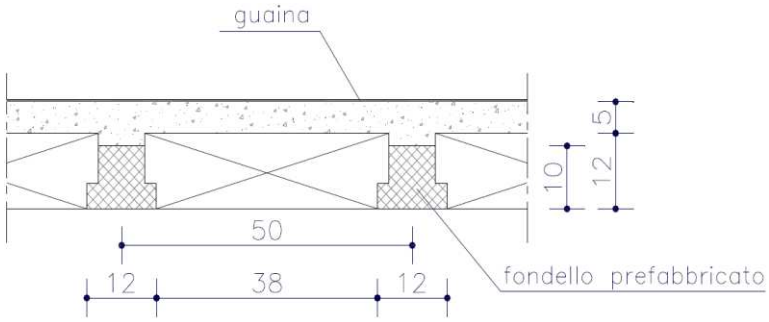

1.2.3. External Infill Walls

Samples on external infill walls were carried out mainly in order to define the structure, therefore the degree of connection with the frames in c.a., and the weight. The investigations carried out are summarized in Table 1-3 .

Table 1-3: External Infill Walls

Element	**Building A: 1° floor: External infill walls**
Investigation site	Stairwell
Structural characteristics	Sub-window in perforated brick blocks 25 cm thick. No curbs

Element	**Building A: 2° floor: External infill walls**
Investigation site	**Corridor**
Structural characteristics	Sub-window in perforated brick blocks 12 cm thick. No curbs

1.2.4. Investigations on reinforcement

The building A and the building G are equal and symmetrical, therefore pacometric measurements were carried out only on building G and apply to building A.

Table 1-4: Pacometric Investigation

Building	Sign	Element	Step Bars [cm]							
			Column: from the lower node				Column: from the upper node			
			Beam: from left node				Beam: from right node			
G	G0 CP1: G0 SP1	Ground floor Building G: Column	26	25	24	29	24	26	28	24
	G0 CT2: G0 ST4	Ground floor Building G: Beam	28	25	25	32	32	25	30	21
	G1 CP1: G1 SP1	1° floor Building G: Column	28	24	25	11	11	20	23	26
	G-1 CP1: G-1 SP1	Basement floor Building G: Column	22	23	20	20	13	20	20	23
	G1 CT2: G1 ST4	1° floor Building G: Beam	26	32	27	25	25	26	27	21

	G-1 CT2: G-1 ST4	Basement floor Building G: Beam	23	31	26	27	31	27	27	32
	G2 CP1: G2 SP1	2° floor Building G: Column	30	26	23	30	18	26	27	26
	G2 CT2: G2 ST4	2° floor Building G: Beam	24	22	23	24	19	32	20	24
	G3 CP1: G3 SP1	3° floor Building G: Column	21	26	Short Column					
	G3 CT2: G3 ST4	3° floor Building G: Beam	20	18	13	28	28	20	16	17

1.2.5. Investigations on the steel's mechanical properties

Table 1-5: Mechanical characteristics of steels

Position	Diameter	Section	Agt	fy	ft	(ft/fy)k
	(mm)	(mm2)	(%)	(N/mm2)	(N/mm2)	≥1,15, e ≤1,35
Column Building A Floor –1 (smooth reinforcement)	16,11	203,84	16,11	359,30	543,86	1,51

1.2.6. Investigations on the properties of concrete

Sonic and sclerometric investigations

Table 1-6: Non-destructive investigations on concrete (Building A)

Sign	Element Investigated	Sclerometric Investigations	ULTRASONIC
		Bounce index I averaged over 8 measurements	Vmedia [m/s]
A-1 CP1 A-1 SP1	Basement floor Building A: Column	29,1	3830
A-1 SP2		26,7	3863
A-1 SP3		32, 0	3879
A-1 CT2 A-1 ST4	Basement floor Building A: Beam	32,1	3897
A-1 ST5		34,7	4055
A-1 ST6		36,3	4110
A0 CP1 A0 SP1	Ground floor Building A: Column	29,2	3933
A0 SP2		30,2	3948
A0 SP3		29,0	3917
A0 CT2 A0 ST4	Ground floor Building A: Beam	28,1	3782
A0 ST5		31,5	3949
A0 ST6		36,5	3951
A1 CP1 A1 SP1	1° floor Building A: Column	30,8	3847
A1 SP2		33,2	3830
A1 SP3		33,3	3921

A1 CT2 A1 ST4	1° floor Building A: Beam	35,4	3967
A1 ST5		32,2	3948
A1 ST6		34,3	3931
A2 CP1 A2 SP1	2° floor Building A: Column	33,4	3880
A2 SP2		32,8	3897
A2 SP3		34,4	3863
A2 CT2 A2 ST4	2° floor Building A: Beam	38,7	3965
A2 ST5		35,8	3863
A2 ST6		36,4	3879
A3 CP1 A3 SP1	3° floor Building A: Column	33,2	3913
A3 SP2		32,8	3863
A3 SP3		33,4	3913
A3 CT2 A3 ST4	3° floor Building A: Beam	34,8	3863
A3 ST5		38,7	3913
A3 ST6		33,3	3830

Table 1-7: Destructive investigations on concrete

Sign	Cylinder diameter [cm]	Ratio h/d	Mass [kg/dm3]	Strength [MPa]
A1CP1	7,4	1	2,313	9,23
A-1CT2	9,2	1	2,324	14,67
A3CP1	9,2	1	2,304	13
A0CT2	9,2	1	2,332	12,5
A-1CP1	9,2	1	2,347	13,58
A1CT2	9,2	1	2,285	9,42
A0CP1	9,2	1	2,348	10,55
A3CT2	9,2	1	2,285	12,41
A2CP1	9,2	1	2,332	16,17
A2CT2	9,2	1	2,291	16,86

1.2.7. The mechanical characteristics of concretes and steels

The values of the resistances obtained from destructive investigations on concrete have been transformed into equivalent cylindrical resistances through the methodology proposed in G. Manfredi, A. Masi, R. Pinho, G. Verderame, M. Vona, Evaluation of existing buildings in Reinforced Concrete.

The values of ultrasonic and sclerometric investigations have been converted into equivalent resistances with the Sonreb method. Table 1-8 summarizes the results obtained. Table 1-9, on the other hand, shows the values of the average yield stresses adopted in the structural analyses.

Table 1-8: Summary of the results of the tests carried out for the mechanical characterization of the concrete

	Average destructive investigations [MPa]	**Average sonreb** [MPa]	**Average sonreb beam** [MPa]	**Average sonreb Column** [MPa]
Building A	15,54	14,71	15,35	14,08

Table 1-9: Mechanical characteristics of steels

Position	**fym** [MPa]
Building A (smooth reinforcement)	360

1.2. Report on Materials

1.2.1. Existing Buildings Materials

The steel and concrete characteristics of the existing buildings are deduced from the results of the investigations, destructive and non-destructive tests, described in the previous chapter, and by subsequent investigations carried out in the retrofitting project. The Knowledge Level of the materials (LC) is Adequate (LC2), therefore a confidence factor of FC = 1.2 was adopted.

Concrete

$$R_{ck} = \mathbf{17,12\ N/mm^2}$$

$$f_{ck} = 0{,}83 R_{ck} = \mathbf{14,21\ N/mm^2}$$

$$f_{cd} = \frac{f_{ck}}{1{,}5} = \mathbf{9,47\ N/mm^2}$$

$$E = 22000 \left(\frac{f_{ck}}{10}\right)^{0,3} = \mathbf{24.443,38\ N/mm^2}$$

Reinforcement

The tests carried out on the samples taken from the buildings (A, B, C, D, F and G) provided a unitary yield point that gives rise to the characteristic yield strength value shown below. This average value between the various building was used for the building A object of study.

$$f_{yk} = 430\ \frac{N}{mm^2})$$

$$f_{yk} = 353\ \mathbf{N/mm^2}$$

$$f_{yd} = \frac{f_{yk}}{1{,}15} = 306{,}96\ \mathbf{N/mm^2}$$

$$E = \mathbf{210.000\ N/mm^2}$$

1.2.2. Materials for dissipative towers

Concrete for foundations: piles and slabs

It was used a cement conglomerate packaged according to the following modes:
- Cement type 425 350 kg / mc;
- Gravel 0.8 mc / mc;
- Sand 0.4 mc / mc;
- Water 120 lt / mc.

Use of hydraulic binders such as cements defined by applicable regulations.

Natural or crushing aggregates, consisting of non-freezing elements, not friable and free of silty or clay organic substances, gypsum etc., harmful to the hardening of the conglomerate and to the preservation of the steell reinforcements. Gravel or crushed stone of maximum dimensions correlated to the characteristics of the carpentry of the jet and to the encumbrance of the metallic reinforcements.

Clear water and salt-free in harmful percentage.

The granulometric distribution of the aggregates, the type of cement and the consistency of the mixture will be adequate for the purpose.

Mechanical characteristics:

For foundation a concrete of class "C 25/30" (Rck = 30 N / mm2) was used.

General characteristics:

$$E = \mathbf{31.447\ N/mm^2}$$

$$f_{ck} = 0{,}83R_{ck} = \mathbf{24,9\ N/mm^2}$$

Ultimate Limit State:

$$\gamma_c = \mathbf{1,5}$$

$$f_{cd} = \frac{f_{ck}}{1{,}5} = \mathbf{16,60\ N/mm^2}$$

Concrete structures in elevation: towers bases

It was used of a cement conglomerate packaged according to the following:
- Cement type 425 350 kg / mc;
- Gravel 0.8 mc / mc;
- Sand 0.4 mc / mc;
- Water 120 lt / mc.

Use of hydraulic binders such as cements defined by applicable regulations.

Natural or crushing aggregates, consisting of non-freezing elements, not friable and free of silty or clay organic substances, gypsum etc., harmful to the hardening of the conglomerate and to the preservation of the steel reinforcements.

Gravel or crushed stone of maximum dimensions correlated to the characteristics of the carpentry of the jet and to the encumbrance of the metallic reinforcements.

Clear water and salt-free in harmful percentage.

The granulometric distribution of the aggregates, the type of cement and the consistency of the mixture adequate for the purpose of the casting.

Reinforcement Bars

Improved adhesion bars of the B450C type were used.
Mechanical Characteristics:

$$f_{tk} = \mathbf{540\ N/mm^2}$$

$$f_{yk} = \mathbf{450\ N/mm^2}$$

$$Minimum\ elongation\ at\ break = \mathbf{7,5}\%$$

$$Minimum\ ratio\ \frac{f_t}{f_y} = \mathbf{1,15}$$

$$Maximum\ ratio\ \frac{f_t}{f_y} = \mathbf{1,35}$$

$$E = \mathbf{210.000\ N/mm^2}$$

Ultimate Limit State:

$$\gamma_c = \mathbf{1,15}$$

$$f_{yd} = \frac{f_{yk}}{1{,}15} = 391{,}3\ \mathbf{N/mm^2}$$

Steel for construction

The steel structures of the towers are in steel type "S 275" (UNI EN 10025-2) with the following characteristics:

$$f_{tk} \geq \mathbf{430\ N/mm^2}$$

$$f_{yk} \geq \mathbf{275\ N/mm^2}$$

The bolted connections realized with high strength bolts having the following characteristics:

- Screw class 8.8 (UNI EN ISO 898-1: 2001)
- $f_{tb} \geq \mathbf{800\ N/mm^2}$
- $f_{yb} \geq \mathbf{649\ N/mm^2}$
- nut Class 8 (UNI EN 20898-2: 1994)
- rosettes C50 (UNI EN 10083-2: 2006)

Steel for connections, mechanical components and devices

Structures in metallic carpentry such as connections, mechanical components and devices, intended as viscous heat sinks and spherical bearings, are made of steel type "S 355 H" (UNI EN 10025-2) having the following characteristics:

$$t \leq 40\ mm \ \rightarrow f_{th} \geq \mathbf{510\ N/mm^2}$$

$$40\ mm \leq t \leq 80\ mm \ \rightarrow f_{th} \geq \mathbf{470\ N/mm^2}$$

$$t \leq 40\ mm \ \rightarrow f_{yh} \geq \mathbf{355\ N/mm^2}$$

$$40\ mm \leq t \leq 80\ mm \ \rightarrow f_{yh} \geq \mathbf{355\ N/mm^2}$$

The bolted connections realized with high strength bolts having the following characteristics:
- Screw class 8.8 (UNI EN ISO 898-1: 2001)
- $f_{tb} \geq \mathbf{800\ N/mm^2}$
- $f_{yb} \geq \mathbf{649\ N/mm^2}$
- nut Class 8 (UNI EN 20898-2: 1994)
- rosettes C50 (UNI EN 10083-2: 2006)

The bars used for the anchors are B7 reference standard ASTM A 193 special steel having the following characteristics:

$$\phi \leq 65\ mm \ \rightarrow f_{th} \geq \mathbf{860\ N/mm^2}$$

$$\phi \leq 65\ mm \ \rightarrow f_{yh} \geq \mathbf{720\ N/mm^2}$$

1.2.3. External Infill Walls

As shown by the investigation campaign presented in the previous chapter, the thickness of the external infill is 12 cm.

Table 1-10: External Infill Walls

Element	**Building A: 2° floor: External infill walls**
Investigation site	**Corridor**
Structural characteristics	Sub-window in perforated brick blocks 12 cm thick. No curbs

In the first instance, for the properties of the material, it is referred to the average values of Tab. Table C8A.2.1 contained in Annex 2 of NTC08 and shown in Figure 1-13.

Tipologia di muratura	f_m [daN/cm^2]	τ_0 [daN/cm^2]	E [daN/cm^2]	G [daN/cm^2]	w [daN/m^3]
	min - max	min - max	min - max	min - max	
Muratura in pietrame disordinata (ciottoli, pietre erratiche e irregolari)	10.0 18.0	0.20 0.32	6900 10500	2300 3500	1900
Muratura a conci sbozzati, con paramento di limitato spessore e nucleo interno	20.0 30.0	0.35 0.51	10200 14400	3400 4800	2000
Muratura in pietre a spacco con buona tessitura	26.0 38.0	0.56 0.74	15000 19800	5000 6600	2100
Muratura a conci di pietra tenera (tufo, calcarenite, ecc.)	14.0 24.0	0.28 0.42	9000 12600	3000 4200	1600
Muratura a blocchi lapidei squadrati	60.0 80.0	0.90 1.20	24000 32000	7800 9400	2200
Muratura in mattoni pieni e malta di calce	24.0 40.0	0.60 0.92	12000 18000	4000 6000	1800
Muratura in mattoni semipieni con malta cementizia (es.: doppio UNI foratura < 40%)	50.0 80.0	2.40 3.20	35000 56000	8750 14000	1500
Muratura in blocchi laterizi semipieni (perc. foratura < 45%)	40.0 60.0	3.00 4.00	36000 54000	10800 16200	1200
Muratura in blocchi laterizi semipieni, con giunti verticali a secco (perc. foratura < 45%)	30.0 40.0	1.80 1.30	27000 36000	8100 10800	1100
Muratura in blocchi di calcestruzzo o argilla espansa (perc. foratura tra 45% e 65%)	15.0 20.0	0.95 1.25	12000 16000	3000 4000	1200
Muratura in blocchi di calcestruzzo semipieni (foratura < 45%)	30.0 44.0	1.80 2.40	24000 35200	6000 8800	1400

Tabella C8A.2.1 della Circolare 617/2009)

Figure 1-13: Table C8A.2.1

The average values adopted, according to the material underlined in the table, are:

$$f_m = \mathbf{4\ N/mm^2}$$

$$\tau_0 = \mathbf{0,35\ N/mm^2}$$

$$E = \mathbf{4.000\ N/mm^2}$$

$$G = \mathbf{1.350\ N/mm^2}$$

Furthermore, for subsequent processing it was also necessary to obtain the resistance to lateral sliding of the mortar joints which was thus calculated:

$$f_{sr} = 1{,}5 \cdot \tau_0 = \mathbf{0,525\ N/mm^2}$$

1.2.4. Internal Infill Walls

The mechanical characteristics of internal infill walls have been derived from dynamic experimental identification. The following are the essential points of this work taken by Nicoletti, Speranza et al. [2019].

The impact load tests were carried out on internal masonry panels with the aim of identifying their out-of-plane modal parameters. Measurements were performed on one panel with dimension of 6.10 x 3.22 m, located at the third floor of the building and composed by hollow clay bricks with dimensions of 8 x 25 x 25 cm with bed and head mortar joints of thickness variable between 0.5-1.5 cm. This infill is coated with a 1.5 cm thick plaster layer

on each side, for a total thickness of the wall of about 11 cm. The panel is analysed in an accurate way to allow the identification of several resonance frequencies and mode shapes. Different panels with the same geometric characteristics and similar positions are tested with simplified procedures. In detail, only resonance frequencies are determined monitoring only one point, which are found to be similar to that of the panel subjected to extensive tests.

The instrumentation used for the test consists of two uniaxial piezoelectric accelerometers (PCB 353B43) with nominal sensitivity of 300 mV/g, one instrumented hammer with load cell type Dytran 5802, a 24bit-four-channel data acquisition module (NI 9234) and a 8-slots chassis (NI cDAQ-9178) connected to a laptop, the latter equipped with software for signal acquisition and processing. The panel is divided with a grid of 25 points identified with an alphanumeric code and two accelerometers are fixed at two grid points, measuring in the out-of-plane direction, in order to get two set of data within the same test. Impulse forces, instead, are applied at each grid point and at least three hammer impacts are applied to obtain a reliable data set. By measuring both the input force and the infill response, the Frequency Response Functions can be computed at each point and the modal parameters identified according to the well-known Experimental Modal Analysis procedure Figure 1-14 shows the out-of-plane modal parameters obtained experimentally, in terms of frequencies and mode shapes.

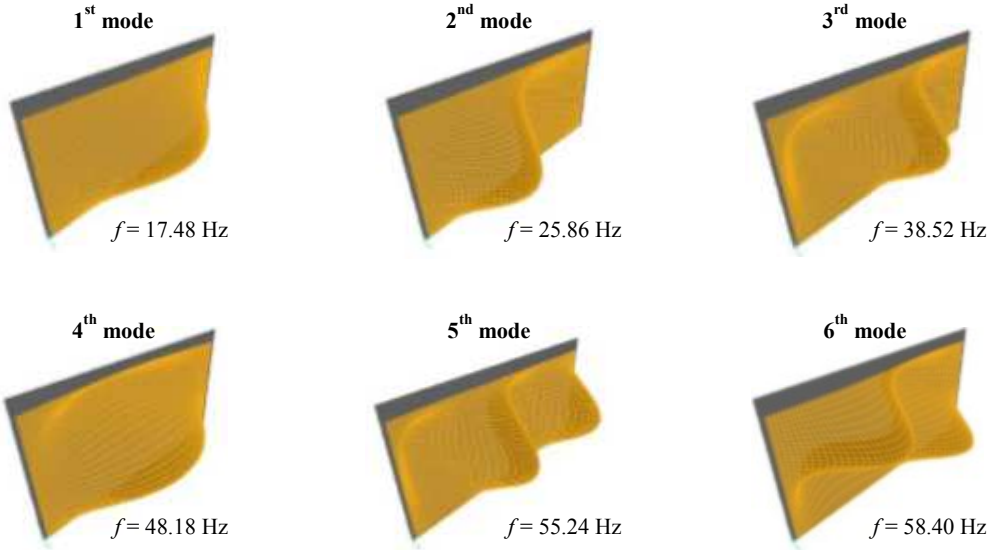

Figure 1-14: Experimental mode shapes and frequency values for the tested panel

Subsequently a f.e. model of the investigated panel was developed in SAP2000 [CSI Computer & Structures, Inc SAP2000 advanced, 2009]. The wall was modelled with bi-dimensional elements having thickness equal to that of the real wall and density estimated starting from the material weights. Fixed boundary conditions are considered, and the masonry material is assumed to be homogeneous, elastic and isotropic. The plate bending behaviour of a thin shell element is governed by the Kirchhoff theory, neglecting transverse shear deformation; hence, the problem can be solved once known the external loads applied (if present) and the bending stiffness of the plate, called *D*. The latter constant depends on

the plate thickness (supposed to be known), the elastic modulus E and the Poisson's coefficient v of masonry material, as illustrated in Eq. (1):

$$D = Eh^3/12(1-v^2) \quad (1)$$

The Poisson's coefficient v is assumed to be constant and equal to 0.2 as its variation does not affect significantly the out-of-plane dynamic behaviour of the plate. Consequently, the only unknown parameter of the material mechanical properties is the elastic modulus E. This parameter is investigated and updated through iterative procedures that end when the numerical out-of-plane modal parameters (i.e. frequencies and mode shapes) fit well the experimental ones found by the in-situ tests. The elastic modulus E obtained at the end of the updating procedure for the tested wall is 3850 MPa [Nicoletti et al., 2018]. The numerical frequencies obtained differ less than 2% with respect to the experimental ones.

$$Elastic\ Modulus = E = \mathbf{3850\ N/mm^2}$$

Table 1-11- Numerical vs. experimental resonance frequencies of the panel.

Mode	Numerical frequency [Hz]	Experimental frequency [Hz]	Error [%]
1	17.82	17.48	1.95
2	25.88	25.86	0.08
3	38.37	38.52	-0.39
4	48.30	48.18	0.25
5	55.39	55.24	0.27
6	58.63	58.40	0.39

1.3. Loads Definition

Permanent actions are distinguished (G1 = own weights of structures, G2 = non-structural permanent) from variable actions (characteristic values Q).

Structural elements in c.a .: G1 = 25 KN / m3

1.3.1. Permanent actions

TYPE 1 LOAD: standard floor slab.
G1 floor weight (h = 12 + 4 cm) = 2.4 (kN / m²)

G2 permanent load = 2.8 (kN / m²)

TYPE 2 LOAD: attic floor.
G1 floor weight (h = 12 + 4 cm) = 2.4 (kN / m²)

G2 permanent load = 0.4 (kN / m²)

TYPE 3 LOAD: roof slab.
G1 floor weight (h = 12 + 4 cm) = 2.4 (kN / m²)

G2 permanent load = 0.6 (kN / m²)

TYPE 4 LOAD: ledge.

G2 permanent load = 2.4 (kN / m²)

TYPE 5 LOAD: staircase.
G1 slab self-weight staircase = 5.0 (kN / m²)

G2 permanent load = 1.6 (kN / m²)

TYPE 6 LOAD: external infill walls.

G2 permanent load = 4.6 (kN / m²)

1.3.2. Variable actions - characteristic values

For stairs and balconies, an operating overload is assumed equal to:

$$Q = 4 \text{ KN / m2}$$

For floors of the standard floor an operating overload is assumed equal to:

$$Q = 3 \text{ KN / m2}$$

For the attic floor, an operating overload is assumed equal to:

$$Q = 0.5 \text{ KN / m2}$$

since it is not practicable.

Snow

For coverings with a height of 691 m above sea level (common altitude of Avezzano), the operating overload due to snow is assumed:

$$Q = 1.25 \text{ KN / m2}$$

Determined as follows (point 3.4.2 NTC):

$$q_s = \mu_i \cdot q_{sk} \cdot C_E \cdot C_t$$

$$q_{sk} = 0{,}51 \left[1 + \left(a_s / 481\right)^2\right] \frac{kN}{m^2} \qquad a_s \geq 200\ m$$

Tabella 3.4.II – *Valori del coefficiente di forma*

Coefficiente di forma	$0° \leq \alpha \leq 30°$	$30° < \alpha < 60°$	$\alpha \geq 60°$
μ_1	0,8	$0{,}8 \cdot \frac{(60 - \alpha)}{30}$	0,0

C_E (coefficiente di esposizione) =1

C_T (coefficiente termico) =1

1.4. Seismic Action

Nominal Life:

$$V_N = 50 \text{ years}$$

Class III is assumed for use class (Construction whose use includes significant crowding ...);

$$C_U = 1.5$$

By obtaining a reference period for the seismic action equal to:

$$V_R = V_N \cdot C_U = 75 \text{ years}$$

With regard to the subsoil category, reference is made to what is reported in the geological report, where soil's category is B.
The topographical condition of the site is T1 (Flat surface, isolated slopes and reliefs with average inclination i≤15 °).

It is therefore possible to define the elastic response spectra for the different limit states considered, depending on the characteristics of the site, from the earthquake return period T_R, from the reference period V_R, and from the probability of exceeding the limit state considered PVR.
The elastic response spectra of reference, relative to the geographical coordinates of the site and defined on terrain of category A and topographical condition T1, according to the probability of exceeding the reference period in each of the 4 limit states provided for by the NTC are shown in the diagram following.

SLATO LIMITE	T_R [anni]	a_g [g]	F_o [-]	T_C^* [s]
SLO	45	0.092	2.347	0.280
SLD	75	0.118	2.315	0.290
SLV	712	0.284	2.384	0.348
SLC	1462	0.363	2.415	0.364

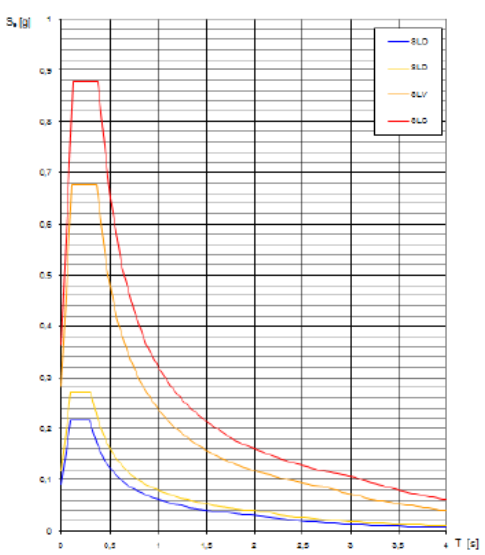

Figure 1-15: Elastic spectrum

The design spectra defined by the NTCs for the limit state of operation (SLO) and of life preservation (SLV) for the conditions of the site in question (terrain category B and topographic surface T1) are reported.

Spettri di risposta (componenti orizz. e vert.) per lo stato lim SLO

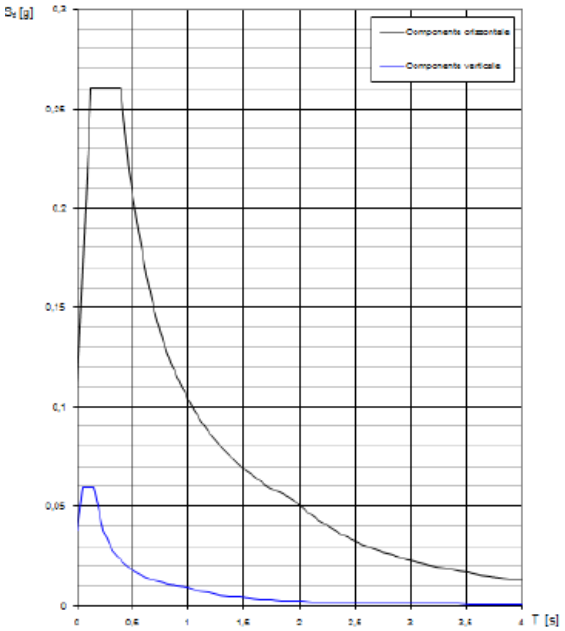

Parametri indipendenti

STATO LIMITE	SLO
a_g	0,092 g
F_o	2,347
T_C^*	0,280 s
S_S	1,200
C_C	1,419
S_T	1,000
q	1,000

Parametri dipendenti

S	1,200
η	1,000
T_B	0,132 s
T_C	0,397 s
T_D	1,970 s

Funzione spettro SLO orizzontale

	T[s]	Se[g]		T[s]	Se[g]		T[s]	Se[g]	T[s]	Se[g]
	0,000	0,111		1,296	0,080		2,453	0,034	3,807	0,014
T_B	0,132	0,260		1,371	0,075		2,550	0,031	3,903	0,013
T_C	0,397	0,260		1,445	0,072		2,646	0,029	4,000	0,013
	0,472	0,219		1,520	0,068		2,743	0,027		
	0,547	0,189		1,595	0,065		2,840	0,025		
	0,622	0,166		1,670	0,062		2,936	0,024		
	0,697	0,148		1,745	0,059		3,033	0,022		
	0,772	0,134		1,820	0,057		3,130	0,021		
	0,846	0,122		1,895	0,055		3,227	0,020		
	0,921	0,112	T_D	1,970	0,052		3,323	0,018		
	0,996	0,104		2,066	0,048		3,420	0,017		
	1,071	0,097		2,163	0,044		3,517	0,016		
	1,146	0,090		2,260	0,040		3,613	0,016		
	1,221	0,085		2,356	0,037		3,710	0,015		

Figure 1-16: SLO spectrum

Spettri di risposta (componenti orizz. e vert.) per lo stato lim SLV

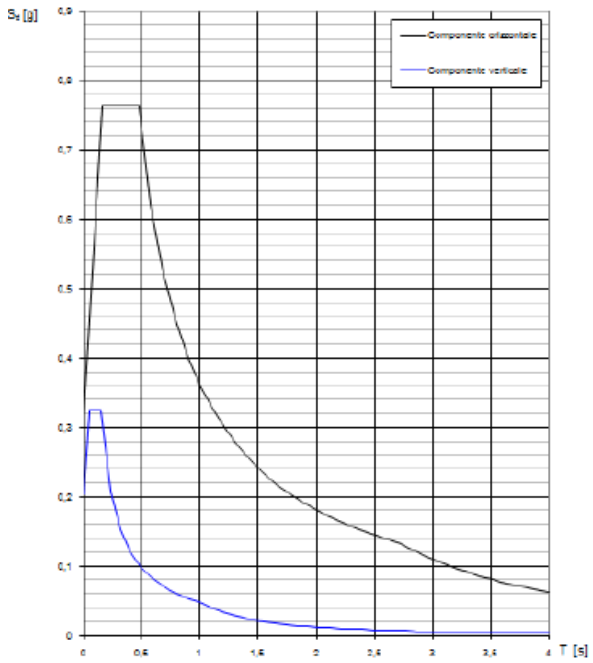

Parametri indipendenti

STATO LIMITE	SLV
a_g	0,284 g
F_o	2,384
T_C^*	0,348 s
S_S	1,129
C_C	1,358
S_T	1,000
q	1,000

Parametri dipendenti

S	1,129
η	1,000
T_B	0,158 s
T_C	0,473 s
T_D	2,735 s

Funzione spettro SLV orizzontale

	T[s]	Se[g]		T[s]	Se[g]		T[s]	Se[g]		T[s]	Se[g]
	0,000	0,320		1,766	0,205		3,036	0,107		3,880	0,066
T_B	0,158	0,764		1,873	0,193		3,096	0,103		3,940	0,064
T_C	0,473	0,764		1,981	0,183		3,157	0,099		4,000	0,062
	0,581	0,622		2,089	0,173		3,217	0,096			
	0,689	0,525		2,196	0,165		3,277	0,092			
	0,796	0,454		2,304	0,157		3,337	0,089			
	0,904	0,400		2,412	0,150		3,398	0,086			
	1,012	0,357		2,519	0,144		3,458	0,083			
	1,119	0,323		2,627	0,138		3,518	0,080			
	1,227	0,295	T_D	2,735	0,132		3,578	0,077			
	1,335	0,271		2,795	0,127		3,639	0,075			
	1,443	0,251		2,855	0,121		3,699	0,072			
	1,550	0,233		2,916	0,116		3,759	0,070			
	1,658	0,218		2,976	0,112		3,819	0,068			

Figure 1-17: SLO spectrum

1.5. Simulated project

As can be seen in the section on building A investigation, there is no information regarding the amount of longitudinal reinforcement in the structural elements, therefore, in order to overcome this lack of information, the simulated project was carried out as specified below.

The construction dates to the 1970s, so it was decided to adopt the method of the admissible stresses for the calculation of reinforcement.

COLUMN

The reinforcement of the Columns was carried out by inserting the minimum reinforcement provided by the standard of the 1970s. In the R.D. 2229/39 reads:

Along≥0.8% concrete area up to 2000 cm^2

Along≥0.5% concrete area up to 8000 cm^2

All the Columns of the building measuring 60x30 = 1800 cm^2, so the calculated reinforcement is:

18000x0,008 = 14,4cm^2

However, it was decided to adopt a minor quantity of reinforcement (penalizing for the analyses) equal to 6Φ16 corresponding to a total area of 12.06 cm^2.

BEAM

The beams used in the construction have the following sections: 30x60, 30x45 and 45x16.

The admissible stresses on the steel side and on the concrete side have been calculated based on the formulas:

$$\sigma_c = 60 + \frac{R_{ck} - 150}{4} \ [kg/cm^2]$$

$$\sigma_s = 255 \ N/mm^2$$

The maximum bending moments on the beam were calculated at the supports and at the centreline of the spans.

For this purpose, the beams have been grouped with similar characteristics (section, length and loads) and for each group bending moments were calculated.

TRANSVERSAL BEAMS (DIR.Y) OF THE 1-2-3 FLOORS - CENTRAL

Section 300x600	Central Beam		
L [mm]	G1+G2+P.P [N/mm]	Q [N/mm]	Qtot [N/mm]
6500	24,42	11,7	36,12
2900	24,42	11,7	36,12
3600	24,42	11,7	36,12

n	s	ξ	r	t	σ N/mm	$\sigma_{c,adm}$ >σ	μ	α	r	t	Reinf. eq.
15	0,27	0,91	0,86	0,005	10,73	NO	0,25	0,1	0,9	0,003	4 ϕ 16
15	0,27	0,91	1,92	0,002	2,137	SI	\	\	\	\	2 ϕ 12
15	0,27	0,91	1,55	0,003	3,293	SI	\	\	\	\	3 ϕ 12
15	0,27	0,9075	1,2164	0,003553	5,367	SI	\	\	\	\	3 φ 16
15	0,27	0,90	2,72	0,0015	1,068	SI	\	\	\	\	1 φ 12
15	0,27	0,90	2,19	0,0019	1,646	SI	\	\	\	\	2 φ 12

TRANSVERSAL BEAMS (DIR.Y) OF THE 1-2-3 FLOORS – PERIMETER

Section 300x600	Perimeter Beam		
L [mm]	G1+G2+P.P [N/mm]	Q [N/mm]	Qtot [N/mm]
6500	24,42	11,7	36,12
2900	24,42	11,7	36,12
3600	24,42	11,7	36,12

n	s	ξ	r	t	σ N/mm	$\sigma_{c,adm}$ >σ	μ	α	r	t	Reinf. eq.
15	0,28	0,91	0,98	0,004	8,23	NO	0,25	0,07	0,91	0,003	3 φ 16
15	0,28	0,91	2,20	0,002	1,64	SI	\	\	\	\	2 φ 12
15	0,28	0,91	1,77	0,002	2,52	SI	\	\	\	\	3 φ 12
15	0,28	0,91	1,39	0,003	4,11	SI	\	\	\	\	2 φ 16
15	0,28	0,91	3,11	0,001	0,82	SI	\	\	\	\	1 φ 12
15	0,28	0,91	2,51	0,002	1,26	SI	\	\	\	\	1 φ 12

TRANSVERSAL BEAMS (DIR.Y) OF THE ATTIC FLOORS - CENTRAL

Section 300x600	Central Beam		
L [mm]	G1+G2+P.P [N/mm]	Q [N/mm]	Qtot [N/mm]
6500	14,8	1,15	15,95
2900	14,8	1,15	15,95
3600	14,8	1,15	15,95

n	s	ξ	r	t	σ N/mm	$\sigma_{c,adm}$ >σ	μ	α	r	t	Reinf. eq.
15	0,28	0,91	1,29	0,003	4,74	SI	\	\	\	\	3 φ 16
15	0,28	0,91	2,90	0,001	0,94	SI	\	\	\	\	2 φ 12
15	0,28	0,91	2,34	0,002	1,45	SI	\	\	\	\	3 φ 12
15	0,28	0,91	1,83	0,002	2,37	SI	\	\	\	\	2 φ 16
15	0,28	0,91	4,10	0,001	0,47	SI	\	\	\	\	1 φ 12
15	0,28	0,91	3,30	0,001	0,73	SI	\	\	\	\	1 φ 12

TRANSVERSAL BEAMS (DIR.Y) OF THE ATTIC FLOORS - PERIMETER

Section 300x600	Perimter Beam		
L [mm]	G1+G2+P.P [N/mm]	Q [N/mm]	Qtot [N/mm]
6500	11,09	0,98	12,07
2900	11,09	0,98	12,07
3600	11,09	0,98	12,07

n	s	ξ	r	t	σ N/mm	$\sigma_{c,adm}$ >σ	μ	α	r	t	Reinf. eq.
15	0,28	0,91	1,49	0,003	3,59	SI	\	\	\	\	2 φ 16
15	0,28	0,91	3,33	0,001	0,71	SI	\	\	\	\	1 φ 12
15	0,28	0,91	2,69	0,002	1,10	SI	\	\	\	\	2 φ 12
15	0,28	0,91	2,10	0,002	1,79	SI	\	\	\	\	1 φ 16
15	0,28	0,91	4,72	0,001	0,36	SI	\	\	\	\	1 φ 12
15	0,28	0,91	3,80	0,001	0,55	SI	\	\	\	\	1φ 12

TRANSVERSAL BEAMS (DIR.Y) OF THE ROOF- PERIMETER

Section 300x600	Beam type		
L [mm]	G1+G2+P.P [N/mm]	Q [N/mm]	Qtot [N/mm]
4400	13,76	6,16	19,92

n	s	ξ	r	t	σ N/mm	$\sigma_{c,adm}$ >σ	μ	α	r	t	Reinf. eq.
15	0,28	0,91	1,71	0,003	2,71	SI	\	\	\	\	3 φ 12
15	0,28	0,91	2,42	0,002	1,36	SI	\	\	\	\	2φ 12

LONGITUDINAL BEAMS (DIR.X)

On the longitudinal beams the load is represented by the only external infill, therefore a minimum reinforcement has been adopted.

LONGITUDINAL BEAMS (DIR.X) - STAIRWAY

Section 300x600	Beam type		
L [mm]	G1+G2+P.P [N/mm]	Q [N/mm]	Qtot [N/mm]
4500	26,94	14,94	41,88

n	s	ξ	r	t	σ N/mm	$\sigma_{c,adm}$ >σ	μ	α	r	t	Reinf. eq.
15	0,28	0,91	0,87	0,005	10,61	NO	0,25	0,07	0,91	0,003	3 φ 16
15	0,28	0,91	1,22	0,004	5,30	SI					2φ 16

1.6. Description of the f.e. model

The structure in elevation is schematized with frame elements for the beams and the columns, while shell elements were used for the slabs of floors and stairs and for coverage. The slab behaviour of the floor was simulated by inserting, in each span, a shell element with a thickness equal to that of the slab.

To simulate the nodes stiffness, rigid links have been introduced automatically at the beam and column ends. Loads are assigned directly on the beam elements of the main structures, again based on the surfaces of influence of the floors, stairs, walls and other elements.

The foundation is not included in the numerical model but is schematized with a fix-restrain at the lower node of each ground column, guaranteed by the t-beams girder.

In this case, the compliance of the foundation soil was not taken into account for two reasons:

- the purpose of this thesis is to evaluate the incidence of the modelling of non-structural elements, calibrating their stiffness through vibrational measurements, in the assessment of the seismic vulnerability index. Therefore, a refined modelling is adopted in relation to non-structural elements while standard and simple modelling strategies are used for the rest, to avoid introducing uncertainties in the interpretation of the results;
- The calibration of f.e. model was carried out by using the result of the operational modal analysis, thus using environmental vibrations as input; in this case, as recognized in the literature and as usual for practical applications the assumption of fix-restrain at the base is justified.

While for the f.e. model post-retrofitting, where the dissipative towers are inserted, the viscous dissipation devices, are modelled with appropriate non-linear behaviour elements called "link damper", whose response is a function of velocity.

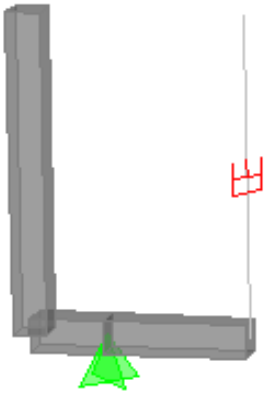

Figure 1-18: link damper

About the reticular steel structure of the dissipative towers, this is shown schematically by means of frame elements, as well as rigid pendulums connected to existing building. At basement level a slab in r.c is inserted, modelled with a shell element. The f.e. model accurately reproduce the actual mass distributions and stiffness of the structure.

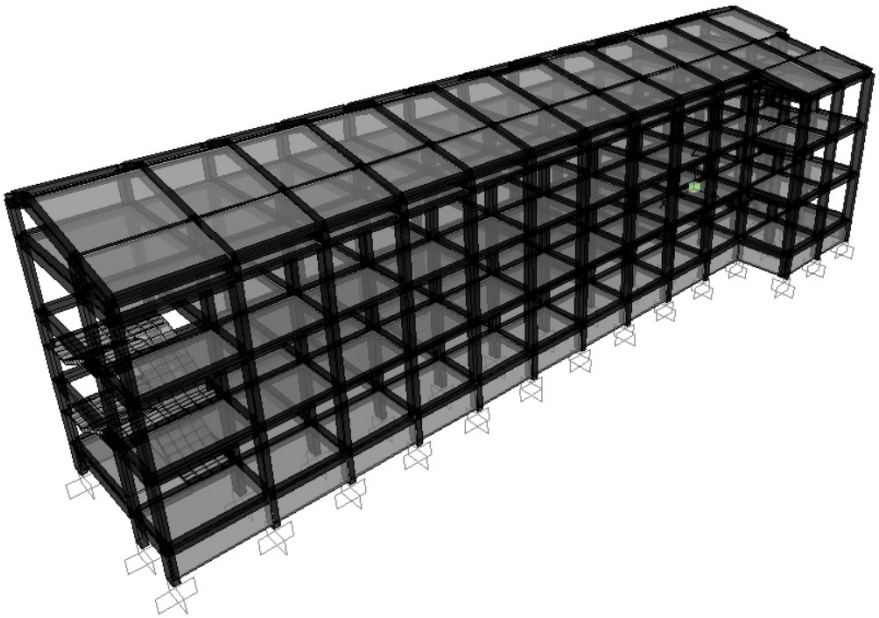

Figure 1-19: F.e. model before retrofitting

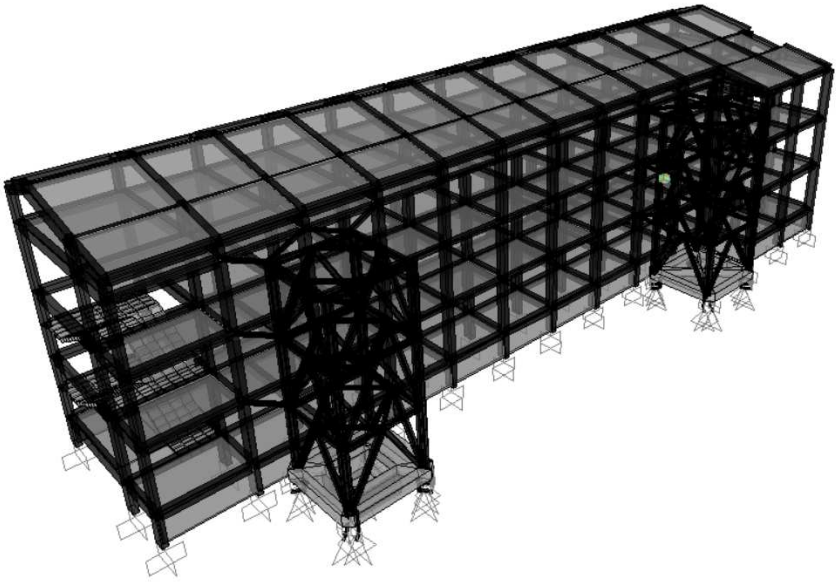

Figure 1-20: F.e. model after retrofitting

1.7. Modelling of Masonry Infill Walls

The masonry infill wall of the structure is modelled according to Decanini, which assumes that the contribution of the masonry infill panel to the response of the infilled frame can be modelled by replacing the panel by a system of two diagonal masonry compression struts. The individual masonry struts are considered to be ineffective in tension. The combination of both diagonal struts provides a lateral load resisting mechanism for positive as well as negative direction of loading. The experiment proposed by the author led to the following results:

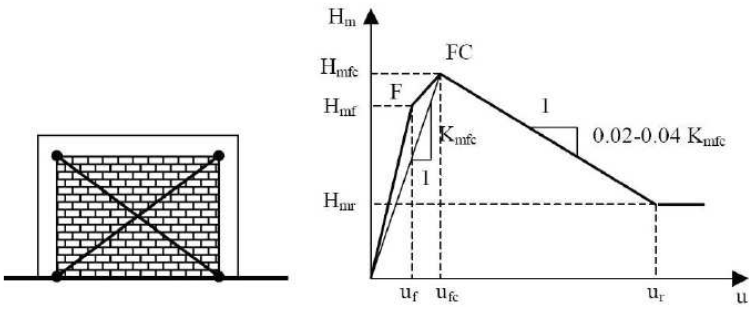

Figure 1-21: Force-displacement envelope curve of the equivalent strut.

The curve of the lateral force-displacement (H_m-u) relationship consider four branches; the first linear elastic ascending branch corresponds to the uncracked stage; the second branch refers to the post-cracking phase up to the development of the maximum strength (H_{mfc}). The point FC corresponds to the complete cracking stage of the infill panel. The third branch of the curve describes the deterioration post-peak strength of the infill; after that the curve continues horizontally. The model needs of the definition of the width of the equivalent strut ω, the stiffness at complete cracking stage K_{mfc}, and the strength H_{mfc}, as a function of the geometric and mechanical characteristics of the frame.

The width of the strut ω is introduced by means of the relative stiffness parameter λh proposed by Stafford-Smith [11] and by two constants K1 and K2 calibrated on the basis of experimental tests:

$$w = \left(\frac{K_1}{\lambda h} + K_2\right) d$$

where λh is a non-dimensional parameter depending on the geometric and mechanical characteristics of the frame-infill system, K1 and K2 are coefficients that change according to λh, as we can see from Figure 1-22: Value for K1 and K2 constant parameters., and d is the length of the equivalent strut.

	$\lambda h < 3.14$	$3.14 < \lambda h < 7.85$	$\lambda h > 7.85$
K_1	1.30	0.707	0.47
K_2	-0.178	0.01	0.04

Figure 1-22: Value for K1 and K2 constant parameters.

The parameter λh, originally proposed by Stafford-Smith [11], is defined by the following expression:

$$\lambda h = \sqrt[4]{\frac{E_m e \sin(2\theta)}{4 E_c I h_m}}$$

where Em is the elastic equivalent modulus corresponding to the complete cracking stage of the infill, Ec is the elastic modulus of concrete, t is the slope of the strut to the respect of the horizontal axis, e is the thickness of the masonry panel, h is the story height, h_m is the height of the masonry panel, I is momentum of inertia of the columns. The stiffness of the equivalent strut K_{mfc} at complete cracking stage is given by the following relation:

$$K_{mfc} = \frac{E_m e w}{d} cos^2\theta$$

The resistance of the infill panel was simulated by a fictitious failure compressive stress σ_{br}, Four basic failure modes are considered, with the corresponding equivalent failure compressive stresses: (a) diagonal tension, $\sigma_{br}(1)$; (b) sliding shear along horizontal joints, $\sigma_{br}(2)$; (c) crushing in the corners in contact with the frame, $\sigma_{br}(3)$; (d) diagonal compression, $\sigma_{br}(4)$.

$$\sigma_{br(1)} = \frac{0{,}6\tau_{m0} + 0{,}3\sigma_0}{\frac{w}{d}}$$

$$\sigma_{br(2)} = \frac{(1{,}2\sin\theta + 0{,}45\cos\theta)f_{sr} + 0{,}3\sigma_0}{\frac{w}{d}}$$

$$\sigma_{br(3)} = \frac{(1{,}12\sin\theta\cos\theta)}{K_1(\lambda h)^{-0{,}12} + K_2(\lambda h)^{0{,}88}}\sigma_{mo}$$

$$\sigma_{br(4)} = \frac{1{,}16\,\sigma_{mo}\tan\theta}{K_1 + K_2\lambda h}$$

where σ_{m0} is the vertical compression strength measured on masonry specimens, τ_{m0} is the shear strength measured with the diagonal compression test, f_{sr} is the slide resistance in the joints measured form the triplet test, and σ_0 is the vertical stress due to working loads. Once determined the fictitious failure compressive stresses corresponding to the different failure modes, the minimum value $(\sigma_{br})_{min}$ defines the most probable failure mode, the lateral strength of the equivalent strut is given by:

$$H_{mfc} = \sigma_{br\,(min)} ewcos\theta$$

To trace the constitutive law shown in Figure 1-21 we consider that the first elastic stretch has stiffness equal to:

$$K_A = 4K_{mfc}$$

The maximum resistance that the connecting rod manifests in the elastic field is:

$$H_{mf} = 0{,}8H_{mfc}$$

While the stretch with negative stiffness has a slope of:

$$K_C = 0{,}02 - 0{,}04\,K_{mfc}$$

1.8. Operational Modal Analysis and calibration of f.e. models

Ambient vibration tests were performed, before and after the retrofitting works, on the blocks A and G to obtain the modal parameters of the structures, such as natural vibration frequencies, mode shapes and damping ratio in operating conditions. Here we will analyse the results obtained for building A in terms of natural frequencies and modal forms.

1.8.1. Before retrofitting works

Ambient vibration tests were carried out on the whole building. Three accelerometers per floor were positioned: two sensors, measuring along two orthogonal axes (transverse and longitudinal), were placed in the same point at a side of the building while the third, measuring along the transverse direction, was located in the opposite side of the building, far from the first two, to better catch the rotational component of the floor, as we can see from the figure . Other two sensors were placed at the ground floor.

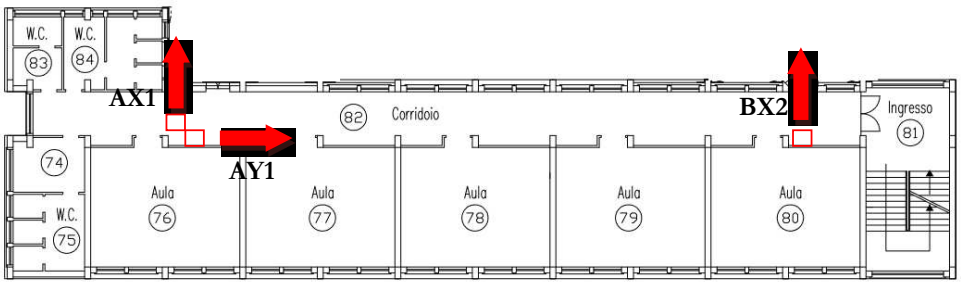

Figure 1-23: Accelerometers layout for each floor.

Tests are carried out using a 24-bit data acquisition system connected to 14 low-noise accelerometers by means of coaxial cables. Four different tests were performed by varying the sampling frequency (from 250 to 1000 Hz) and the time of acquisition (from 1 to 20 minutes). The modal parameters are extracted by means of the Enhanced Frequency Domain Decomposition (EFDD). Firstly, the recorded data are suitably processed by applying a baseline correction, by filtering in the frequency range 0.1-25 Hz, and finally by downsampling at 50 Hz. The EFDD, which is an extension of the Frequency Domain Decomposition, allows estimating damping ratios, in addition to the natural frequencies and mode shapes. According to this technique, working in the frequency domain, modes are extracted by simply peak picking from the Singular Value Decomposition of the spectral densities of accelerations. For each peak, a frequency band is selected evaluating the MAC value between the shape relevant to the peak and to the neighbour frequencies, while all the rest is set to zero. The Power Spectral Density function is taken back to the time domain using the Inverse Discrete Fourier Transform obtaining an approximation of the correlation function of the SDOF system. [Roia et al. 2013]. Resonance frequencies are listed in Table 1-12 while Figure 1-24 shows the relevant mode shapes. The first three frequencies are very close to each other and can be associated to the first two translational modes (in the transverse and longitudinal directions, respectively) and to the rotational mode. The fourth natural frequency is much higher and corresponds to an in-plane distortional mode. More details about execution and results of ambient vibration tests can be found in Roia et al. [2013].

Table 1-12- Experimental resonance frequencies of the building.

Mode number	Mode type	Frequency [Hz]
1	1st transversal	5.23
2	1st longitudinal	5.58
3	1st torsional	6.26
4	in-plane distortional	10.37

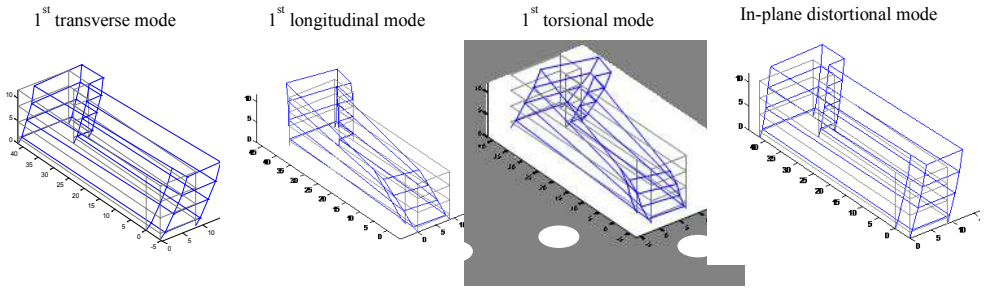

Figure 1-24: Experimental mode shapes of the building

Considering the experimental modal parameters, the finite element model was calibrated. Since the primary purpose of the thesis; calculating the security level of the structure through non-linear analyses, we opted for the use of a model that did not compromise the computational management of non-linear analyses. Therefore, the calibration was performed on a complete model of both external and internal infill walls; modelled with equivalent connecting rods according to "Decanini", in order not to aggravate the computational burden. In particular, in order to use the Decanini's law it was necessary to use a calibration procedure that would allow the use of the same constitutive law but modified in the first section (elastic stretch) in order to catch the modal frequencies and modal shapes obtained through OMA procedure. The results obtained are shown below for every type of equivalent connecting struts, in relation to the width of the frame.

Table 1-13: EXTERNAL INFILL WALLS - Values of the elastic modulus for the equivalent connecting struts

	1	2	3	4	5	6	7
E [kN/mq]	9836738	7596311	3420402	2858878	4893203	9359503	5464696
w [m]	0.84	1.09	2.42	2.89	1.69	0.88	1.51
s [m]	0.12	0.12	0.12	0.12	0.12	0.12	0.12

As regards the internal infill walls, these have been divided into longitudinal and transversal infills to take into account the different incidence of the frame on the panel stiffness. In particular, the elastic modulus used are:

Table 1-14: INTERNAL INFILL WALLS - Values of the elastic modulus for the equivalent connecting struts

	LONG.	TRANSV.

E [kN/mq]	10875694,52	5703809,46
w [m]	1.09	2.89
s [m]	0.12	0.12

The concrete elastic modulus is assumed to be 27500 N/mm^2, corresponding to about 1.125 times the static one indirectly derived from the cylindrical compressive strength obtained from destructive tests.

$$E_{conc.} = 27500\ N/mm^2$$

Numerical resonance frequencies obtained from a classical modal analysis are compared with the experimental ones, resulting from the OMA (Table 1-15). Experimental and numerical values show a very good agreement.

Table 1-15: Experimental vs. analytical values of the building resonance frequencies

Mode	Experimental Frequency [Hz]	Analytical Frequency [Hz]	Percentage error [%]	Mode type
1	5.23	5.26	0.57%	1st transverse
2	5.58	5.73	2.69%	1st longitudinal
3	6.26	6.25	0.16%	1st torsional
4	10.37	10.51	1.35%	in-plane distortional

The following is a comparison between modal shapes obtained from the OMA procedures and those obtained from the f.e. model.

Mode shapes		
	Experimental	Analytical
1	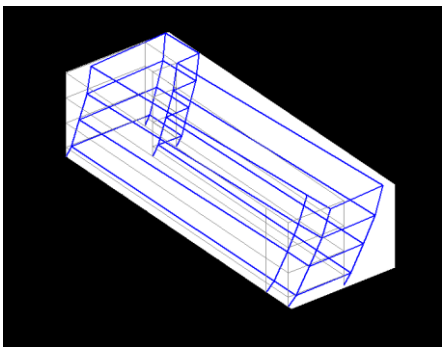	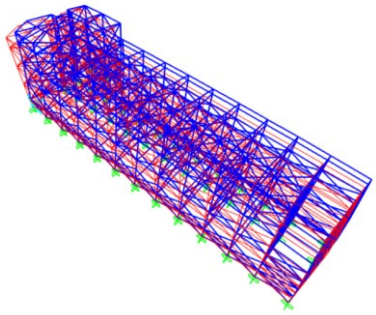
	5.23 Hz	5.26 Hz

2	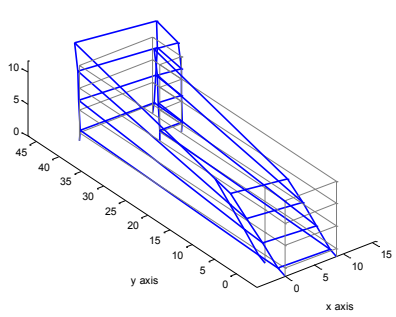	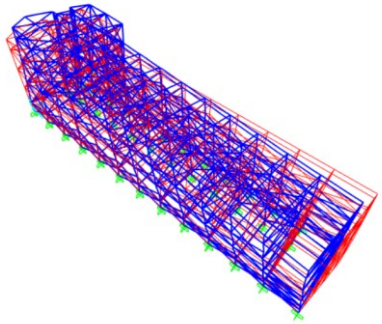
	5.58 Hz	5.73 Hz
3	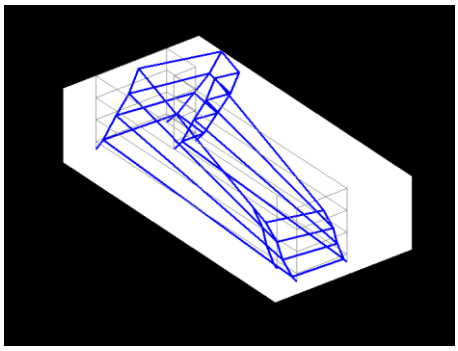	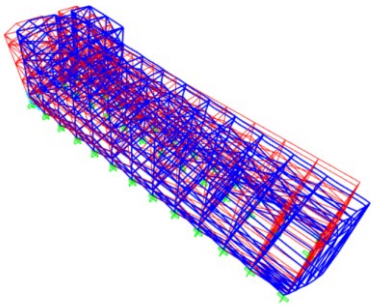
	6.26 Hz	6.25 Hz
4	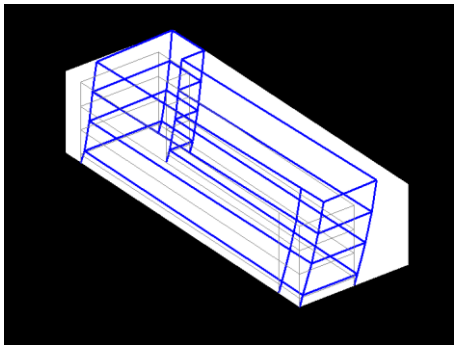	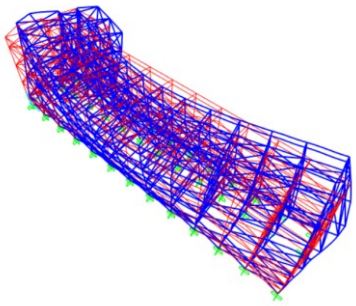
	10.37 Hz	10.51 Hz

Figure 1-25: Experimental mode shapes vs. analytical mode shapes

The mode shapes were compared using the MAC (Modal Assurance Criterion), calculated as the normalized scalar product of two sets of vectors $\phi_{th,i}$ and $\phi_{e,i}$, respectively representing the theoretical and experimental modal form of the i-th mode considered:

$$MAC_i = \frac{\left(\phi_{th,i}^T \cdot \phi_{e,i}\right)^2}{\left(\phi_{th,i}^T \cdot \phi_{th,i}\right) \cdot \left(\phi_{e,i}^T \cdot \phi_{e,i}\right)}$$

The results of the Modal Assurance Criterion between experimental and analytical modal displacements are also shown.

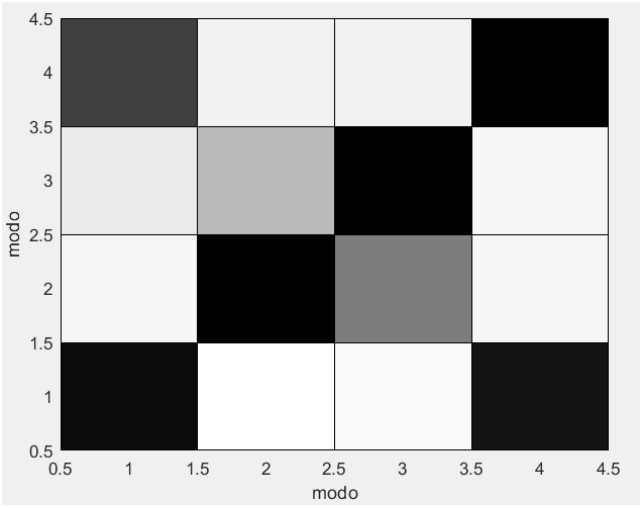

Figure 1-26: Mac Matrix experimental vs. analytical displacements

As we can see from the MAC matrix the experimental modal shapes are quite decoupled therefore, they represent the first 4 natural modes of the structure. Except for the first and fourth modes, among which we could note a certain dependence due to problems of spatial aliasing. In fact, the fourth modal shape results in bending in the plane and it would have been impossible to be able to catch it with the test configuration adopted.

This thesis is supported by the results collected by the autoMAC matrix, where we can see the similarity between the first and the fourth mode shapes.

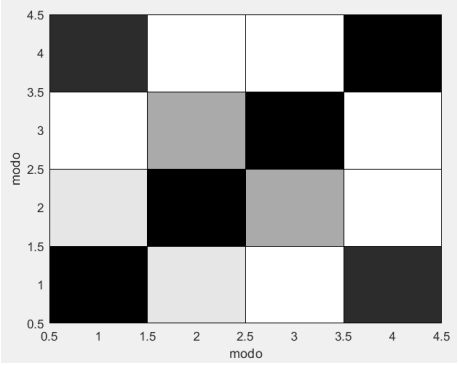

Figure 1-27: AutoMac Matrix

1.8.2. After retrofitting works

After retrofitting works on block A were performed ambient vibration tests and snap back test, in order to assess the dissipative capacity of the new structural system at greater input energy level. Below are shown the modal parameters obtained by OMA procedures after retrofitting, with the same accelerometers configurations.

Table 1-16- Experimental resonance frequencies of the building after retrofitting.

Mode number	Mode type	Frequency [Hz]
1	1st transversal	5,42
2	1st longitudinal	5,70
3	1st torsional	6,50
4	in-plane distortional	10,18

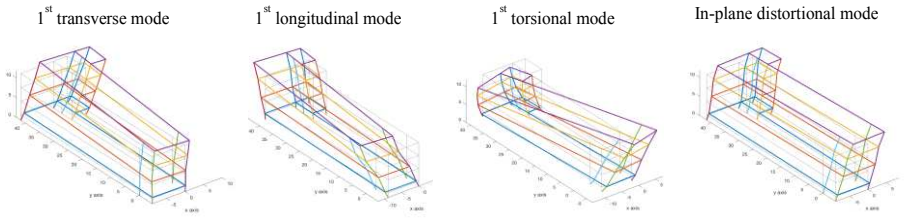

Figure 1-28: Experimental mode shapes of the building after retrofitting

As we can see, there are no significant variations in the natural frequencies and in the modal shapes of the structure, proving that the dissipative towers do not modify the dynamic behaviour of the original building.

With reference to the calibration phase of the model, the geometry, the characteristics of the materials and any other data have been kept identical to the previous case, to which the structures of the dissipative towers have simply been added. However, since the after-retrofitting model must be subjected to a higher computational burden, because the presence of viscoelastic dissipators requires the use of non-linear dynamic analyses to calculate the level of safety, the shell mesh has been slightly increased. This fact, notoriously, has the consequence of an implementation of the global stiffness of the model which cannot be eliminated, therefore the natural analytical frequencies will be slightly above the experimental ones.

Table 1-17: Experimental vs. analytical values of the building resonance frequencies

Mode	Experimental Frequency [Hz]	Analytical Frequency [Hz]	Percentage error [%]	Mode type
1	5.42	5.67	4.61%	1st transverse
2	5.70	5.96	4.56%	1st longitudinal
3	6.50	6.77	4.15%	1st torsional
4	10.18	15.74	54.62%	in-plane distortional

The following is a comparison between the modal shapes obtained from the OMA procedures and those obtained from the f.e. model.

	Mode shapes	
	Experimental	**Analytical**
1	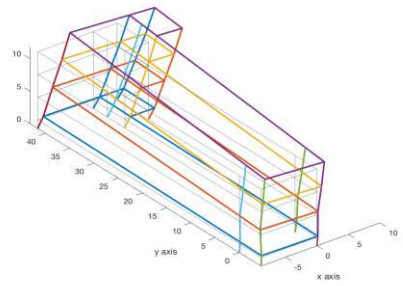	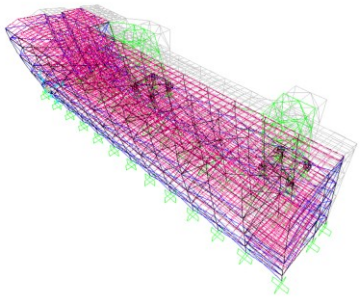
	5.42 Hz	5.67 Hz
2	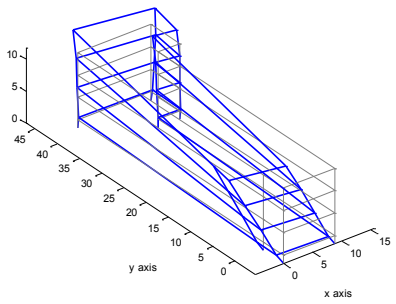	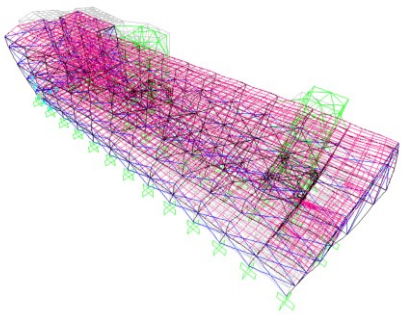
	5.70 Hz	5.96 Hz

3	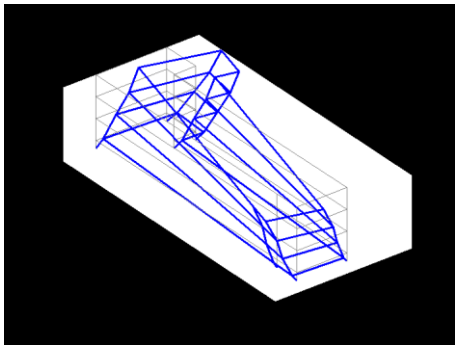	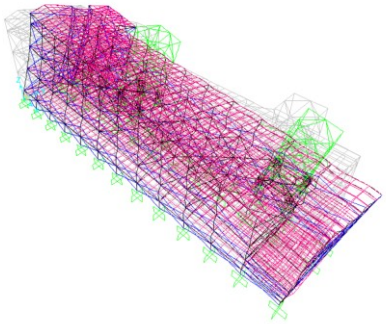
	6.50 Hz	6.77 Hz
4	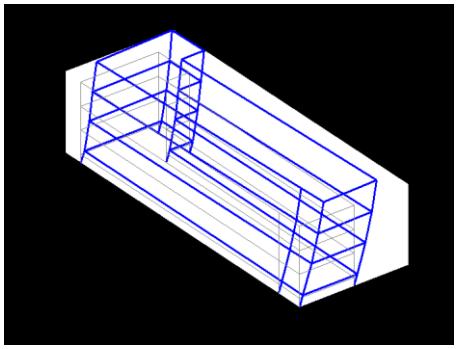	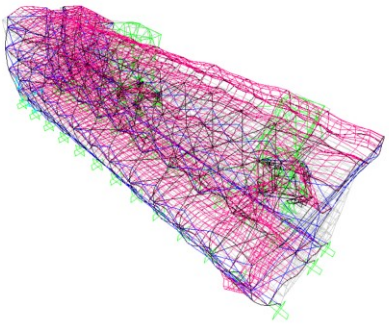
	10.18 Hz	15.74 Hz

Figure 1-29: Experimental mode shapes vs. analytical mode shapes after retrofitting

The results of the Modal Assurance Criterion between experimental and analytical modal displacements are also shown.

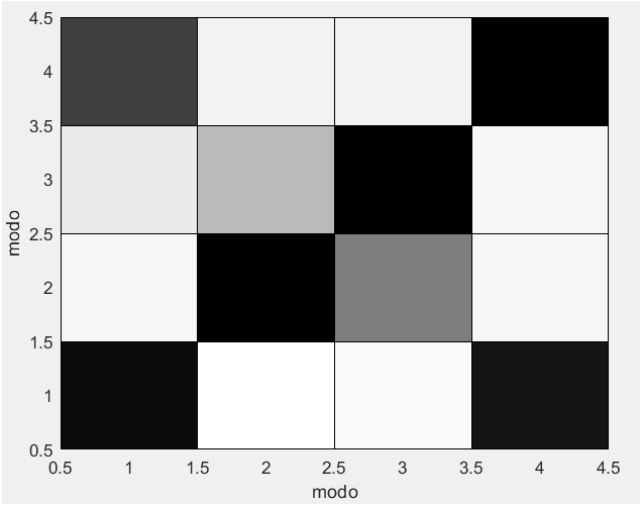

Figure 1-30: Mac Matrix experimental vs. analytical displacements

1.9. Vulnerability Index Before Retrofitting Works

As already mentioned in the introduction, the purpose of this thesis work is to evaluate how much the accuracy in finite element modelling affects the calculation of the seismic vulnerability index of the structures. Considering this aim, three models have been implemented, characterized by increasing degree of accuracy:

- Model A: frame without non-structural elements
- Model B: frame with external infill walls modelled with equivalent rods according to literature
- Model C: frame with external infill walls modelled with equivalent connecting rods and calibrated by OMA and internal infill walls modelled with equivalent connecting rods and calibrated by EMA.

The modelling of external and internal infill walls, as anticipated in chap. 1.7, was carried out through the introduction of equivalent connecting rods according to the "Decanini" theory. The seismic vulnerability index was calculated through non-linear static analysis (Pushover).

1.9.1. Non-linear Static Analysis – Pushover

Notoriously, the purpose of the pushover analysis is to investigate the post-elastic behaviour of the structure, for this purpose, it is necessary to model the post-elastic behaviour

of the structural elements; a concentrated plasticity model (plastic hinge) was used to this purpose. The non-linear static analysis consists in applying the gravitational loads to the structure and, for the considered direction of the seismic action, a system of distributed horizontal forces, at each level of the construction, proportionally to the resulting inertial forces Fb.

These forces are scaled so that the horizontal displacement of a control point grows monotonically, both in a positive and in a negative direction and until the conditions of local or global collapse are reached.

The plastic hinges represent the areas of the structural elements where the inelastic behaviour is concentrated; outside these areas the elements remain in the elastic range. The constitutive laws of the hinges can describe different phenomena (flexural behaviour, combined compressive and bending stress., Shear, etc.). The points where the plastic hinges are inserted depends precisely on the behaviour they describe.

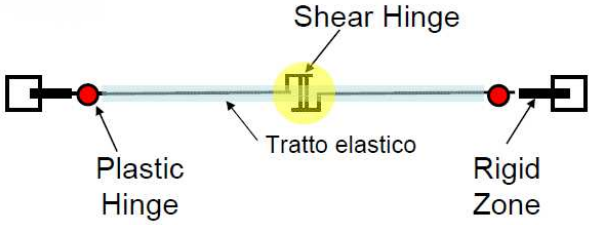

Figure 1-31: Positioning of plastic hinges

Hinges with bending and combined compressive and bending behaviour

The plastic hinges implemented in the f.e. model through SAP2000 program refer to FEMA 356, which for the Nonlinear Static Procedure (NSP), uses the generalized load-deformation relation shown in Figure 1-32 to defining behaviour under monotonically increasing deformation.

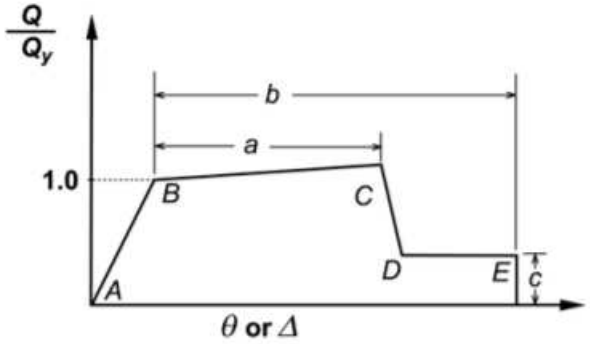

Figure 1-32: Generalized Force-Deformation Relations for Concrete Elements or Components

The generalized load-deformation relation shown in Figure 1-32 is described by linear response from A (unloaded component) to an effective yield B, then a linear response at reduced stiffness from point B to C, then sudden reduction in lateral load resistance to point

D, then response at reduced resistance to E, and final loss of resistance thereafter. The slope from point B to C, ignoring effects of gravity loads acting through lateral displacements, shall be taken between zero and 10% of the initial slope unless an alternate slope is justified by experiment or analysis. Point C shall have an ordinate equal to the strength of the component and an abscissa equal to the deformation at which significant strength degradation begins. Representation of the load-deformation relation by points A, B, and C only (rather than all points A–E), shall be permitted if the calculated response does not exceed point C. Numerical values for the points identified in Figure 1-32 shall be as specified in Figure 1-33 and Figure 1-34.

Table 6-7 ***Modeling Parameters and Numerical Acceptance Criteria for Nonlinear Procedures—Reinforced Concrete Beams***

			Modeling Parameters[3]			Acceptance Criteria[3]				
						Plastic Rotation Angle, radians				
						Performance Level				
			Plastic Rotation Angle, radians		Residual Strength Ratio		Component Type			
							Primary		Secondary	
Conditions			a	b	c	IO	LS	CP	LS	CP
i. Beams controlled by flexure[1]										
$\frac{\rho-\rho'}{\rho_{bal}}$	Trans. Reinf.[2]	$\frac{V}{b_w d\sqrt{f'_c}}$								
≤ 0.0	C	≤ 3	0.025	0.05	0.2	0.010	0.02	0.025	0.02	0.05
≤ 0.0	C	≥ 6	0.02	0.04	0.2	0.005	0.01	0.02	0.02	0.04
≥ 0.5	C	≤ 3	0.02	0.03	0.2	0.005	0.01	0.02	0.02	0.03
≥ 0.5	C	≥ 6	0.015	0.02	0.2	0.005	0.005	0.015	0.015	0.02
≤ 0.0	NC	≤ 3	0.02	0.03	0.2	0.005	0.01	0.02	0.02	0.03
≤ 0.0	NC	≥ 6	0.01	0.015	0.2	0.0015	0.005	0.01	0.01	0.015
≥ 0.5	NC	≤ 3	0.01	0.015	0.2	0.005	0.01	0.01	0.01	0.015
≥ 0.5	NC	≥ 6	0.005	0.01	0.2	0.0015	0.005	0.005	0.005	0.01
ii. Beams controlled by shear[1]										
Stirrup spacing ≤ d/2			0.0030	0.02	0.2	0.0015	0.0020	0.0030	0.01	0.02
Stirrup spacing > d/2			0.0030	0.01	0.2	0.0015	0.0020	0.0030	0.005	0.01
iii. Beams controlled by inadequate development or splicing along the span[1]										
Stirrup spacing ≤ d/2			0.0030	0.02	0.0	0.0015	0.0020	0.0030	0.01	0.02
Stirrup spacing > d/2			0.0030	0.01	0.0	0.0015	0.0020	0.0030	0.005	0.01
iv. Beams controlled by inadequate embedment into beam-column joint[1]										
			0.015	0.03	0.2	0.01	0.01	0.015	0.02	0.03

1. When more than one of the conditions i, ii, iii, and iv occurs for a given component, use the minimum appropriate numerical value from the table.
2. "C" and "NC" are abbreviations for conforming and nonconforming transverse reinforcement. A component is conforming if, within the flexural plastic hinge region, hoops are spaced at ≤ d/3, and if, for components of moderate and high ductility demand, the strength provided by the hoops (V_s) is at least three-fourths of the design shear. Otherwise, the component is considered nonconforming.
3. Linear interpolation between values listed in the table shall be permitted.

Figure 1-33: Modelling Parameters and Numerical Acceptance Criteria for Nonlinear Procedures— Reinforced Concrete Beams

Table 6-8 *Modeling Parameters and Numerical Acceptance Criteria for Nonlinear Procedures—Reinforced Concrete Columns*

Conditions			Modeling Parameters[4]			Acceptance Criteria[4]				
			Plastic Rotation Angle, radians		Residual Strength Ratio	Plastic Rotation Angle, radians				
						Performance Level				
							Component Type			
							Primary		Secondary	
			a	b	c	IO	LS	CP	LS	CP
i. Columns controlled by flexure[1]										
$\frac{P}{A_g f'_c}$	Trans. Reinf.[2]	$\frac{V}{b_w d \sqrt{f'_c}}$								
≤ 0.1	C	≤ 3	0.02	0.03	0.2	0.005	0.015	0.02	0.02	0.03
≤ 0.1	C	≥ 6	0.016	0.024	0.2	0.005	0.012	0.016	0.016	0.024
≥ 0.4	C	≤ 3	0.015	0.025	0.2	0.003	0.012	0.015	0.018	0.025
≥ 0.4	C	≥ 6	0.012	0.02	0.2	0.003	0.01	0.012	0.013	0.02
≤ 0.1	NC	≤ 3	0.006	0.015	0.2	0.005	0.005	0.006	0.01	0.015
≤ 0.1	NC	≥ 6	0.005	0.012	0.2	0.005	0.004	0.005	0.008	0.012
≥ 0.4	NC	≤ 3	0.003	0.01	0.2	0.002	0.002	0.003	0.006	0.01
≥ 0.4	NC	≥ 6	0.002	0.008	0.2	0.002	0.002	0.002	0.005	0.008
ii. Columns controlled by shear[1, 3]										
All cases[5]			—	—	—	—	—	—	.0030	.0040
iii. Columns controlled by inadequate development or splicing along the clear height[1,3]										
Hoop spacing ≤ d/2			0.01	0.02	0.4	0.005	0.005	0.01	0.01	0.02
Hoop spacing > d/2			0.0	0.01	0.2	0.0	0.0	0.0	0.005	0.01
iv. Columns with axial loads exceeding $0.70P_o$[1, 3]										
Conforming hoops over the entire length			0.015	0.025	0.02	0.0	0.005	0.01	0.01	0.02
All other cases			0.0	0.0	0.0	0.0	0.0	0.0	0.0	0.0

1. When more than one of the conditions i, ii, iii, and iv occurs for a given component, use the minimum appropriate numerical value from the table.
2. "C" and "NC" are abbreviations for conforming and nonconforming transverse reinforcement. A component is conforming if, within the flexural plastic hinge region, hoops are spaced at ≤ $d/3$, and if, for components of moderate and high ductility demand, the strength provided by the hoops (V_s) is at least three-fourths of the design shear. Otherwise, the component is considered nonconforming.
3. To qualify, columns must have transverse reinforcement consisting of hoops. Otherwise, actions shall be treated as force-controlled.
4. Linear interpolation between values listed in the table shall be permitted.
5. For columns controlled by shear, see Section 6.5.2.4.2 for acceptance criteria.

Figure 1-34: Modelling Parameters and Numerical Acceptance Criteria for Nonlinear Procedures—Reinforced Concrete Columns

Shear hinges

For what concerns shear hinges it was considering a brittle-type fracture as shown in Figure 1-35.

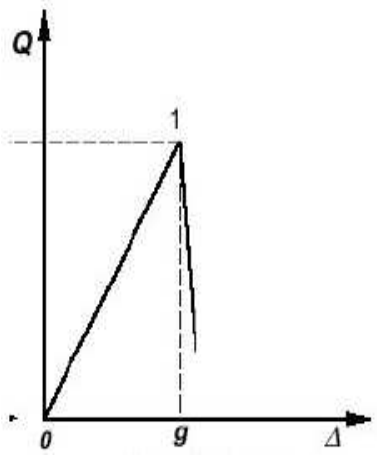

Figure 1-35: Force-Deformation Relations for brittle type fractures.

The shear hinges inside the SAP2000 have been inserted manually, calculating the maximum resistant shear in the two directions X (local axis 3) and Y (local axis 2). Considering the low quantity of transversal reinforcement (1.2.4) the shear strength of the non-reinforced section was evaluated using the formula:

$$V_{rd} = \left[\frac{0{,}18}{\gamma_c} \cdot k \cdot (100 \cdot \rho_l \cdot f_{ck})^{1/3} + 0{,}15 \cdot \sigma_{cp}\right] \cdot b_w \cdot d \geq \left(v_{min} + 0{,}15 \cdot \sigma_{cp}\right) \cdot b_w \cdot d$$

The shear hinges have been defined as follows in SAP2000:

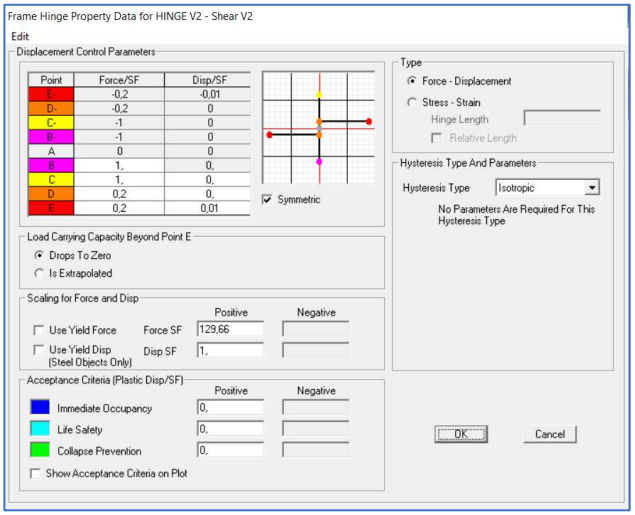

Figure 1-36: Constitutive law of the hinge with shear oriented towards Y.

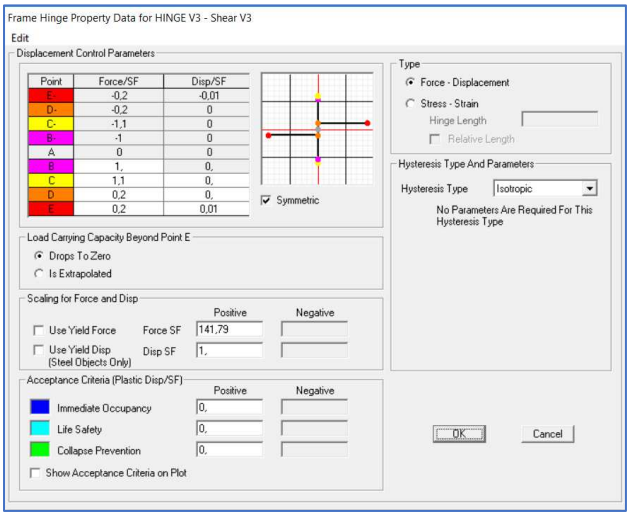

Figure 1-37: Constitutive law of the hinge with shear oriented towards X.

1.9.2. Non-linear Static Analysis – Distribution of forces

According to the NTC08 (NTC 2008 § 7.3.4.1) at least two distributions of the inertia forces must be considered, one in the main distributions (Group 1) and the other in the secondary distributions (Group 2) illustrated below.

Group 1 - Main distributions

- distribution proportional to the static forces (linear static analysis), applicable only if the fundamental vibration mode in the considered direction has a mass participation of not less than 75% and on condition of using the second distribution as the second one;
- distribution corresponding to a distribution of accelerations proportional to the vibration mode, applicable only if the fundamental vibration mode in the considered direction has a mass participation of not less than 75%;
- distribution corresponding to the distribution of the plan shear calculated in a linear dynamic analysis, applicable only if the fundamental period of the structure is greater than Tc.

Group 2 - Secondary distributions

a) uniform distribution of forces, to be understood as derived from a uniform distribution of accelerations along the height of the construction;

b) adaptive distribution, which changes as the displacement of the control point increases as a function of the plasticization of the structure.

As the Ordinance PCM 3431 (03.05.2005) suggests, generally two distributions of forces are considered:

- one proportional to the masses;
- one proportional to the product of the masses for the deformation corresponding to the first mode.

They are respectively equivalent to the first of Group 2 and the second of Group 1.

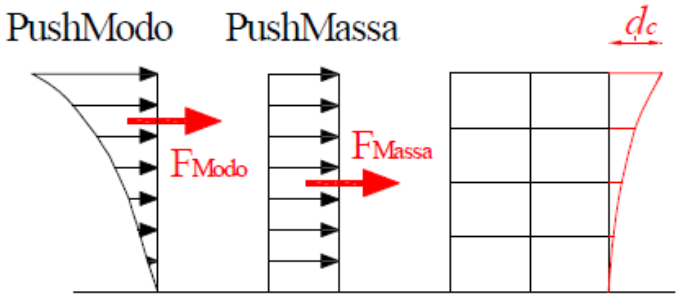

Figure 1-38: Distribution forces

The analysis has as an initial condition of undeformed structure: the case of non-linear static analysis "Grav" (only with gravitational loads).

In particular in this work the "Grav" case is defined by the forces and coefficients shown in Figure 1-39: Load case “GRAV”.

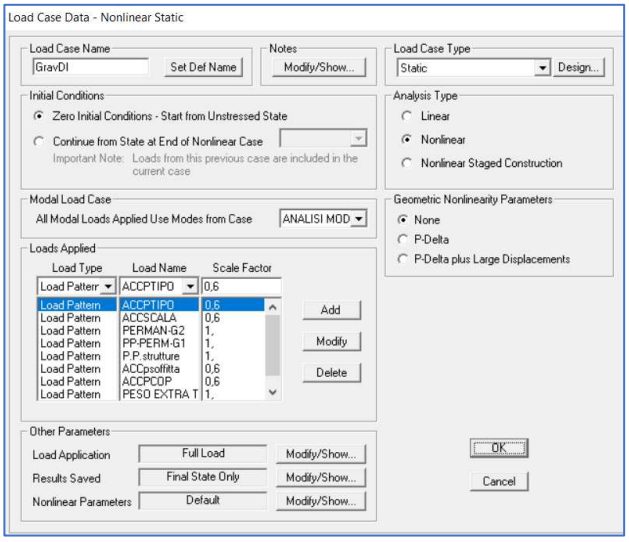

Figure 1-39: Load case “GRAV”

To take into account the spatial variability of the seismic motion, as well as any uncertainties in the location of the masses, at the center of mass an accidental eccentricity must be attributed to its position.

For buildings only and in the absence of more accurate determinations accidental eccentricity in any direction cannot be considered inferior to 0.05 times the size of the building measured perpendicularly to the direction of application of the seismic action. This eccentricity is assumed to be constant, by entity and direction, on all the horizontal sections.

The cases to be evaluated are the following:

1. PushmassaX+TP
2. PushmassaX+TN
3. PushmassaX-TP
4. PushmassaX-TN
5. PushmassaY+TP
6. PushmassaY+TN
7. PushmassaY-TP
8. PushmassaY-TN
9. PushmodeX+TP
10. PushmodeX+TN
11. PushmodeX-TP
12. PushmodeX-TN
13. PushmodeY+TP
14. PushmodeY+TN
15. PushmodeY-TP
16. PushmodeY-TN

where:

- Pushmassa: distribution of force proportional to the masses;
- Pushmode: force distribution proportional to the fundamental mode of vibration in the direction of analysis;
- +, -: push direction (in relation to the global reference system of the structural model);
- TP: torque associated with the horizontal thrust accidental positive (defined with reference to the axis z of the global structural model system).
- TN: torque associated with the horizontal thrust accidental negative (defined with reference to the axis z of the global structural model system).

The load distribution inserted for load case "pushmassa" is shown in Table 1-18: Load distribution "Pushmassa"

Table 1-18: Load distribution "Pushmassa"

	Mass [kN*s²/m]	**Force [kN]**	**PushMass**
Floor 1	541,77	5314,76	0,89
Floor 2	561,99	5513,12	0,92
Floor 3	557,19	5466,03	0,92
Floor 4	608,22	5966,64	1,00

The load distribution inserted for load case "pushmodo" is shown in Table 1-19.

Table 1-19: Load distribution "Pushmodo"

	U1 [m]	**U2 [m]**	**Mass [kN*s²/m]**	**U1*Mass**	**U2*Mass**	**Pushmodo X**	**Pushmodo Y**
Floor 1	0,0017	-0,0021	541,77	0,939	-1,122	0,049	0,060
Floor 2	0,0116	-0,0125	561,99	6,523	-7,009	0,338	0,377
Floor 3	0,0233	-0,0230	557,19	12,959	-12,838	0,671	0,690
Floor 4	0,0317	-0,0306	608,22	19,310	-18,614	1,000	1,000

The seismic vulnerability index was calculated using the CSM (Capacity Spectrum Method) method and it is presented for the three f.e. models previously described and characterized by increasing accuracy: model A, model B and model C. Furthermore, for each of these, two cases have been distinguished: fragile and ductile. In the first case, all the types of plastic hinge presented are included, including those with brittle fractures, in the second case, instead, the possible fragile mechanisms are omitted assuming that these can be avoided through local interventions (FRP wrapping for short Column).

1.9.3. Model A: Seismic Vulnerability Index

As already mentioned, the A model, characterized by a lower level of accuracy, is composed only of structural components.

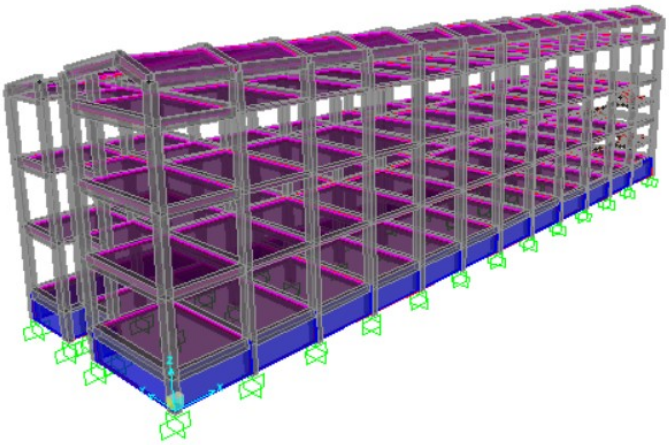

Figure 1-40: Extruded view of Model A

$$E_{conc} = 50\% E_{conc\ el}$$

The results obtained for the four most important analysis cases are summarized in the table

Table 1-20: Summarize of seismic vulnerability index for model A

	I_R SLD	**I_R SLV BRITTLE**	**I_R SLV DUCTILE**
Pushmass X+	0,328	0,443	0,778
Pushmodo X+	0,270	0,390	0,658
Pushmass Y+	0,354	0,293	0,880
Pushmodo Y+	0,301	0,404	0,780

1.9.4. Model B: Seismic Vulnerability Index

Model B, characterized by an intermediate level of accuracy, is composed of external infill walls modelled as equivalent rods according to literature, in addition to the structural components.

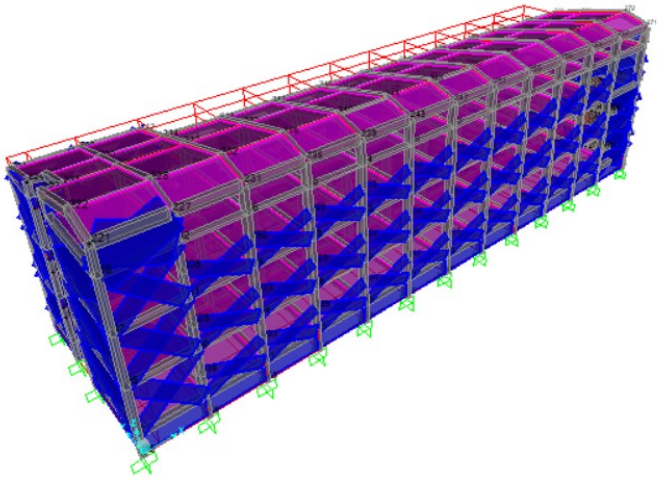

Figure 1-41: Extruded view of Model B

$$E_{conc} = 50\% E_{conc\ el}$$

The constitutive laws and the corresponding law of the plastic hinge inserted in the model are shown below:

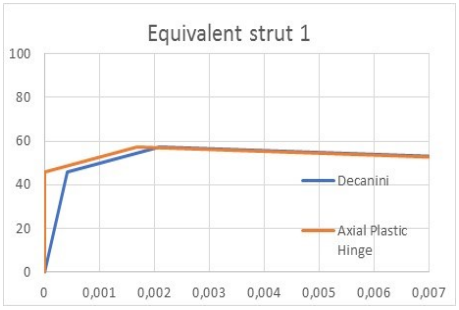

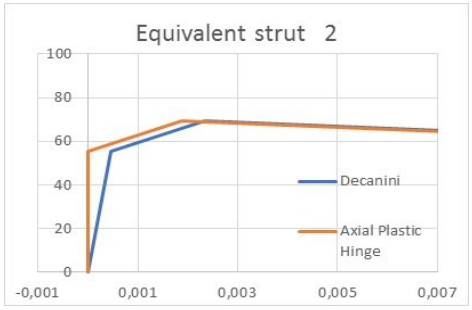

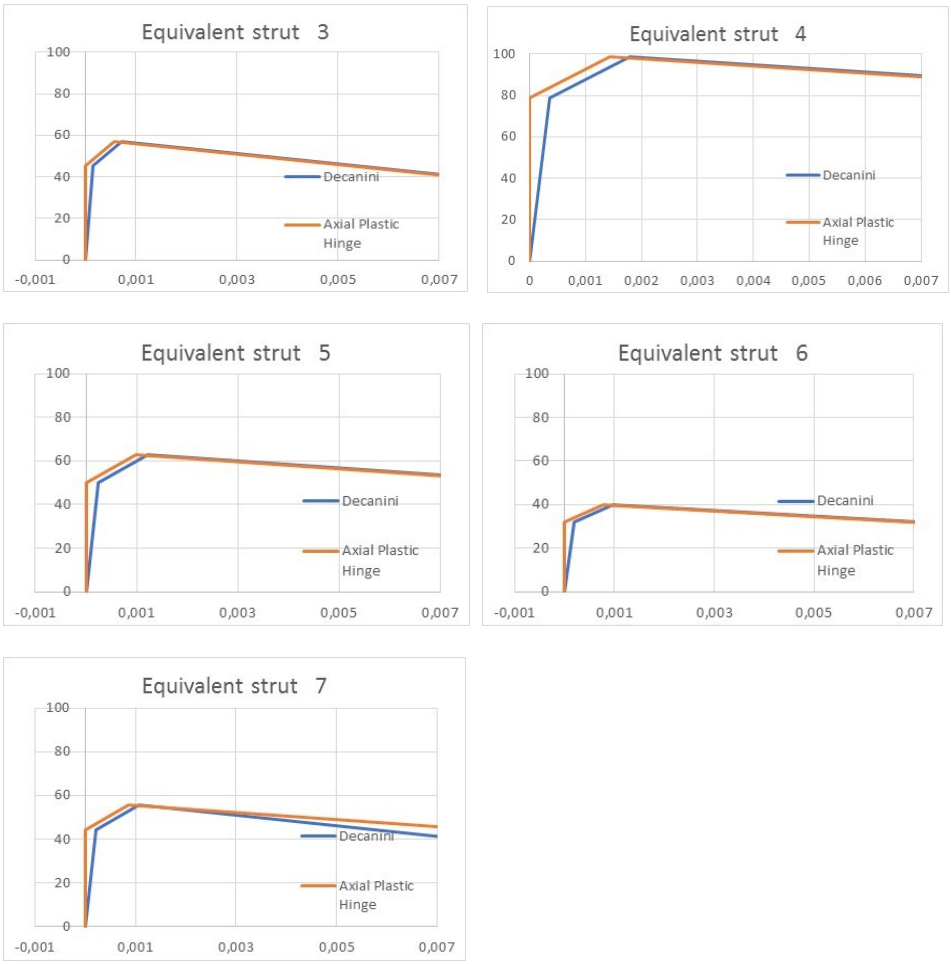

Figure 1-42: The constitutive laws of the equivalent strut and the corresponding law of the plastic hinge

The results obtained for the four most important analysis cases are summarized in the table:

Table 1-21: Summarize of seismic vulnerability index for model B

	I_R SLD	I_R SLV BRITTLE	I_R SLV DUCTILE
Pushmass X+	0,603	0,681	1,151
Pushmodo X+	0,537	0,559	0,961
Pushmass Y+	0,465	0,312	0,952
Pushmodo Y+	0,373	0,358	1,016

1.9.5. Model C: Seismic Vulnerability Index

Model C, characterized by a higher level of accuracy, is composed of external and internal infill walls, in addition to the structural components, modelled as equivalent connecting rods and calibrated through experimental tests; the first one through OMA procedures and the second one through EMA procedures.

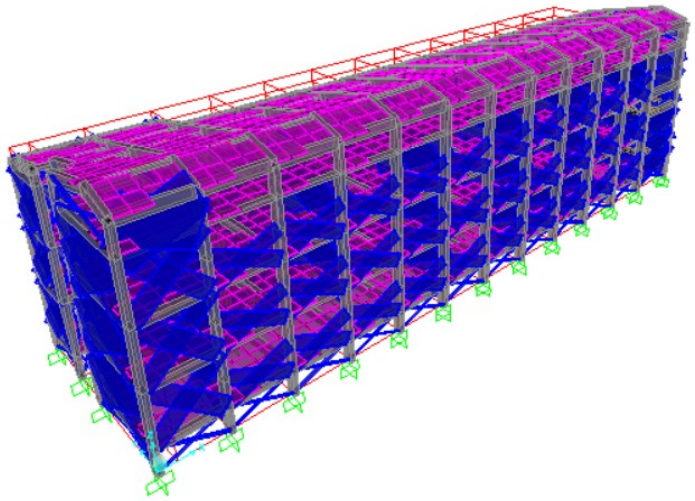

Figure 1-43: Extruded view of Model C

Obviously, the calibrated model C is different from the model C on which the push-over was performed. This is because a dynamic elastic modulus of concrete was used for the calibration Ed = 27500 N / mm^2 and also the accidental loads were not inserted since the OMA tests were performed with the empty building. In order to pass from this model to the one on which the pushover was made, the module of cracked concrete was adopted, and accidental loads were added.

$$E_{conc} = 50\% E_{conc\ el}$$

The constitutive laws and the corresponding law of the plastic hinge inserted in the model are shown below:

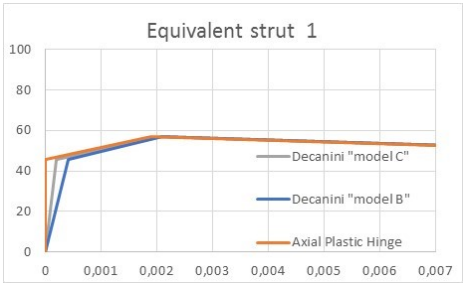

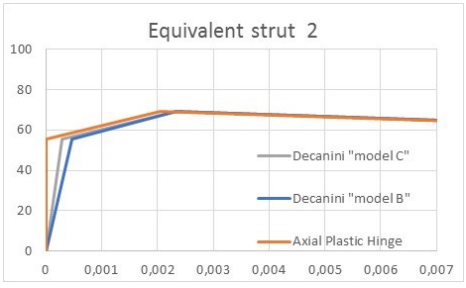

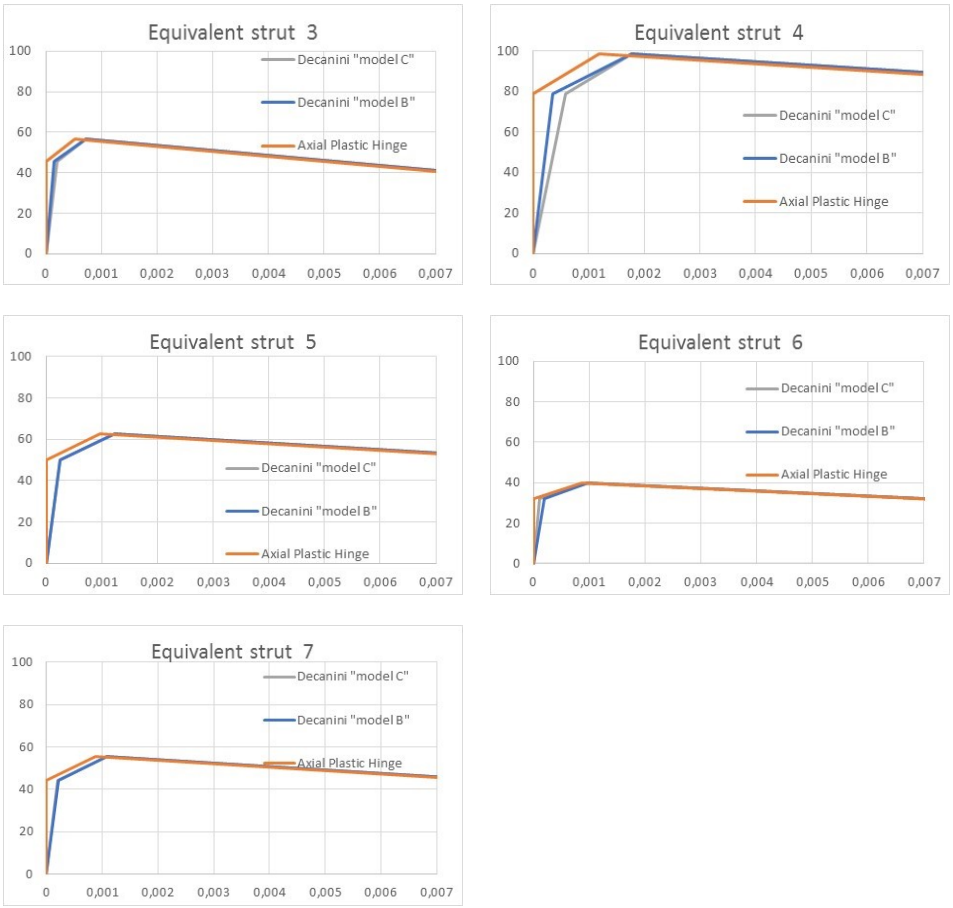

Figure 1-44: The constitutive laws of the equivalent strut and the corresponding law of the plastic hinge

The results obtained for the four most important analysis cases are summarized in the Table 1-22.

Table 1-22: Summarize of seismic vulnerability index for model C

	I_R SLD	I_R SLV BRITTLE	I_R SLV DUCTILE
Pushmass X+	0,822	0,708	1,252
Pushmodo X+	0,768	0,782	1,225
Pushmass Y+	0,548	0,235	1,107
Pushmodo Y+	0,389	0,226	1,069

1.9.6. Comparisons between models

Below, the SLV seismic vulnerability index of the structure is compared for the three models implemented, for the push direction.

Table 1-23: seismic vulnerability index obtained for the most severe load cases, for models containing brittle fracture mechanisms, based on the push direction

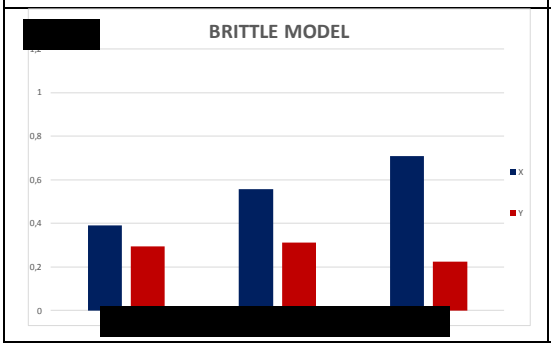

Table 1-24: seismic vulnerability index obtained for the most severe load cases, for models without brittle fracture mechanisms, based on the push direction

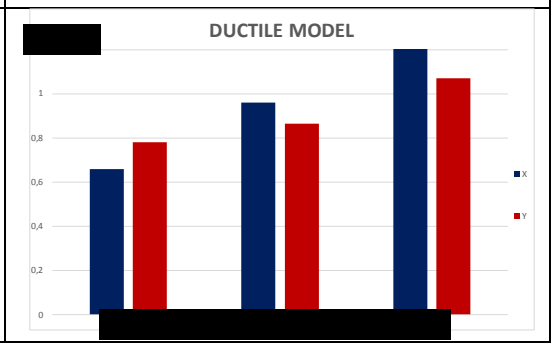

From these graphs we can appreciate how, along the transversal direction "Y", the increase of the modelled infill (from model A to model C) leads to anticipating the arrival of fragile mechanisms at the base. On the contrary, in the corresponding ductile models, to the increase of the precision of the modelling and the infill there is instead an increase of the seismic vulnerability index.

In addition, a comparison between different model is shown in terms of intensity level of the seismic action necessary to reach the SLD.

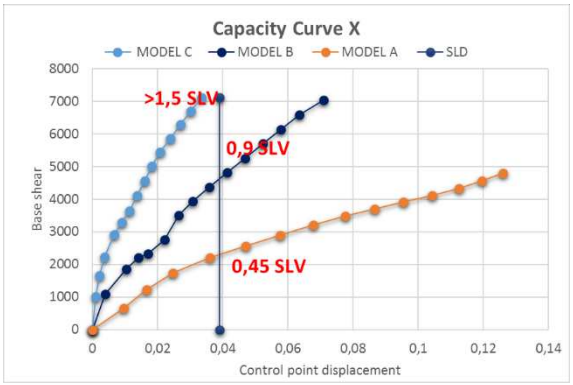

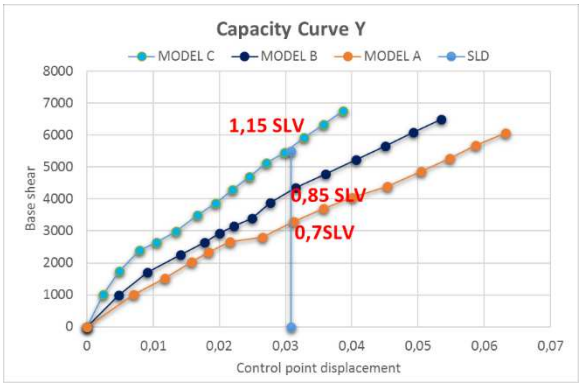

Figure 1-45: Comparison between different model in terms of intensity level of the seismic action necessary to reach the SLD

From the figures it has been noted that the level of seismic energy necessary to reach the SLD limit displacement increases as the degree of detail of the model increases. The level of seismic energy necessary to reach the SLD limit displacement in X direction for model C is greater than 1.5 SLV, compared to a level equal to 0.45 SLV necessary to reach the SLD for model A. However, the striking results obtained for SLD must be read carefully in the right perspective. The fundamental period of model A without infill walls, model B and model C with calibrated internal and external infill walls, fall between the fundamental periods of the spectrum: Tb and Tc, therefore correspond to the maximum seismic acceleration. Consequently, the striking difference found derives, in part, from the fact that the model C is characterized by a stiffness much greater than models A and B, despite having their same seismic acceleration. On the other hand, the common engineering practice leads to considering the results obtained as an overvalue of the elastic stiffness stretch of the infill walls. The choice of evaluate the elastic modulus of the infill panel through experimental modal analysis, characterized by very low level of dynamic input, can lead to the overvalue of this parameter in the assessment of seismic vulnerability index in linear field (SLD). Probably, the real elastic stretch of the infill walls stiffness lies between the one measured by experimental dynamic tests (calibrated on low input level, non-destructive test), and the one proposed in literature (calibrated on high input level, failure test), because the seismic energy level connected to the SLD is greater than the one related to the dynamic identification tests and less than the one associated with the breaking tests on infill panels present in the literature.

1.9.7. Seismic classification

For the determination of the Risk Class, reference is made hereinafter to two parameters: (i) the expected average annual loss (PAM), which takes into account the economic losses associated with structural and non-structural element damage, and referring to the cost of reconstruction (CR) of the building without its contents, and (ii) the safety index (IS-V) of

the structure defined as the ratio between the peak ground acceleration (PGA, Peak Ground Acceleration) which determines the reaching the State of the Life Protection Limit (SLV), capacity in PGA - PGAC, and the PGA that the standard indicates, in the specific site where the building is located and for the same limit state, as a reference for the design of a new building, application in PGA - PGAD. The seismic vulnerability index (IS-V) of the structure is better known to technicians under the name of "Risk Index". The PAM parameter can be assimilated to the cost of repair of the damage caused by seismic events that occur during the life of the building, divided annually and expressed as a percentage of the reconstruction cost. It can be evaluated, as required for the application of the conventional method, such as the subtended area to the curve representing direct economic losses, based on the average annual frequency of exceeding (equal to the inverse of the average return period) the events that cause the achievement of one state limit for the structure. This curve, in the absence of more precise data, can be discretized. The smaller the area subtended by this curve, the lower the expected average annual loss (PAM).

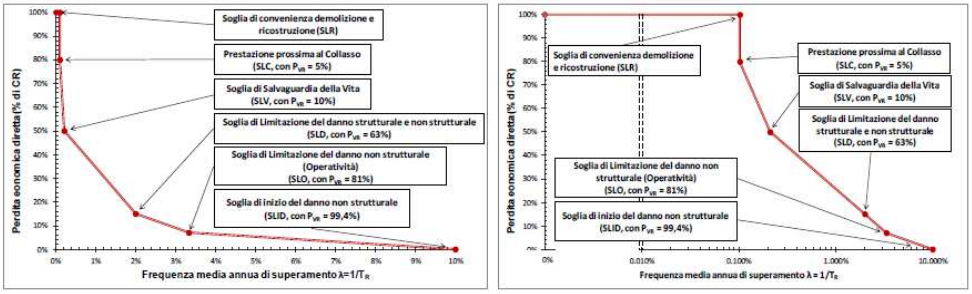

Figure 1-46: Trend of the curve that identifies the PAM, referring to a construction with a nominal life of 50 years and belonging to the use class II. In the image on the right, to better identify the points close to the ordinate axis, the abscissas are on a logarithmic scale.

The conventional method assigns to the construction in question, a Risk Class according to the economic parameter PAM and the seismic vulnerability index of the IS-V structure. In order to evaluate these parameters it is necessary to calculate, referring to the site construction, the peak ground accelerations for which the SLO, SLD, SLV and SLC limit states are reached, using the usual safety checks to the limit states provided for by the Technical Standards for Buildings. The reference values for the definition of the PAM Classes are shown in Figure 1-47.

Perdita Media Annua attesa (PAM)	Classe PAM
PAM ≤ 0,50%	A^+_{PAM}
0,50% < PAM ≤ 1,0%	A_{PAM}
1,0% < PAM ≤ 1,5%	B_{PAM}
1,5% < PAM ≤ 2,5%	C_{PAM}
2,5% < PAM ≤ 3,5%	D_{PAM}
3,5% < PAM ≤ 4,5%	E_{PAM}
4,5% < PAM ≤ 7,5%	F_{PAM}
7,5% ≤ PAM	G_{PAM}

Figure 1-47: Assignment of the PAM Risk Class based on the amount of expected average annual Losses

The reference values of the safety index from which to derive the Class IS-V, linked to safeguarding human life, are shown in Figure 1-48.

Indice di Sicurezza	Classe IS-V
100% < IS-V	A^+_{IS-V}
80% ≤ IS-V < 100%	A_{IS-V}
60% ≤ IS-V < 80%	B_{IS-V}
45% ≤ IS-V < 60%	C_{IS-V}
30% ≤ IS-V < 45%	D_{IS-V}
15% ≤ IS-V < 30%	E_{IS-V}
IS-V ≤ 15%	F_{IS-V}

Figure 1-48: Seismic class in relation to the safety index for life

Therefore, for the attribution of the risk class we proceed by carrying out the analysis of the structure and determining the values of ground accelerations of capacity, PGA_C (SLi), which induce to reach the limit states indicated by the standard (SLC, SLV, SLD, SLO). It is possible, in a simplified way, to carry out the checks only to the SLV (limit state for the safeguarding of life) and the SLD (damage limit state). If the PAM is evaluated by determining the points corresponding to only two limit states, to the other two limit states the following values may be assigned: $\lambda_{SLO} = 1{,}67\lambda_{SLD}$, $\lambda_{SLC} = 0{,}49\lambda_{SLV}$. Note the ground accelerations, PGAC, which produce the attainment of the mentioned limit states, determine the corresponding return periods, T_{rC}, associated with the earthquakes that generate these accelerations. In the absence of more specific assessments, the transition from PGA_C to the values of the period of return can be performed using the following relationship:

$$T_{rC} = T_{rD}\left(\frac{PGA_C}{PGA_D}\right)^{\eta}$$

η=1/0,41

For each of the periods identified above, the value of the average annual frequency of exceeding $\lambda = 1/ T_{rC}$ is determined. It is useful to underline that, for the calculation of the return time TrC associated with the attainment of the operating limit states (SLD and SLO) it is necessary to assume the lower value between that obtained for these limit states and that evaluated for the safeguard limit state of the life. It is assumed, in fact, that one cannot reach the limit state of safeguarding life without having reached the limit states of operation and damage. Damage Start Limit (SLID) is defined as the state that can be associated with a zero economic loss at a seismic event and whose return period is conventionally assumed to be 10 years, $\lambda = 0{,}1$. Reconstruction Limit State (SLR) is defined as that to which, given the general criticality that the construction presents to the point of making it almost impossible to carry out an intervention other than demolition and reconstruction, it is in any case associated with an economic loss of 100%. Conventionally it is assumed that this limit state occurs at a seismic event whose return period is equal to that of the Limit State of the Collapse (SLC).

For each of the limit states considered, it is associated with the corresponding value of λ the value of percentage of reconstruction cost according to the following Figure 1-49.

Stato Limite	CR(%)
SLR	100%
SLC	80%
SLV	50%
SLD	15%
SLO	7%
SLID	0%

Figure 1-49: Percentage of reconstruction cost (CR), associated with the achievement of each limit state

Subsequently the PAM is evaluated (in percentage value), or the area subtended to the line identified by the pairs of points (λ, CR) for each of the above indicated limit states, to which the point is added (λ=0, CR=100%) by the following expression:

$$PAM = \sum_{i=1}^{5} \lambda(SL_i) - \lambda(SL_{i-1}) * \frac{[CR(SL_i) + CR(SL_{i-1})]}{2} + \lambda(SL_C) * CR(SL_R)$$

The PAM Class is then identified, using the Figure 1-47 that associates the class with the range of values assumed by the PAM.

Once identified the class linked to the PAM, it determines the security index for the IS-V life.

The Class IS-V is identified by means of the Figure 1-48 which associates the class with the range of values assumed by the IS-V Life Safety Index, evaluated as the ratio between the PGA_C (SLV) and PGA_D (SLV).

The Construction Risk Class is the worst between the PAM Class and the IS-V Class.

Having obtained in the previous chapter the seismic vulnerability indexes for the various models, the various push cases, for the limit states SLD and SLV (ductile and fragile case) we proceed now reporting the final summary of the seismic classification for the worst load cases of each model, divided into two directions.

Table 1-25: Seismic classes obtained for the most severe load cases, for models containing brittle fracture mechanisms, based on the thrust direction

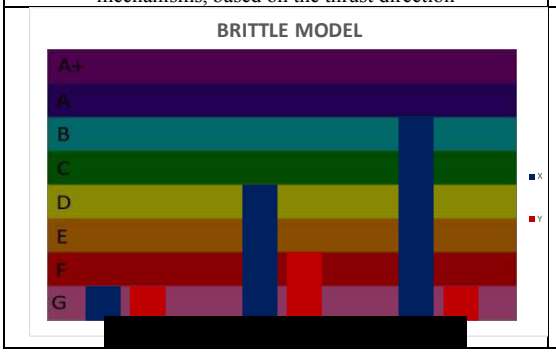

Table 1-26: Seismic classes obtained for the most severe load cases, for models without brittle fracture mechanisms, based on the thrust direction

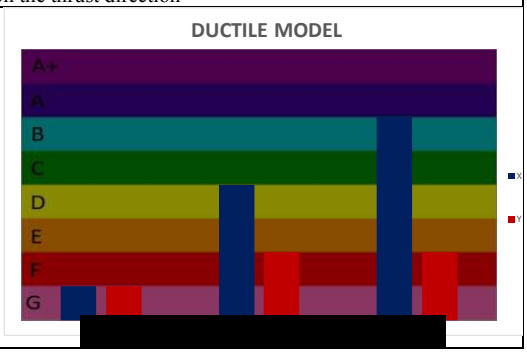

As can be seen, regarding the longitudinal stress direction "X" of the building, the increase in the seismic class as the model becomes more accurate is remarkable. In fact, most of the connecting rods are oriented in this direction and cooperate with the frame, which reaches the various limit states for greater base shear, because of the substantial increase in stiffness.

The difference instead, is less evident in the opposite stress direction, also due to the small number of infills oriented in this direction.

For what concerns the brittle model, a better seismic class is obtained for the B model compared to the C model. The motivation probably lies in the fact that the increase in stiffness of the habitable floors negatively affects the fragile mechanisms of the columns below the ground floor, reaching the condition of a soft floor more quickly.

1.10. Vulnerability Index After Retrofitting Works

For what concerns post-retrofitting, as already mentioned, the f.e. models are the same as pre-retrofitting with the addition of dissipative towers. Therefore, the geometrical and material characteristics and the degree of accuracy are the same as described in the previous chapter. Also, in this case, three models have been implemented, characterized by increasing degree of accuracy:

- Model A: frame without non-structural elements
- Model B: frame with external infill walls modelled with equivalent rods according to literature

- Model C: frame with external infill walls modelled with equivalent connecting rods and calibrated by OMA and internal infill walls modelled with equivalent connecting rods and calibrated by EMA.

1.10.1. Incremental Dynamic Analysis – I.D.A

The IDA analysis (Incremental Dynamic Analysis) arises from the need to investigate the dynamic behaviour of a structure at different levels of seismic intensity, to do this given an accelerogram, different dynamic analyzes are carried out on the same structure but with a seismic input, scaled in an increasing manner, until reaching the collapse of the structure or a predetermined level of deformation or displacement. An analysis of this type offers further advantages with respect to a single dynamic analysis: it allows to observe the evolution of the structural behaviour of the building with the growth of the seismic forcing. In particular, it is possible to understand how the structure reaches the crisis, what kind of crisis triggers, where the structural weaknesses are found, where the first plastic hinges are formed, what is the elastic behaviour and the post-yielding behaviour, how the dynamic response moving from linear to non-linear behaviour, as in the case of pushover analysis.

The IDA analysis, presented by D. Vamvatsikos and C. A. Cornell [2002], plans to subject the structure model to a series of accelerograms, each scaled with multiple levels of intensity. In this way one or more response curves parameterized with the intensity level are obtained.

From the operational point of view, it is a series of non-linear dynamic analyzes, performed with scaled accelerograms. Through this simple method of analysis, different objects can be achieved:

- Improve the understanding of the evolution of the seismic response / demand ratio at the various stress levels;
- More accurate interpretation of the structural implications of earthquakes of great intensity;
- Evaluation of changes in behaviour of buildings in terms of deformability, induced by the degradation of strength and stiffness of the structure.
- Determination of the seismic stress that causes the achievement of the different performance levels of the structure.

This type of analysis should provide the results closest to the real behaviour of the structure; but its application is conditioned by a series of critical issues connected, among other things, to: i) the selection of a set of sufficiently significant earthquakes (both in terms of number and of seismological characteristics); ii) the definition of the damping properties of the structure; iii) the schematization of the cyclic behaviour of plastic hinges, especially in relation to the definition of the degradation laws.

The following paragraphs will describe the choices made in order to obtain reliable results by solving the described criticalities.

1.10.2. Definition of the seismic action

The choice of a set of significant earthquakes was made by determining artificial spectrum-compatible accelerograms obtained as foreseen in par. 3.2.3.6 of the NTC'08. The program

used to generate accelerograms compatible with assigned response spectra is the SIMQKE-1 (SIMulation of earthQuaKE ground motions). The program automatically calculates the response spectra according to the indications of the Technical Standards for Construction (Ministerial Decree 14-1-2008) and of the Order of the President of the Council of Ministers No. 3274 (OPCM 3274). Below, in Figure 1-50, the captured images of the program are shown, they show respectively the generated spectrum-compatible acceleration and its overlap with the elastic spectrum at the SLV.

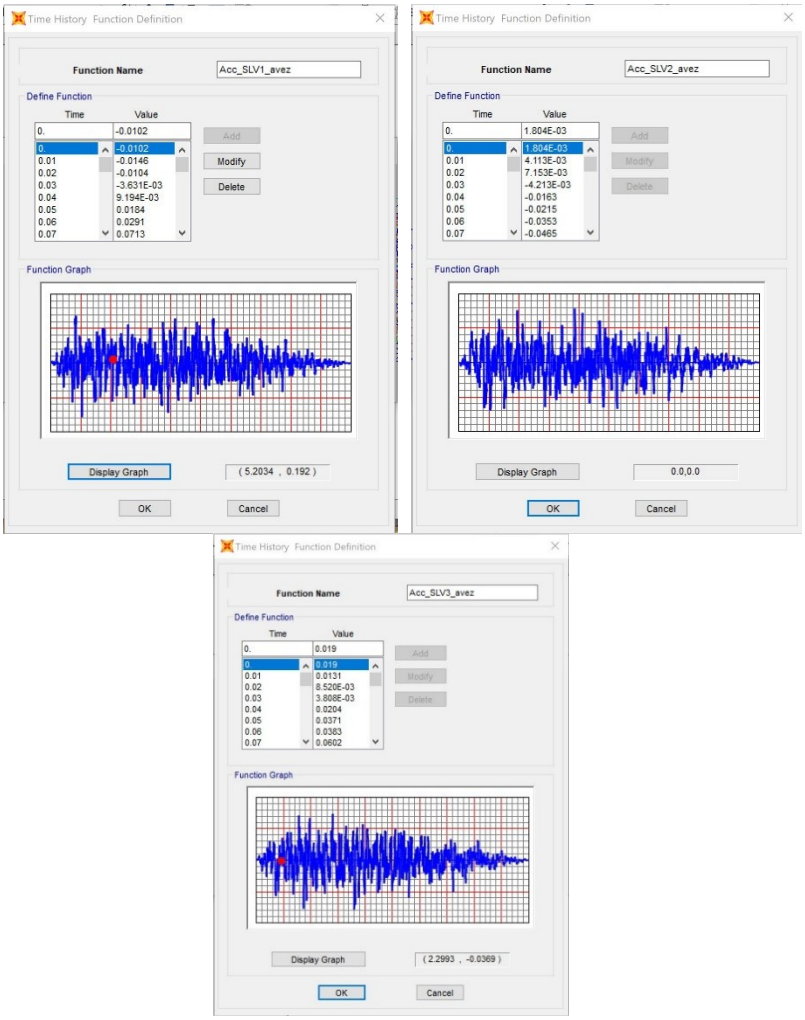

Figure 1-50: Spectro-compatible accelerograms SLV 1 - SLV 2 - SLV3

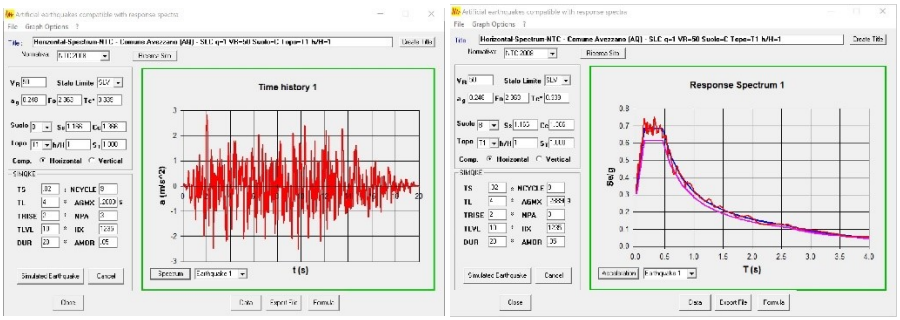

Figure 1-51: SIMQUAKE - superposition of the elastic spectrum with spectrum-compatible acceleration

In this study, due to the high computational burden, we chose to use only the SLV1 accelerogram in the analyzes, applying it in different models.

1.10.3. Modelling of viscous damping

For simplicity, the energy dissipation sources contained within the real structures can be enclosed in a single term of linear viscous damping.

The damping models proportional to mass or stiffness allow to set a modal damping coefficient based on the selection of the coefficients a0 and a1.

In order to allow greater control of modal damping along a fixed frequency range, a Rayleigh damping model is often assumed (Rayleigh, 1945). The damping matrix is expressed as the sum of a term proportional to mass and a term proportional to stiffness (both initial and tangent). Both the Rayleigh damping for initial stiffness and tangent can be defined by the following expression:

$$C = a_0 M + a_1 K_i$$

With M = mass matrix and Ki = initial elastic stiffness matrix

In this case, the modal damping coefficient must be specified for two different frequencies, based on the coefficients a_0 and a_1. Assuming that the modal damping coefficient $\xi i = \xi j = \xi$, the Rayleigh damping coefficients have been defined by Chopra (2001), as:

$$a_0 = \xi \cdot \frac{2\omega_i \omega_j}{\omega_i + \omega_j}$$

$$a_1 = \xi \cdot \frac{2}{\omega_i + \omega_j}$$

Where ω_i and ω_j are the circular frequencies to which the damping coefficient is applied.

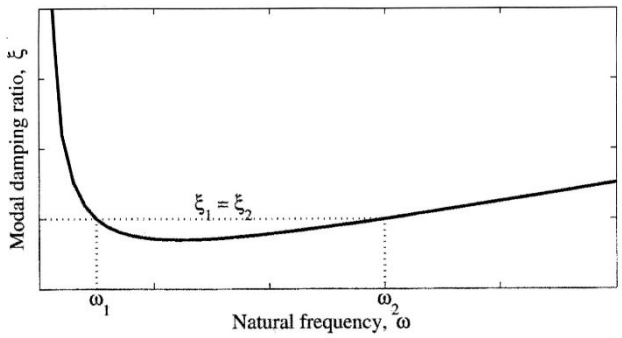

Figure 1-52: Modal damping coefficients for the Rayleigh model

In this thesis work, the values assumed to determine the viscous damping of the building in question are divided into two groups:

- I.D.A. pre retrofitting:

ω_i	ω_j	ξ	$a_{0=0,2285}$
0,2T	0,9T	0,05	$a_{1=1,042*10\text{^}-3}$

- I.D.A. post retrofitting:

ω_i	ω_j	ξ	$a_{0=0,5712}$
0,2T	0,9T	0,02	$a_{1=2,604*10\text{^}-3}$

1.10.4. Plastic Hinges and Takeda model

Takeda's hysteretic model (Takeda et al., 1970) is commonly used to represent the non-linear behavior of concrete structures, in which non-linearity is modelled using concentrated plastic hinges. The model is trilinear type and takes into account the yield, the cracking and therefore the degradation of the material.

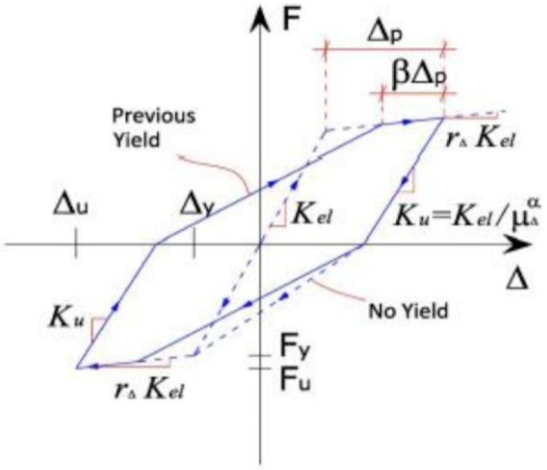

Figure 1-53: Takeda's hysteretic model

These laws are characterized by a lower discharge and reloading stiffness than the initial elastic one.

In the Takeda model the values of α are variable between 0 and 0.5; if α = 0 a drain is considered with a stiffness equal to the initial elastic. The reloading phase of the second and subsequent cycles does not lead directly to the point of maximum displacement reached in the previous cycle, but to a point distant from the latter of the quantity β Δp, along the plasticization direction with inclination $r_\Delta K_{el}$. For the beams in c.a., built with attention to detail, values considered appropriate are: α = 0.3 and β = 0.6.

In the SAP2000 v20 calculation program it is possible to select, in the characteristics of the plastic hinges, Takeda's hysteretic cycle and Figure 1-54 the scheme used by the program is shown. The definition of plastic hinges is the same as in the case of pre-retrofitting seen in the paragraph 1.9.1.

Figure 1-54: Takeda's hysteretic model in SAP2000 V.20

Also in this case, the seismic vulnerability index was calculated using the CSM (Capacity Spectrum Method) method and is presented for the three f.e. models previously described and characterized by increasing accuracy: model A, model B and model C. Compared to the pre-retrofitting case, in this case the analyzes refer to the ductile model only; without plastic shear hinges. It should be noted that the capacity curves obtained by I.D.A analysis by discretizing the input accelograms must be converted to be compared, in the ADRS plane, with the demand. At this point the capacity curve should have been bilinearized, in order to find the performance point, however the aforementioned capacity curve of the structure do not, in any case, reach the SLV, thus always maintaining itself in the elastic range. Therefore, the aforementioned bilinearization would have had no meaning and therefore the comparison between capacity and demand takes place only in graphic terms, from which it is possible to see that the capacity is always higher than the demand, for each model and for each limit state.

1.10.5. Model A: Seismic Vulnerability Index

As already mentioned, the A model, characterized by a lower level of accuracy, is composed only of structural components.

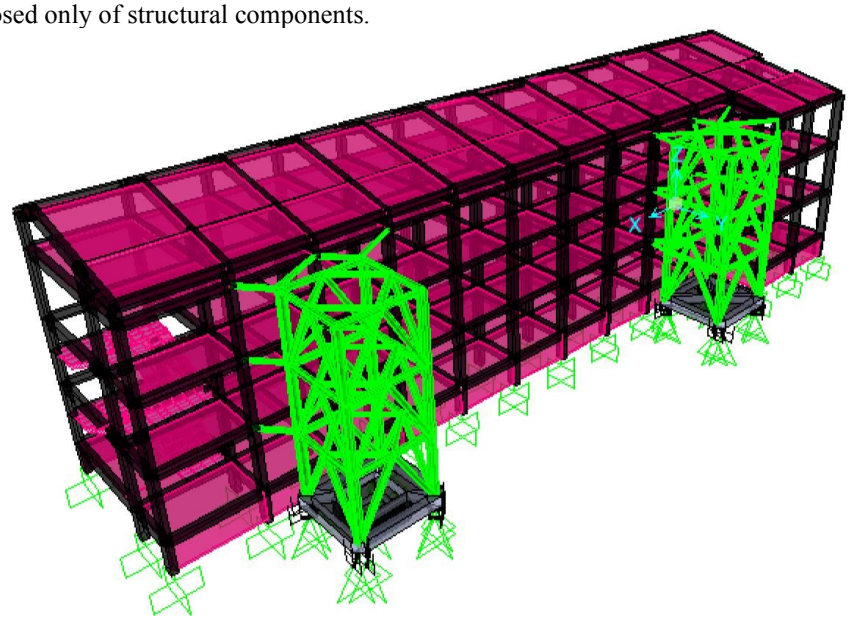

Figure 1-55: Extruded view of Model A

$$E_{conc} = 50\% E_{conc\ el}$$

The accelerogram used to determine the capacity curve is scaled in a range between 0.1 and 1.4 per step of 0.1.

The capacity curves obtained in the ADRS plane compared to the corresponding demand curves are shown from Figure 1-53 to Figure 1-56.

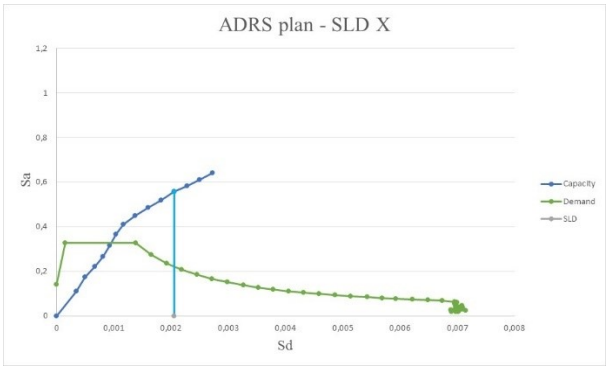

IRSLD > 1

Figure 1-56: SLD – X DIRECTION

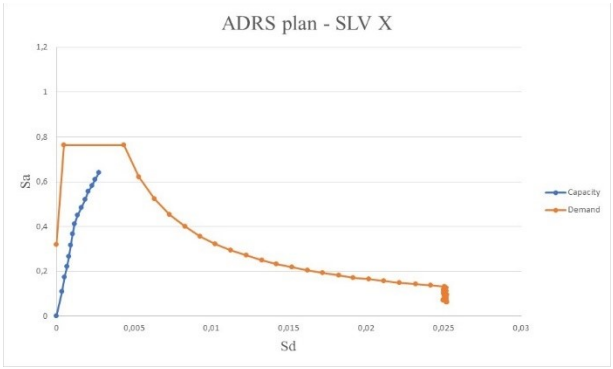

IRSLV > 1

Figure 1-57: SLV – X DIRECTION

IRSLD > 1

Figure 1-58: SLD – Y DIRECTION

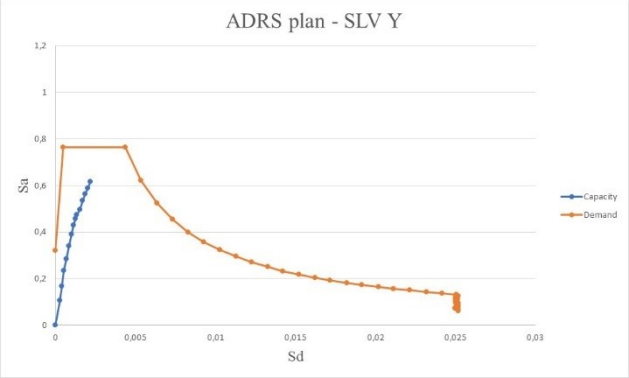

IRSLV > 1

Figure 1-59: SLV – Y DIRECTION

1.10.6. Model B: Seismic Vulnerability Index

Model B, characterized by an intermediate level of accuracy, is composed of external infill walls modelled as equivalent rods according to literature, in addition to the structural components.

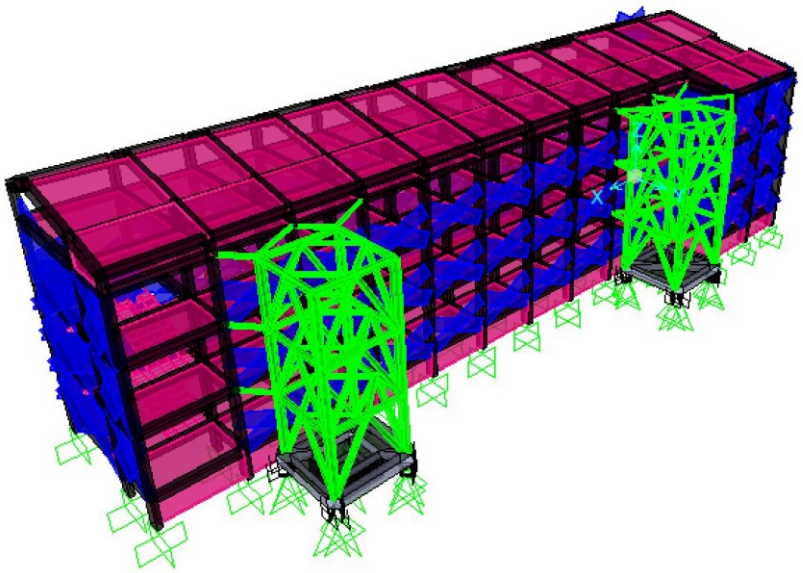

Figure 1-60: Extruded view of Model B

$$E_{conc} = 50\% E_{conc\ el}$$

The accelerogram used to determine the capacity curve is scaled in a range between 0.1 and 1.4 per step of 0.1.

The capacity curves obtained in the ADRS plane compared to the corresponding demand curves are shown from Figure 1-58 to Figure 1-61.

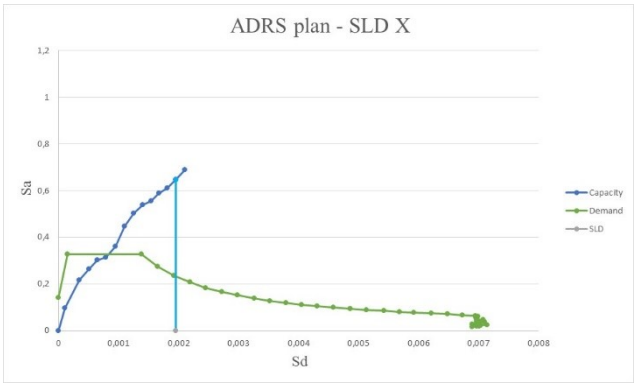

IRSLD > 1

Figure 1-61: SLD – X DIRECTION

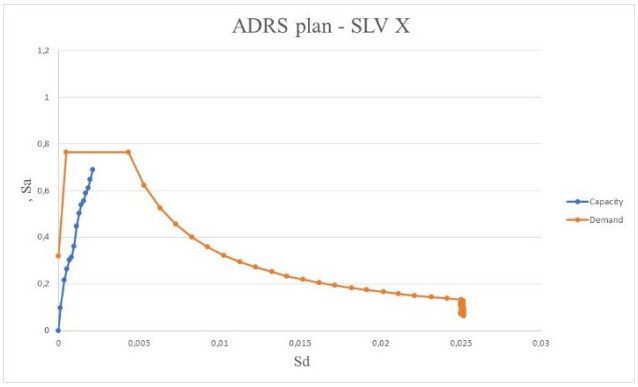

IRSLV > 1

Figure 1-62: SLV – X DIRECTION

IRSLD > 1

Figure 1-63: SLD – Y DIRECTION

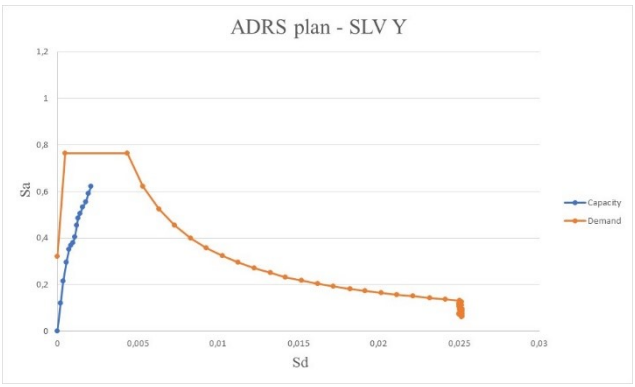

IRSLV > 1

Figure 1-64: SLV – Y DIRECTION

1.10.7. Model C: Seismic Vulnerability Index

Model C, characterized by a higher level of accuracy, is composed of external and internal infill walls, in addition to the structural components, and modelled as equivalent connecting rods and calibrated through experimental tests; the first one through OMA procedures and the second one through EMA procedures.

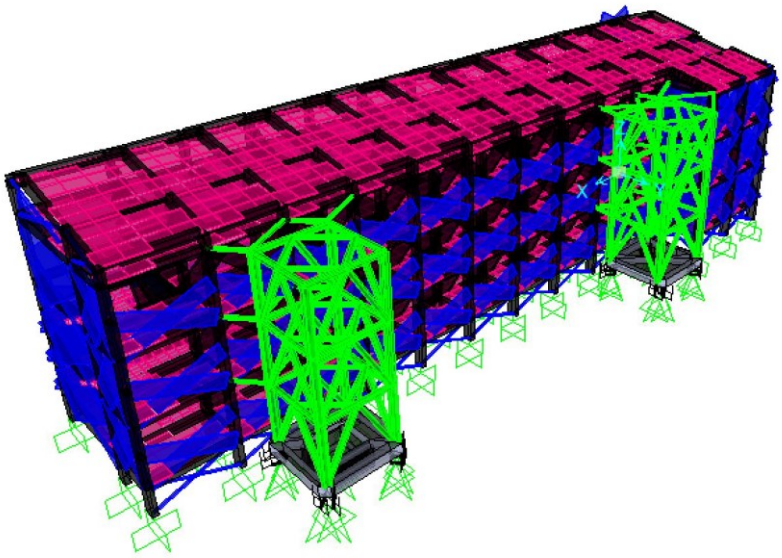

Figure 1-65: Extruded view of Model C

Obviously, the calibrated model C is different from the model C on which the I.D.A was performed. This is because a dynamic elastic modulus of concrete was used for the calibration Ed = 27500 N / mm^2 and also the accidental loads were not inserted since the OMA tests were performed with the empty building. In order to pass from this model to the one on which the pushover was made, the module of cracked concrete was adopted, and accidental loads were added.

$$E_{conc} = 50\% E_{conc\ el}$$

The accelerogram used to determine the capacity curve is scaled in a range between 0.1 and 1.4 per step of 0.1.

The capacity curves obtained in the ADRS plane compared to the corresponding demand curves are shown from Figure 1-58 to Figure 1-61.

IRSLD > 1

Figure 1-66: SLD – X DIRECTION

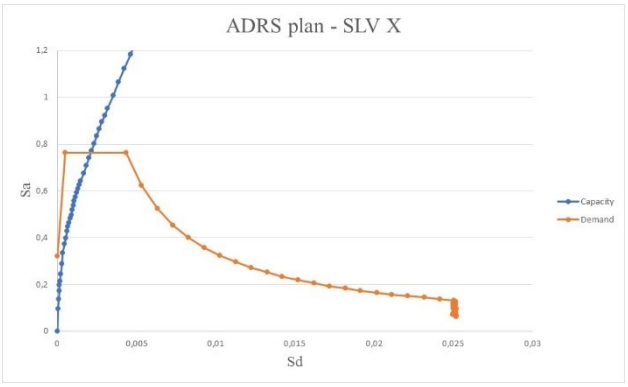

IRSLV > 1

Figure 1-67: SLV – X DIRECTION

IRSLD > 1

Figure 1-68: SLD – Y DIRECTION

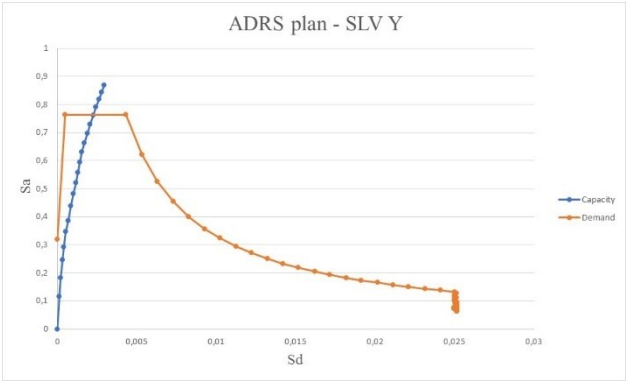

IRSLV > 1

Figure 1-69: SLV – Y DIRECTION

1.10.8. Comparisons between models

In order to evaluate the effectiveness of dissipative towers, IDA analyses were also performed on pre-retrofitting models. Below are shown, in Figure 1-67, 1-68, 1-69, the obtained capacity curves referred to each model with and without the presence of dissipative towers.

- Model A

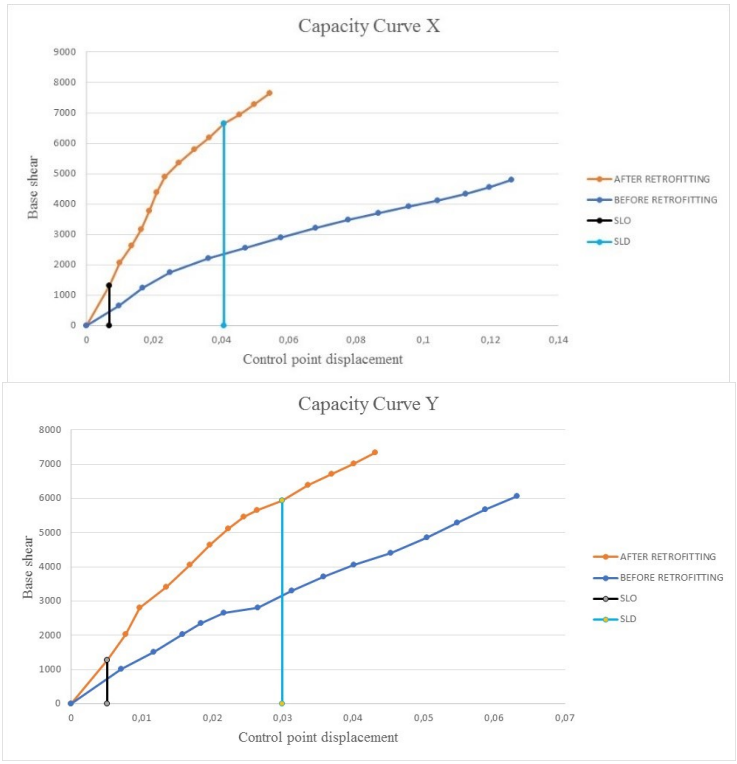

Figure 1-70: Comparison of pre and post retrofitting capacity curves for model A

- Model B

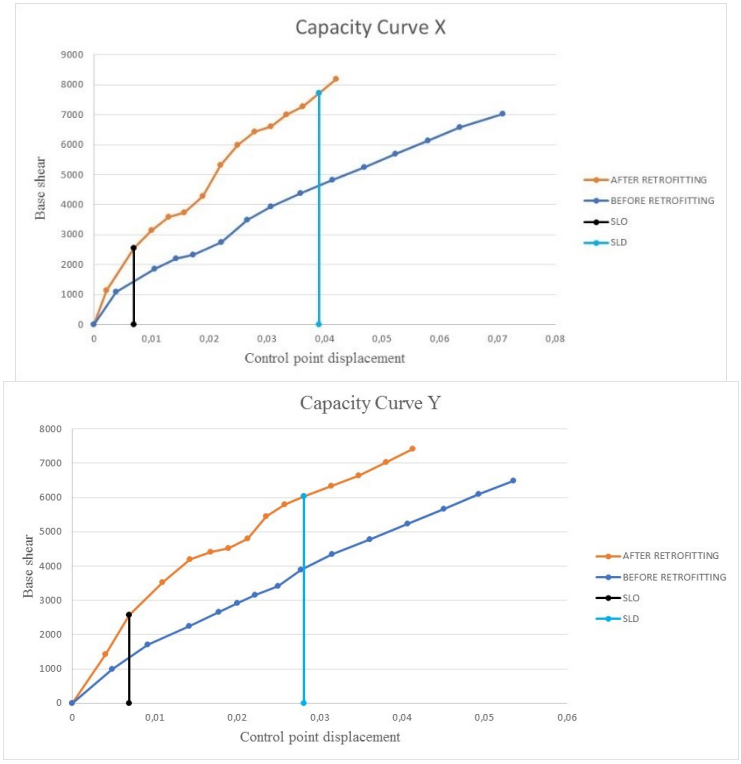

Figure 1-71: Comparison of pre and post retrofitting capacity curves for model B

- Model C

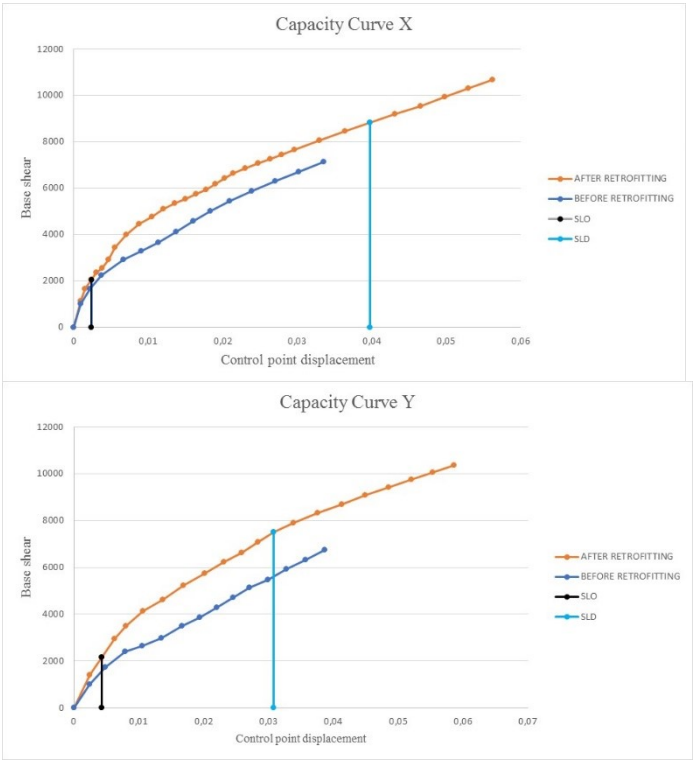

Figure 1-72: Comparison of pre and post retrofitting capacity curves for model C

These results show that after retrofitting works, an increase in the structural capacity was obtained both in terms of increase in shear base and reduction of the maximum displacements of the control point.

In addition, a comparison between different model is shown in terms of intensity level of the seismic action necessary to reach the SLD.

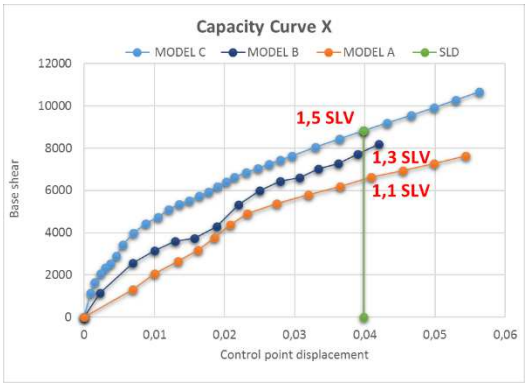

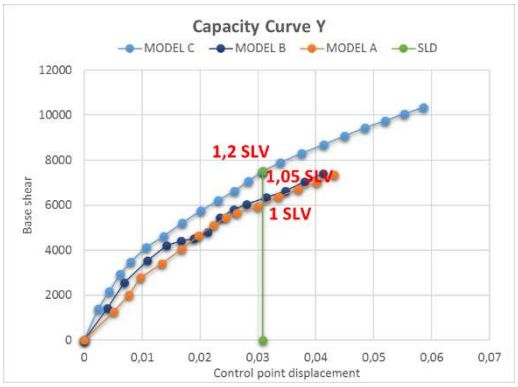

Figure 1-73: Comparison between different model in terms of intensity level of the seismic action necessary to reach the SLD – After retrofitting

Also in this case, it has been noted that the level of seismic energy necessary to reach the SLD limit displacement increases as the degree of detail of the model increases. However, less evident results were obtained in post-retrofitting, because the effectiveness of dissipative towers obscures the accuracy problem of the model.

Moreover, from the comparison between the situation before and after retrofitting it is noted that the shear on the columns does not change significatively because the predominant part of this increase is absorbed by the dissipative towers.

This difference is shown through Figure 1-74 of shear related to two columns in the pre- and post-retrofitting works, respectively.

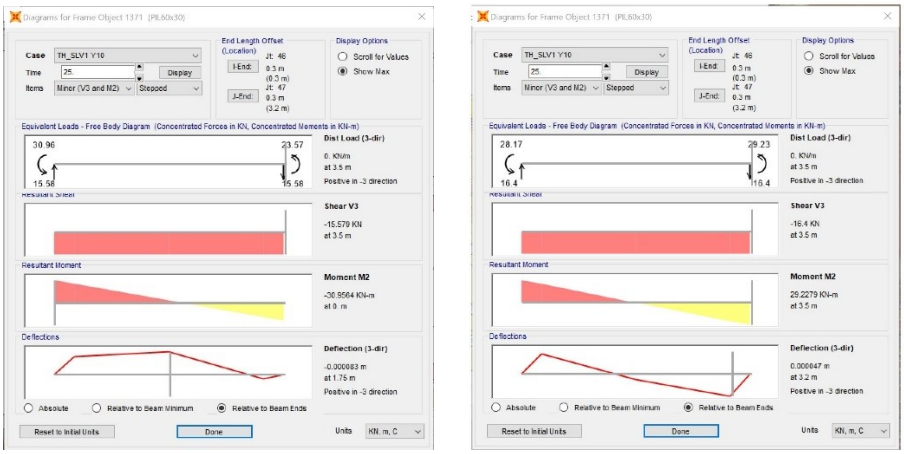

Figure 1-74: Comparison of shear on the Column pre and post-retrofitting respectively

There are also benevolent effects due to retrofitting in the plastic field. It is possible to see from the energy balances how the dissipation of energy by the structural elements has decreased.

Figure 1-75 shows the hysteresis cycles recorded on a type damper at the base of the towers in the analyses with the SLV1 accelerograms. From the hysteresis loops of the damper it is possible to deduce the amplitude of the elongations and the maximum shortening of the damper, as well as the maximum work force.

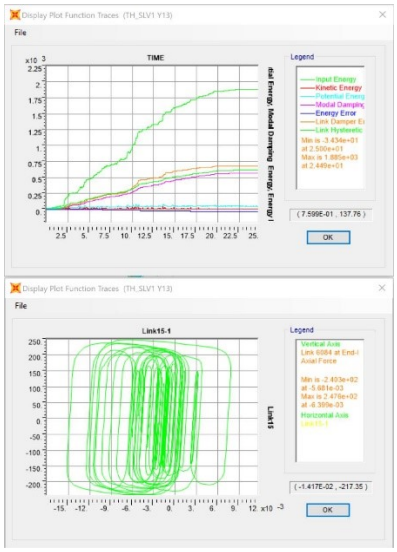

Figure 1-75: Energy balance and hysteretic cycles of damper

To further demonstrate the effectiveness of the dissipative system, the hysteretic cycles of two flexural hinges referring to the pre- and post-retrofitting situation are reported.

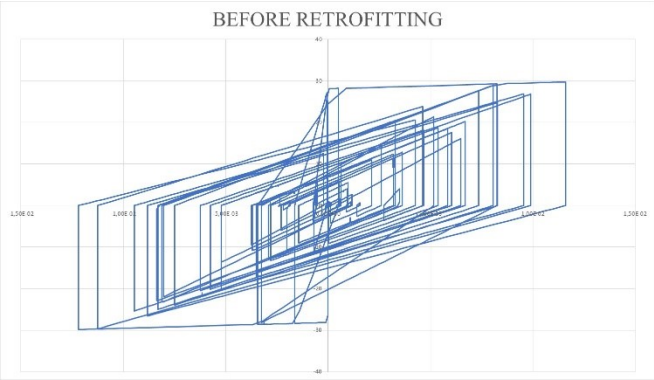

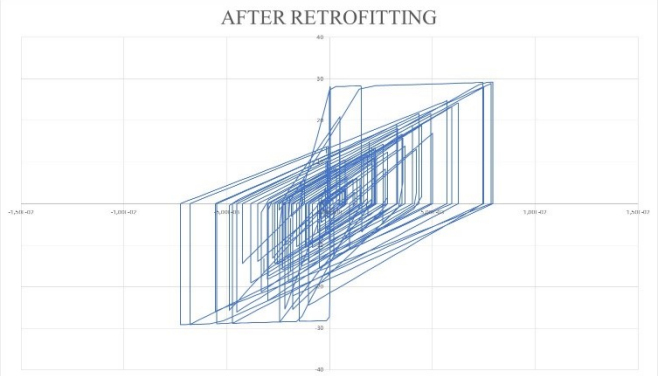

Figure 1-76: Hysteretic cycles of pre and post retrofitting flexural hinges

The graphs show that the area inside the cycle, which represents the energy dissipated, of the model without towers is greater than the area of the model cycle with towers. This proves that energy dissipation is entrusted to viscous devices and not only to structural elements.

1.10.9. Seismic classification

For the theoretical discussion of the seismic classification, see the chapter 1.9.7.

In this case the seismic vulnerability index relative to each of the limit states and to each of the tested models is greater than the unit, therefore being all the analysis situations attributable to the same result it is reported univocally.

The calculation of the PAM parameter in the post retrofitting case leads to the value of:

$$PAM = 0{,}873$$

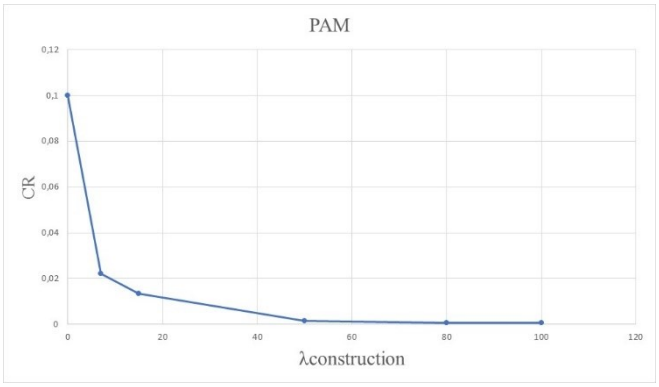

Figure 1-77: PAM

This value of the PAM parameter falls in the class A range. While the seismic vulnerability index greater than 1 falls in class A +; therefore the risk class is identified as the lower of the two.

CLASS A

1.10.10. Conclusions

Below is shown a summary table of the seismic risk classes obtained in the pre and post-retrofitting cases, for the three models implemented.

Table 1-27: Risk class for pre and post retrofitting case

	PRE-RETROFITTING	**POST-RETROFITTING**
MODEL A	CLASS G	CLASS A
MODEL B	CLASS F	CLASS A
MODEL C	CLASS F	CLASS A

As can be seen from the results obtained, the incidence of modelling is significant only in the pre retrofitting, as in the post retrofitting the improvement obtained through the inclusion of dissipative towers largely overcomes the problems related to modelling f.e.m.

Chapter 2. Case study: High School “Varano” in Camerino.

2.1 Description of the building

2.1.1 High School “Varano” in Camerino

The building is located in Camerino in Largo Feliciangeli, adjacent to the Palazzo Ducale. Figure 2-1 shows an image taken from Google Maps.

Figure 2-1: Territorial framework

The building has an in-plan L shape, formed by two wings, identified respectively as the building "A" and "B", separated from each other by a construction joint of about 2 cm constant for all buildings floor and not seismically adequate.

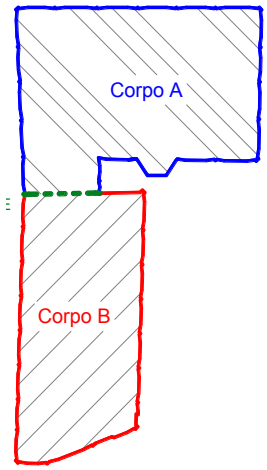

Figure 2-2: In-Plan view of the Institute with indication of the buildings

There is also a further construction joint, not seismically adequate, which divides the A wing into two parts. In total, therefore, there are three statically independent building: A1, A2 and B. It should be noted that the second joint was highlighted by the earthquake of 30 October 2017, so it was not known during the interventions carried out on the structure recently therefore the modelling has been carried out without taking into account this second joint.

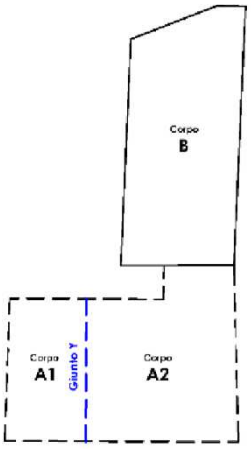

Figure 2-3: Basement floor plan -2

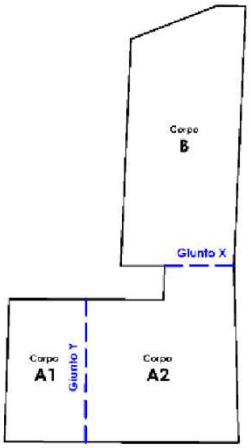

Figure 2-4: Basement floor plan -1

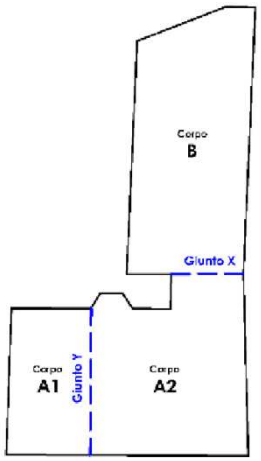

Figure 2-5: Ground floor plan

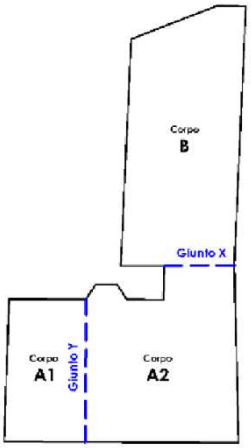

Figure 2-6: First floor plan

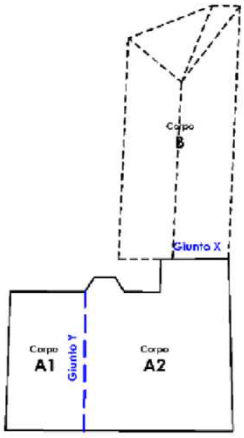

Figure 2-7: Second floor plan

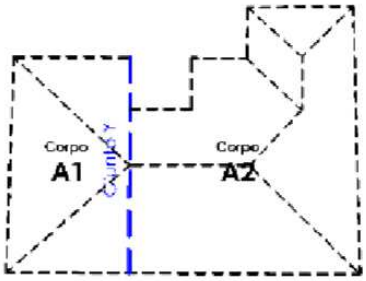

Figure 2-8: Attic floor plan

The in-plane dimensions are: wing A 25x19 m and wing B 13x27 m. Wing A has four floors, one above ground plus the attic for a total of 20.40 m height; while wing B is entirely headed on the massive historical walls of the former convent by means of foundation plinths, and extends above ground by three floors plus the attic for a total of 14.05 m height. Overall, the structure is based on a sandstone rock base. Wing A has a constant inter-floor of 3.80 m height on the intermediate floors, 3.60 m height on the top floor and much more in the basement with the North-West side of 6.00 m height and the opposite part of 4,80 m height; wing B coplanar to the intermediate floors of wing A has a constant inter-floor of 3.80 m height.

The building is reinforced concrete structure and is composed of columns which, for strictly architectural reasons, have rhomboidal shape, in particular, square shape rotated of 45° with respect to the frame direction, with a constant 35x35 cm section for all the elevations; only exceptions are two central columns of wing A which have dimensions of 42x42 cm. There are all emerging beams and in particular the perimeter beams have variable section both in height and thickness, so as to form a polyhedral surface. The particular geometry of the main structural elements makes the building classifiable as shear type, meaning that beams are much stiffer than columns: this leads to a greater vulnerability of the columns under seismic actions. Furthermore, the fact that the columns are rotated with respect to the axis of the beams leads to a non-optimal behavior due to the compound bending stress. The reinforced concrete and hollow tiles mixed floor with a thickness of 20 + 4 cm can be considered rigid for the purpose of transferring seismic loads. The perimeter infill walls of the building consist of a masonry of 1.20 m height. Difference can be seen in the basement of wing A where the infill walls consist of a vaulted ceiling in solid brick and stone of 40 cm thick. The internal partitions are constituted by perforated brick, or, as result of subsequent adjustments, in plasterboard. The large windows significantly reduce the interference with the structure.

Figure 2-9: View of building A with the geometry of beams and columns highlighted

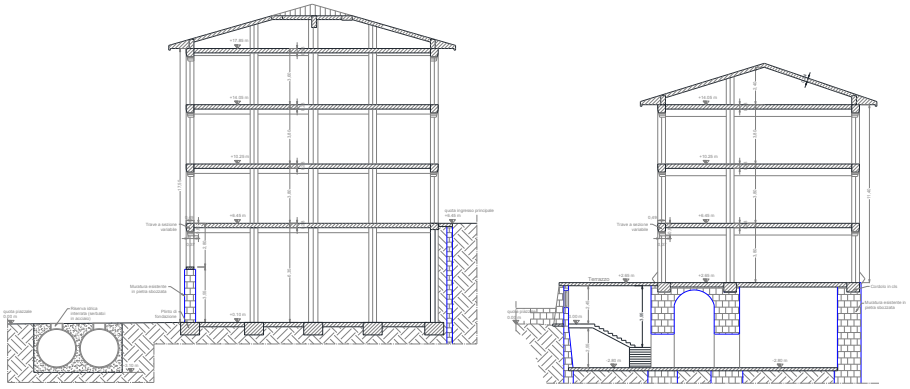

Figure 2-10: Cross section and longitudinal section of the building

Figure 2-11: View of the building resting on the historic walls of the convent

2.1.2 Retrofitting Project

The intervention realizes to reduce the seismic vulnerability of the structure and reach the safety levels required for the complete retrofitting, consists in making the building a whole, sewing the joint between the two buildings with anchors in correspondence of the floors. The joints are sewn together with the triangular columns placed side by side using metal plates,

fixed with chemical anchors. In addition, two dissipative towers connected to the building at floor level have been included, called tower A and tower B, respectively. The towers are connected to the building by means of suitable rigid steel pendulums.

The tower A structure is constituted by HEB 340 profiles for the uprights, by HEB 240 for the diagonals and crosspieces, with the exception of that of the last floor which is a HEB 200, while the bracings of the floor are HEB 160 The base is made up of a r.c. slab of 5.40 m x 5.40 m with 50 cm thick. Below the base is the area dedicated to dissipation with n. 8 dissipative systems equipped with devices type FIP “OTP30 / 110” and a central support with a spherical hinge type FIP “SF 100-180” which rests on a base in r.c. of 75x75 cm and 86.5 cm height.

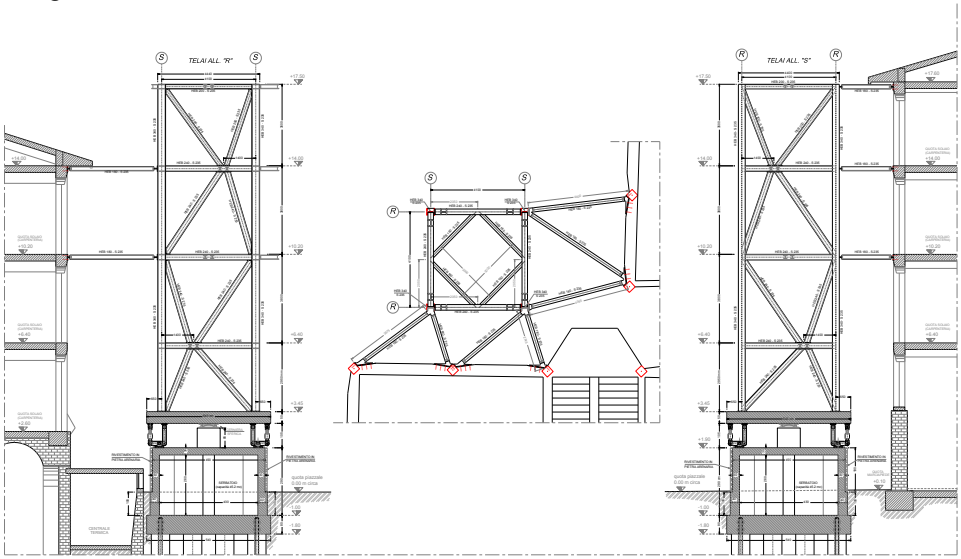

Figure 2-12: Elevations and carpentry of tower A

The tower B structure is constituted by HEB 300 profiles for the uprights, by HEB 200 for the diagonals and crosspieces, while the bracings of the floor are HEB 160. The base consists of an r.c. slab of 4.30 m x 4.30 m and 40 cm thick. Below the base is the area dedicated to dissipation with n. 4 dissipative systems equipped with devices type FIP “OTP30 / 110” and a central support with a spherical hinge type FIP “SF 60-90”, which in turn rests on a base in r.c.. 70x70 cm and 90 cm height.

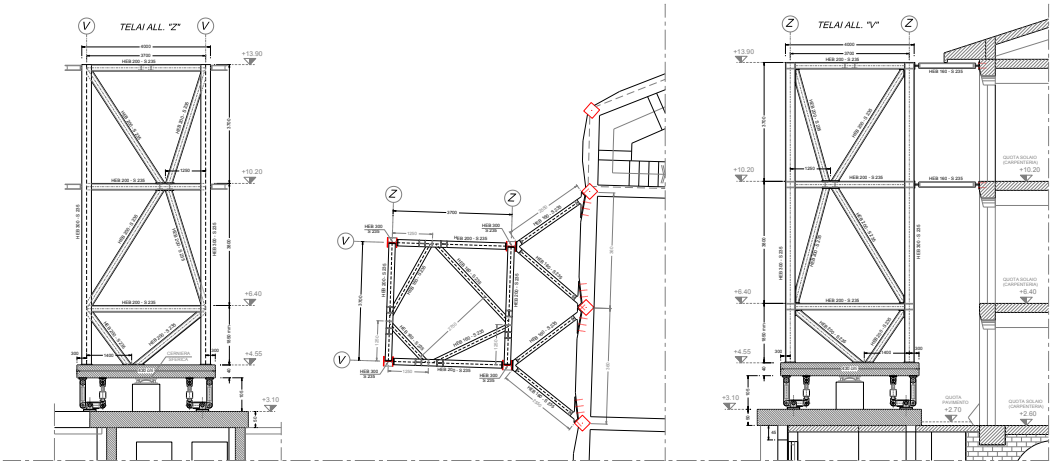

Figure 2-13: Elevations and carpentry of a standard plan of tower B

The in-plane towers position is useful to avoid the manifestation of possible torsional couplings and, consequently, to regularize the dynamic behaviour of the building. Moreover, this choice makes the intervention not very invasive from the point of view of the visual impact with the context (historical city center).

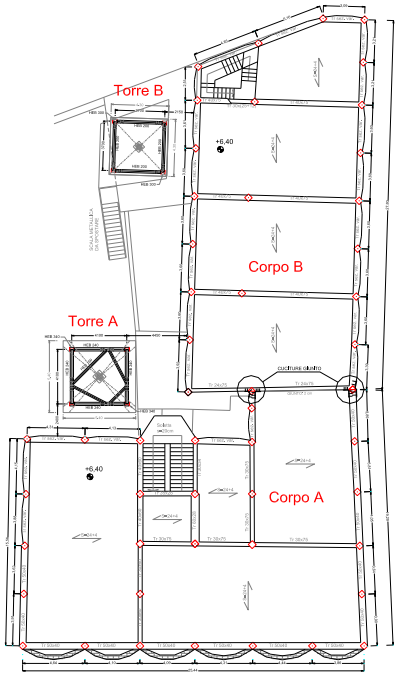

Figure 2-14: In-plane view of Retrofitting project, +6.40 m

The foundations of the base of the towers are constituted by piles and micropiles. Since the towers are positioned outside the building, the foundations of the basements do not interfere with those of the existing building.

2.2 Investigation Campaign

The concrete compressive strength was evaluated by means of n. 22 concrete specimens, taken both from the beams and from the columns, located on the various floors of the building, that provided an average cubic resistance value of: 19,76 N/mmq.

The investigation campaign detected the presence of a technical construction joint not seismically adequate, which separates the two buildings.

Figure 2-15: Construction joint

2.3 Report on Materials

2.3.1 Material Properties of the Existing Building

The mechanical characteristics of materials belonging to the existing buildings are deduced from the results of the investigations.

Concrete

$$R_{ck} = \mathbf{19,76\ N/mm^2}$$

$$f_{ck} = 0{,}83 R_{ck} = \mathbf{16,40\ N/mm^2}$$

$$f_{cd} = \frac{f_{ck}}{1{,}5} = \mathbf{10,93\ N/mm^2}$$

$$E = 22000 \left(\frac{f_{ck}}{10}\right)^{0,3} = \mathbf{25.520\ N/mm^2}$$

Reinforcement bars

For the elevation structures, smooth bars of homogeneous steel were used, similar to an Aq 50 steel.

$$f_{yk} = 375\ N/mm^2$$

$$f_{yd} = \frac{f_{yk}}{1{,}15} = 326{,}087\ \mathbf{N/mm^2}$$

$$E = \mathbf{210.000\ N/mm^2}$$

2.3.2 Materials for the dissipative towers

Concrete for foundations: piles and slabs

It was used a cement conglomerate packaged according to the following modes:
- Cement type 425 350 kg / mc;
- Gravel 0.8 mc / mc;
- Sand 0.4 mc / mc;
- Water 120 lt / mc.

Use of hydraulic binders such as cements defined by applicable regulations.

Natural or crushing aggregates, consisting of non-freezing elements, not friable and free of silty or clay organic substances, gypsum etc., in proportions harmful to the hardening of the conglomerate and to the preservation of the metal reinforcements. Gravel or crushed stone of maximum dimensions correlated to the characteristics of the carpentry of the jet and to the encumbrance of the metallic reinforcements.

Clear water and salt-free in harmful percentage.

The granulometric distribution of the aggregates, the type of cement and the consistency of the mixture will be adequate for the purpose.

Mechanical characteristics:
For r.c. foundation, a concrete class of "C 25/30" (Rck = 30 N / mm2) was used.
General characteristics:

$$E = \mathbf{31.447\ N/mm^2}$$

$$f_{ck} = 0{,}83R_{ck} = \mathbf{24{,}9\ N/mm^2}$$

Ultimate Limit State:

$$\gamma_c = \mathbf{1{,}5}$$

$$f_{cd} = \frac{f_{ck}}{1{,}5} = \mathbf{16{,}60\ N/mm^2}$$

Concrete structures in elevation: towers bases

It was used of a cement conglomerate packaged according to the following modes:
- Cement type 425 350 kg / mc;
- Gravel 0.8 mc / mc;
- Sand 0.4 mc / mc;
- Water 120 lt / mc.

Use of hydraulic binders such as cements defined by applicable regulations.

Natural or crushing aggregates, consisting of non-freezing elements, not friable and free of silty or clay organic substances, gypsum etc., in proportions harmful to the hardening of the conglomerate and to the preservation of the metal reinforcements.

Gravel or crushed stone of maximum dimensions correlated to the characteristics of the carpentry of the jet and to the encumbrance of the metallic reinforcements.

Clear water and salt-free in harmful percentage.

The granulometric distribution of the aggregates, the type of cement and the consistency of the mixture adequate for the purpose.

Reinforcement

Improved adhesion bars of the B450C type were used.
Mechanical Characteristics:

$$f_{tk} = \mathbf{540\ N/mm^2}$$

$$f_{yk} = \mathbf{450\ N/mm^2}$$

$$Minimum\ elongation\ at\ break = \mathbf{7{,}5}\%$$

$$Minimum\ ratio\ \frac{f_t}{f_y} = \mathbf{1{,}15}$$

$$Maximum\ ratio\ \frac{f_t}{f_y} = \mathbf{1{,}35}$$

$$E = \mathbf{210.000\ N/mm^2}$$

Ultimate Limit State:

$$\gamma_c = \mathbf{1,15}$$

$$f_{yd} = \frac{f_{yk}}{1{,}15} = 391{,}3\ \mathbf{N/mm^2}$$

Steel for construction

The steel structures of the towers are in steel type "S 235" (UNI EN 10025-2) with the following characteristics:

$$f_{tk} \geq \mathbf{360\ N/mm^2}$$

$$f_{yk} \geq \mathbf{235\ N/mm^2}$$

The bolted connections realized with high strength bolts having the following characteristics:

- Screw class 8.8 (UNI EN ISO 898-1: 2001)
- $f_{tb} \geq \mathbf{800\ N/mm^2}$
- $f_{yb} \geq \mathbf{649\ N/mm^2}$
- nut Class 8 (UNI EN 20898-2: 1994)
- rosettes C50 (UNI EN 10083-2: 2006)

Steel for connections, mechanical components and devices

Structures in metallic carpentry such as connections, mechanical components and devices, intended as viscous heat sinks and spherical bearings, are made of steel type "S 355 H" (UNI EN 10025-2) having the following characteristics:

$$t \leq 40\ mm \rightarrow f_{th} \geq \mathbf{510\ N/mm^2}$$

$$40\ mm \leq t \leq 80\ mm \rightarrow f_{th} \geq \mathbf{470\ N/mm^2}$$

$$t \leq 40\ mm \rightarrow f_{yh} \geq \mathbf{355\ N/mm^2}$$

$$40\ mm \leq t \leq 80\ mm \rightarrow f_{yh} \geq \mathbf{355\ N/mm^2}$$

The bolted connections realized with high strength bolts having the following characteristics:

- Screw class 8.8 (UNI EN ISO 898-1: 2001)
- $f_{tb} \geq \mathbf{800\ N/mm^2}$
- $f_{yb} \geq \mathbf{649\ N/mm^2}$
- nut Class 8 (UNI EN 20898-2: 1994)
- rosettes C50 (UNI EN 10083-2: 2006)

The bars used for the anchors are B7 reference standard ASTM A 193 special steel having the following characteristics:

$$\phi \leq 65\ mm \ \rightarrow f_{th} \geq \mathbf{860\ N/mm^2}$$

$$\phi \leq 65\ mm \ \rightarrow f_{yh} \geq \mathbf{720\ N/mm^2}$$

2.3.3 External and Internal Infill Walls

For what concerns wing A, the external and internal infill walls have a thickness of 40 cm, 20 cm and 12 cm respectively. The walls against the ground, the external infill walls and the internal infill walls of the wing B are represented in their real position, while the internal infill walls of the wing A are grouped according to the principal guidelines identified by the r.c. frames. The walls in ancient masonry of wing B are modelled with shell-thin elements of variable thickness between 0.50 m, 1.4 m and 1.8 m. As regards the mechanical characteristics (respectively compressive strength, shear strength, normal elasticity modulus, tangential elasticity modulus) of the external infill walls, reference is made to the average values indicated in table C8A.2.1 of the following rule.

Tipologia di muratura	f_m [daN/cm^2] min - max	τ_0 [daN/cm^2] min - max	E [daN/cm^2] min - max	G [daN/cm^2] min - max	w [daN/m^3]
Muratura in pietrame disordinata (ciottoli, pietre erratiche e irregolari)	10.0 18.0	0.20 0.32	6900 10500	2300 3500	1900
Muratura a conci sbozzati, con paramento di limitato spessore e nucleo interno	20.0 30.0	0.35 0.51	10200 14400	3400 4800	2000
Muratura in pietre a spacco con buona tessitura	26.0 38.0	0.56 0.74	15000 19800	5000 6600	2100
Muratura a conci di pietra tenera (tufo, calcarenite, ecc.)	14.0 24.0	0.28 0.42	9000 12600	3000 4200	1600
Muratura a blocchi lapidei squadrati	60.0 80.0	0.90 1.20	24000 32000	7800 9400	2200
Muratura in mattoni pieni e malta di calce	24.0 40.0	0.60 0.92	12000 18000	4000 6000	1800
Muratura in mattoni semipieni con malta cementizia (es.: doppio UNI foratura < 40%)	50.0 80.0	2.40 3.20	35000 56000	8750 14000	1500
Muratura in blocchi laterizi semipieni (perc. foratura < 45%)	40.0 60.0	3.00 4.00	36000 54000	10800 16200	1200
Muratura in blocchi laterizi semipieni, con giunti verticali a secco (perc. foratura < 45%)	30.0 40.0	1.80 1.30	27000 36000	8100 10800	1100
Muratura in blocchi di calcestruzzo o argilla espansa (perc. foratura tra 45% e 65%)	15.0 20.0	0.95 1.25	12000 16000	3000 4000	1200
Muratura in blocchi di calcestruzzo semipieni (foratura < 45%)	30.0 44.0	1.80 2.40	24000 35200	6000 8800	1400

Tabella C8A.2.1 della Circolare 617/2009)

Figure 2-16: Table C8A.2.1

2.4 Loads Definition

Permanent actions are distinguished (G1 = own weights of structures, G2 = non-structural permanent) from variable actions (characteristic values Q).

Structural elements in c.a .: G1 = 25 KN / m3

2.4.1 Permanent actions

TYPE 1 LOAD: standard floor slab.	
G1	3.2 (kN / m²)
G2	1.8 (kN / m²)
TYPE 2 LOAD: attic floor.	
G1	3.2 (kN / m²)
G2	0.6 (kN / m²)
TYPE 3 LOAD: roof slab.	
G1	2.8 (kN / m²)
G2	0.6 (kN / m²)
TYPE 4 LOAD: staircase.	
G2	1.2 (kN / m²)

2.4.2 Variable actions - characteristic values

For stairs and balconies, an operating overload is assumed equal to:

$$Q = 4 \text{ KN / m}^2$$

For floors of the standard floor an operating overload is assumed equal to:

$$Q = 3 \text{ KN / m2}$$

For the attic floor, an operating overload is assumed equal to:

$$Q = 0.5 \text{ KN / m2}$$

since it is not practicable.

Snow
For coverings with a height of 661 m above sea level (common altitude of Camerino), the operating overload due to snow is assumed:

$$Q = 1.96 \text{ KN} / \text{m}^2$$

2.5 Seismic Action

Nominal Life:

$$V_N = 50 \text{ years}$$

Class III is assumed for use class (Construction whose use includes significant crowding ...);

$$C_U = 1.5$$

By obtaining a reference period for the seismic action equal to:

$$V_R = V_N \cdot C_U = 75 \text{ years}$$

With regard to the subsoil category, reference is made to what is reported in the geological report, where soil's category is C.
The topographical condition of the site is T1 (Flat surface, isolated slopes and reliefs with average inclination i≤15 °).
It is therefore possible to define the elastic response spectra for the different limit states considered, depending on the characteristics of the site, from the earthquake return period T_R, from the reference period V_R, and from the probability of exceeding the limit state considered PVR.
The elastic response spectra of reference, relative to the geographical coordinates of the site and defined on subsoil category A and topographical condition T1, according to the probability of exceeding the reference period in each of the 4 limit states provided for by the NTC are shown in the diagram following.

SLATO LIMITE	T_R [anni]	a_g [g]	F_o [-]	T_C^* [s]
SLO	45	0,078	2,440	0,285
SLD	75	0,097	2,433	0,295
SLV	712	0,220	2,544	0,333
SLC	1462	0,277	2,584	0,343

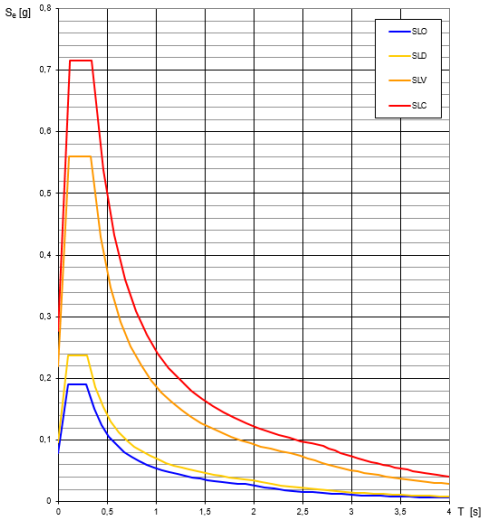

Figure 2-17: Elastic spectrum

The design spectra defined by the NTCs for the SLO, SLD, SLV, SLC for the conditions of the site in question (subsoil category C and topographic surface T1) are reported.

SLO spectrum

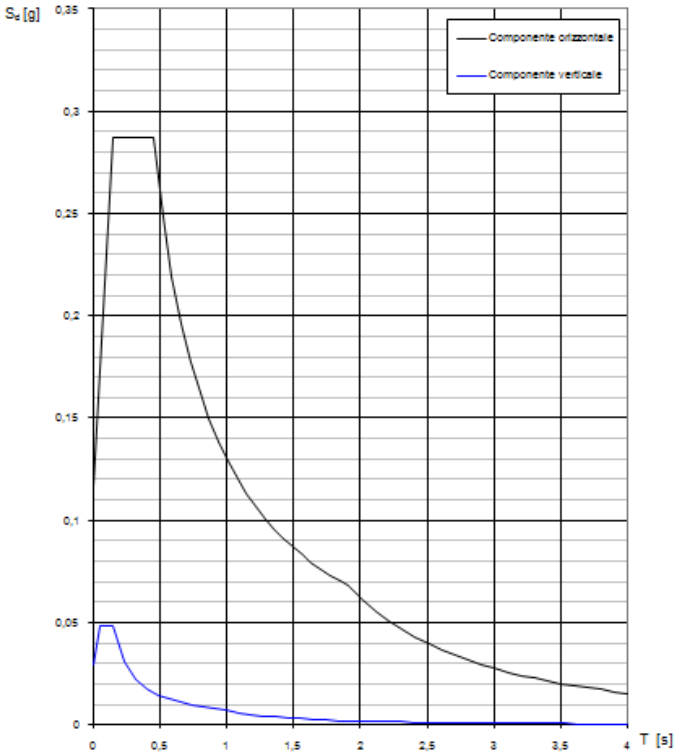

Parametri indipendenti

STATO LIMITE	SLO
a_g	0,078 g
F_o	2,440
T_C^*	0,285 s
S_S	1,500
C_C	1,589
S_T	1,000
q	1,000

Parametri dipendenti

S	1,500
η	1,000
T_B	0,151 s
T_C	0,453 s
T_D	1,913 s

	T[s]	*Se[g]*
	0,000	0,118
T_B	0,151	0,287
T_C	0,453	0,287
	0,522	0,249
	0,592	0,219
	0,662	0,196
	0,731	0,178
	0,801	0,162
	0,870	0,149
	0,940	0,138
	1,009	0,129
	1,079	0,120
	1,148	0,113
	1,218	0,107

	T[s]	*Se[g]*
	1,288	0,101
	1,357	0,096
	1,427	0,091
	1,496	0,087
	1,566	0,083
	1,635	0,079
	1,705	0,076
	1,774	0,073
	1,844	0,070
T_D	1,913	0,068
	2,013	0,061
	2,112	0,056
	2,212	0,051
	2,311	0,047

T[s]	*Se[g]*
2,410	0,043
2,510	0,039
2,609	0,037
2,708	0,034
2,808	0,032
2,907	0,029
3,006	0,027
3,106	0,026
3,205	0,024
3,304	0,023
3,404	0,021
3,503	0,020
3,603	0,019
3,702	0,018

T[s]	*Se[g]*
3,801	0,017
3,901	0,016
4,000	0,016

SLD spectrum

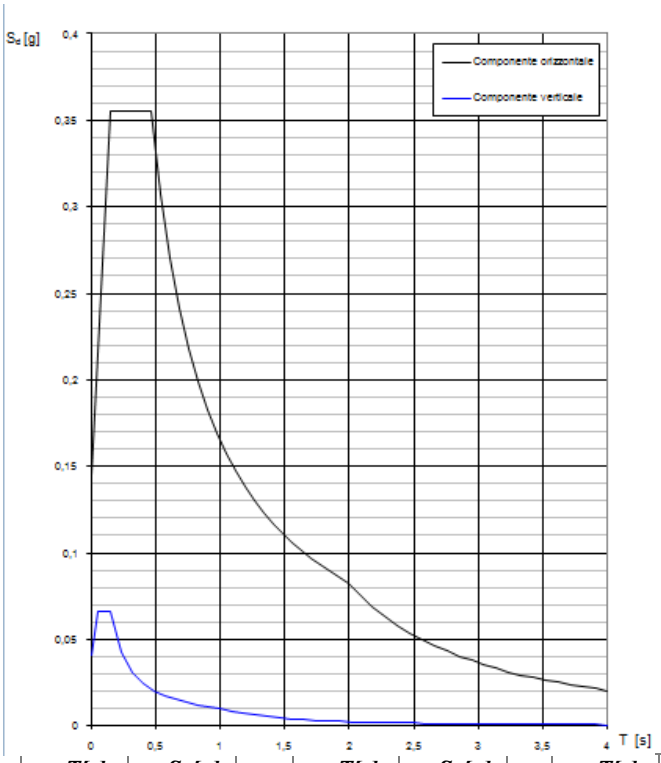

Parametri indipendenti

STATO LIMITE	SLD
a_g	0,097 g
F_o	2,433
T_C^*	0,295 s
S_S	1,500
C_C	1,571
S_T	1,000
q	1,000

Parametri dipendenti

S	1,500
η	1,000
T_B	0,154 s
T_C	0,463 s
T_D	1,989 s

	T[s]	*Se[g]*		*T[s]*	*Se[g]*		*T[s]*	*Se[g]*	*T[s]*	*Se[g]*
	0,000	0,146		1,335	0,123		2,468	0,054	3,809	0,023
T_B	0,154	0,355		1,408	0,117		2,564	0,050	3,904	0,021
T_C	0,463	0,355		1,481	0,111		2,660	0,046	4,000	0,020
	0,536	0,307		1,553	0,106		2,755	0,043		
	0,609	0,271		1,626	0,101		2,851	0,040		
	0,681	0,242		1,699	0,097		2,947	0,038		
	0,754	0,218		1,771	0,093		3,043	0,035		
	0,827	0,199		1,844	0,089		3,138	0,033		
	0,899	0,183		1,917	0,086		3,234	0,031		
	0,972	0,169	T_D	1,989	0,083		3,330	0,030		
	1,045	0,158		2,085	0,075		3,426	0,028		
	1,117	0,147		2,181	0,069		3,521	0,026		
	1,190	0,138		2,277	0,063		3,617	0,025		
	1,263	0,130		2,372	0,058		3,713	0,024		

SLV spectrum

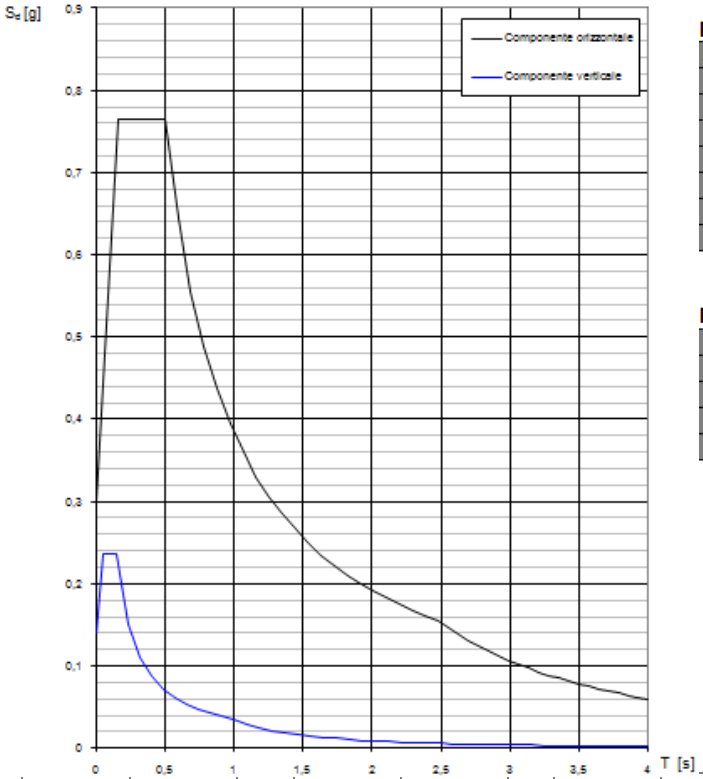

Parametri indipendenti

STATO LIMITE	SLV
a_g	0,220 g
F_o	2,544
T_C^*	0,333 s
S_S	1,364
C_C	1,510
S_T	1,000
q	1,000

Parametri dipendenti

S	1,364
η	1,000
T_B	0,167 s
T_C	0,502 s
T_D	2,482 s

	T[s]	*Se[g]*		*T[s]*	*Se[g]*		*T[s]*	*Se[g]*		*T[s]*	*Se[g]*
	0,000	0,301		1,633	0,235		2,843	0,118		3,855	0,064
T_B	0,167	0,765		1,728	0,222		2,916	0,112		3,928	0,062
T_C	0,502	0,765		1,822	0,211		2,988	0,107		4,000	0,060
	0,597	0,644		1,916	0,200		3,060	0,102			
	0,691	0,556		2,010	0,191		3,132	0,097			
	0,785	0,489		2,105	0,182		3,205	0,093			
	0,879	0,437		2,199	0,175		3,277	0,089			
	0,974	0,394		2,293	0,167		3,349	0,085			
	1,068	0,360		2,388	0,161		3,422	0,081			
	1,162	0,330	T_D	2,482	0,155		3,494	0,078			
	1,256	0,306		2,554	0,146		3,566	0,075			
	1,351	0,284		2,626	0,138		3,639	0,072			
	1,445	0,266		2,699	0,131		3,711	0,069			
	1,539	0,250		2,771	0,124		3,783	0,067			

SLC spectrum

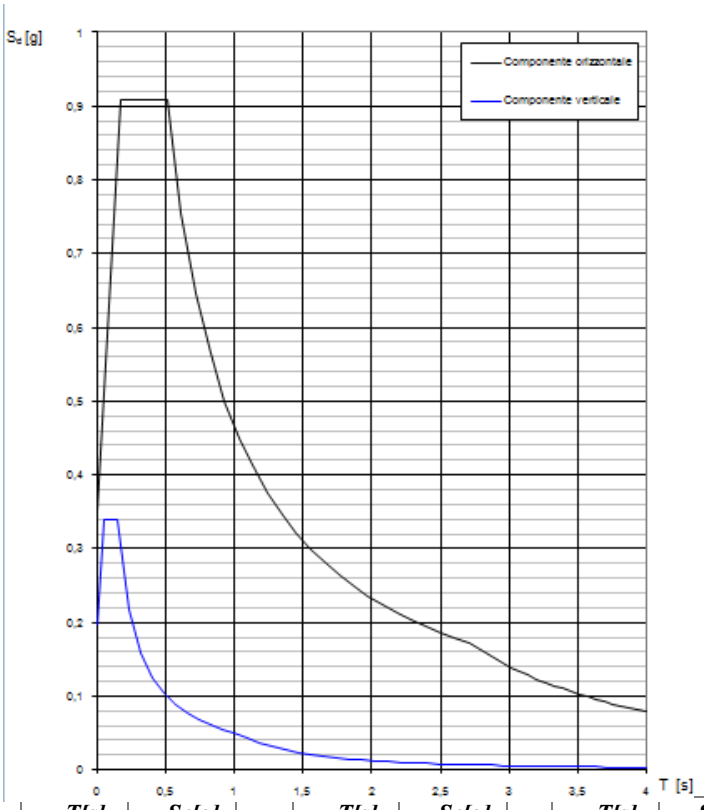

Parametri indipendenti

STATO LIMITE	SLC
a_g	0,277 g
F_o	2,584
T_C^*	0,343 s
S_S	1,271
C_C	1,495
S_T	1,000
q	1,000

Parametri dipendenti

S	1,271
η	1,000
T_B	0,171 s
T_C	0,513 s
T_D	2,707 s

	T[s]	*Se[g]*		*T[s]*	*Se[g]*		*T[s]*	*Se[g]*	*T[s]*	*Se[g]*
	0,000	0,352		1,767	0,264		3,015	0,139	3,877	0,084
T_B	0,171	0,909		1,871	0,249		3,077	0,133	3,938	0,081
T_C	0,513	0,909		1,976	0,236		3,138	0,128	4,000	0,079
	0,617	0,755		2,080	0,224		3,200	0,123		
	0,722	0,646		2,185	0,213		3,261	0,119		
	0,826	0,564		2,289	0,204		3,323	0,114		
	0,931	0,501		2,394	0,195		3,384	0,110		
	1,035	0,450		2,498	0,187		3,446	0,106		
	1,140	0,409		2,603	0,179		3,508	0,103		
	1,244	0,375	T_D	2,707	0,172		3,569	0,099		
	1,349	0,346		2,769	0,165		3,631	0,096		
	1,453	0,321		2,830	0,157		3,692	0,093		
	1,558	0,299		2,892	0,151		3,754	0,090		
	1,662	0,280		2,954	0,145		3,815	0,087		

2.6 Simulated project

The simulated project allows to define, in the absence of the original construction drawings of the building, the quantity and arrangement of the reinforcement in the elements with structural function. To be representative of the construction under investigation, the simulated project must be carried out based on the technical standards in force and the characteristic construction practice at the time of construction.

Below are some indications to be used for buildings constructed before '72.

COLUMNS

The reinforcement of the columns was carried out by inserting the minimum reinforcement provided by the standard of the time. In the R.D. 2229/39 reads:

Along≥0.8% concrete area up to 2000 cm^2

Along≥0.5% concrete area up to 8000 cm^2

In view of these criteria, reinforcement values in the columns have been derived in respect of this requirement for minimum longitudinal reinforcement; in particular, in favour of security, a percentage lower than the minimum required was inserted (0.6%).

$$A_{s,min} = 0{,}006 \cdot A_c$$

Column typology	As			
	Reinforcement bars			cmq
Column 35x35	4	φ	16	8,04
Column 40x40	4	φ	16	8,04
Column 35x35_triangular	3	φ	16	6,03
Column 40x40_triangular	3	φ	16	6,03

BEAMS

The calculation is performed using the admissible stress method; it is a procedure, with deterministic evaluation of the quantities, which controls the safety of the structures for the operating conditions, in the hypothesis of elastic behaviour of the materials. This is done by comparing the calculation stresses σ produced by the external operating actions, with those admissible for the materials $\bar{\sigma}$, deduced from the breaking values.

$$\sigma \leq \bar{\sigma}$$

$$\bar{\sigma}_c = 60 + \frac{R_{ck} - 150}{4} = 71{,}90 \ \ kg/cm^2$$

$$\bar{\sigma}_a = 2200 \ \ kg/cm^2$$

Once the homogenization value of the section n is fixed (equal to the ratio between the elastic modules of the two materials, steel and concrete, generally equal to 15) it is possible to determine the value of the reinforcement stretched to vary the tension at which the concrete works, by means of the use of tabulated values of the coefficients r and t.

On the basis of the above, a summary table of the average reinforcement calculated for each type of beam is shown.

Table 2-1: Summarize table of reinforcement bars of the beam

Beam typology	As,inf				As,sup			
	bars			cmq	bars			cmq
25x24	5	φ	12	5,65	2	φ	12	2,26
30x28	2	φ	12	2,26	2	φ	12	2,26
30x28	5	φ	16	10,05	3	φ	16	6,03
25X45	6	φ	12	6,79	3	φ	12	3,39
25x50	3	φ	12	3,39	2	φ	12	2,26
25x60	2	φ	12	2,26	2	φ	12	2,26
25x75	3	φ	12	3,39	3	φ	12	3,39
25x75	3	φ	16	6,03	2	φ	16	4,02
25x75	5	φ	16	10,05	3	φ	16	6,03
30x24	4	φ	16	8,04	2	φ	16	4,02
30x38	2	φ	12	2,26	2	φ	12	2,26
30x55	3	φ	12	3,39	3	φ	12	3,39
30x55	6	φ	12	6,79	3	φ	12	3,39
30x55	6	φ	16	12,06	4	φ	16	8,04
30x60	3	φ	12	3,39	3	φ	12	3,39
30x60	4	φ	16	8,04	2	φ	16	4,02
30x60	5	φ	16	10,05	3	φ	16	6,03
30x75	3	φ	12	3,39	3	φ	12	3,39
30x75	3	φ	16	6,03	2	φ	16	4,02
30x75	6	φ	16	12,06	6	φ	16	12,06
30x80	2	φ	16	4,02	2	φ	16	4,02
30x85	3	φ	16	6,03	2	φ	16	4,02

30x85	6	φ	16	12,06	5	φ	16	10,05
35x60	3	φ	16	6,03	2	φ	16	4,02
36x28	3	φ	12	3,39	2	φ	12	2,26
36x28	6	φ	16	12,06	4	φ	16	8,04
40x10	6	φ	16	12,06	6	φ	16	12,06
40x20	5	φ	16	10,05	3	φ	16	6,03
40x75	4	φ	12	4,52	4	φ	12	4,52
40x75	7	φ	12	7,92	4	φ	12	4,52
40x75	6	φ	16	12,06	6	φ	16	12,06
50x24	4	φ	16	8,04	2	φ	16	4,02
50x24	6	φ	16	12,06	6	φ	16	12,06
50x28	2	φ	12	2,26	2	φ	12	2,26
50x28	6	φ	12	6,79	3	φ	12	3,39
50x28	6	φ	16	12,06	5	φ	16	10,05
60x28	4	φ	16	8,04	2	φ	16	4,02
60x28	6	φ	16	12,06	4	φ	16	8,04
15x60	3	φ	16	6,03	2	φ	16	4,02
20x60	4	φ	16	8,04	2	φ	16	4,02
20x75	2	φ	12	2,26	2	φ	12	2,26
20x75	4	φ	16	8,04	3	φ	16	6,03
22,5x45	4	φ	12	4,52	2	φ	12	2,26
22,5x60	3	φ	16	6,03	2	φ	16	4,02
22,5x60	4	φ	16	8,04	2	φ	16	4,02
Variable beam 30x80	2	φ	16	4,02	2	φ	16	4,02
Variable beam 40x30 middle	4	φ	16	8,04	2	φ	16	4,02
Variable beam 40x30 middle	6	φ	16	12,06	4	φ	16	8,04
Variable beam 40x30 middle	2	φ	16	4,02	2	φ	16	4,02

2.7 Description of the f.e. model

The structural elements such as beams and columns have been modelled as frame elements, that is as one-dimensional elements with sectional geometry adherent to reality, while the foundation walls, stairs and floors have been modelled with shell-thin elements, which allow to hold considering the in-plane and plate behaviour of these elements. The shell elements have been discretized into elements of about 40 x 40 cm, a value obtained by gradually reducing the mesh to reach a limit size for which even when further decreasing the dimensions, a variation in the structure's frequencies is not obtained.

Modelling criteria adopted:

- The internal beams have been modelled as prismatic elements while the external beams have been attributed a linear variation of the area and quadratic of the moment of inertia as they are beams with a variable rectangular section along their development.
- The columns are modelled with the Section Designer command to faithfully reproduce the rhomboid and triangular geometry of the elements. To take into account the area in the connection between beams and Columns, a “rigid arm” with a stiffness factor of 0.8 is inserted, ie with a 20% reduction compared to full non-deformability.
- At the shells of the floors, in order to take into account the warping, different values were assigned to the inertia modifiers: the values corresponding to the warping direction were increased to 1.48 and to 11.68 respectively for the plate behaviour (bending) and slab (membranes), the value relative to shear in the vertical direction was decreased to 0.72, while the other values are left unchanged at the unit value. The values of these changes are the result of in situ investigations. Moreover, the thickness is assigned with an equivalent value equal both to plate and slab behaviour equal to 12 cm, however the mass and weight of the floors are considered through an added distributed load, therefore the element appears to have zero density. Instead for the roof slabs, which would seem to have no warping, the inertia modifiers are all equal to 1 and the equivalent thickness is 4 cm.
- The joints in the X and Y directions are modelled by separating the adjacent columns into two spaced apart triangular columns, as well as the beams. The continuity of the floor is guaranteed by the presence of the shells, in fact on the joint there is continuity of flooring and probably also of the screed above the floor.
- The stair ramps are modelled with shell-thin elements with equivalent thickness equal to 12 cm those of wing B and equivalent thickness 15 cm those from wing A.
- Even the infill walls are modelled as shell-thin elements. The retaining walls of the wing A, the external and internal infill walls have different material, with equivalent thickness equal to 40 cm, 20 cm and 12 cm respectively. While the walls against the ground, the external infill walls and the internal infill walls of the B wing are represented in their real position, the internal infill walls of the A wing are grouped according to the principal guidelines identified by the frames in c.a. The ancient masonry walls of wing B are modelled with shell-thin elements of variable thickness between 0.50 m, 1.4 m and 1.8 m.

- The frame and shell elements of the lower floor are fix-constrained by their lower end joints, except those relating to the stairs that are hinged. The joints at the base for modelling the foundations have been considered representative of real behaviour as the building is on a cemented sandstone formation. For buildings B, joints were assigned to each node making up the foundation masonry, while for building A, the joints were assigned to the base of the column. Furthermore, along the masonry walls on the back of the ground, elastic springs were applied to the nodes of the individual shells involved in a direction orthogonal to the plane, with horizontal reaction values equal to 8144 kN/m in operation of soil stiffness, which in the case of cemented sandstone is approximately E_{ed} = 19500 - 29500 kN/m^2.

In this case, the compliance of the foundation soil was not taken into account for two reasons:

- the purpose of this thesis is to evaluate the incidence of the modelling of non-structural elements, calibrating their operating stiffness through vibrational measurements, in the assessment of the seismic vulnerability index. Therefore, a refined modelling is adopted in relation to non-structural elements while standard and simple modelling strategies are used for the rest, so that to avoid introducing uncertainties in the interpretation of the results;
- the calibration of f.e. model was carried out by using the result of the operational modal analysis, thus using environmental vibrations as input; in this case, as recognized in the literature and as usual for practical applications the assumption of fix-restrain at the base is justified.

While for the f.e. model post-retrofitting, where the dissipative towers are inserted, the viscous dissipation devices, are modelled with appropriate non-linear behaviour elements called "link damper", whose response is a function of velocity.

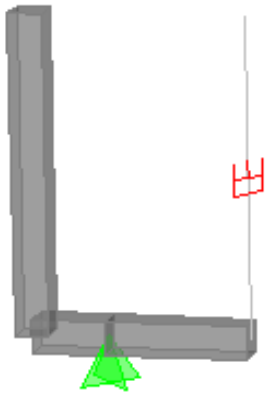

Figure 2-18: link damper

About the reticular steel structure of the dissipative towers, this is shown schematically by means of frame elements, as well as rigid pendulums of connection to the existing building. At basement level a slab in r.c is inserted, modelled with a shell element. The f.e. model accurately reproduce the actual mass distributions and stiffness of the structure.

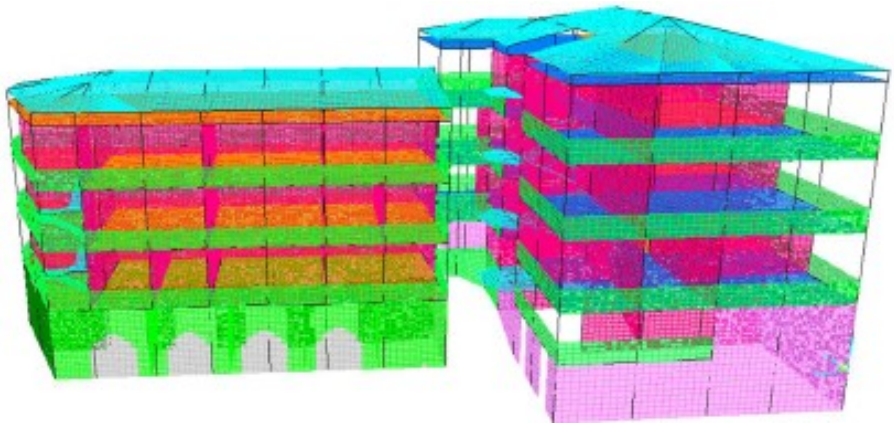

Figure 2-19: 3D view of the model before retrofitting

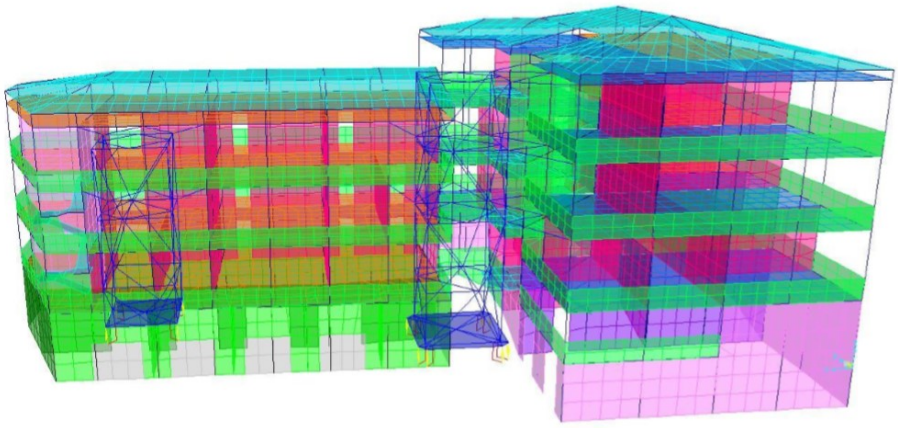

Figure 2-20: view of the model after retrofitting

The f.e. model presented in the figure represents the starting model on which the calibration was performed; in this model the shell elements have been discretized into elements of about 40 x 40 cm, a value obtained by gradually reducing the mesh to a limit size for which even when further decreasing the dimensions, a variation in frequencies is not obtained of the structure.

Also in this second case study, 3 models are proposed:

- Model A: frame without non-structural elements
- Model B: frame with external infill walls modelled with equivalent rods according to literature
- Model C: frame with external and internal infill walls modelled with shell elements characterized by a wider mesh compared to the calibrated starting model in order to perform complex computational analyses.

2.8 Modelling of Masonry External Infill Walls

The external infills of model B were modelled using equivalent connecting rods, whose geometry was also evaluated in this case according to the studies of Decanini et al. (2004). For the analytical discussion, see the paragraph 1.7.

2.9 Operational Modal Analysis – OMA and calibration of f.e. models

Ambient vibration tests were performed, before and after the retrofitting works, in order to obtain the modal parameters of the structures, such as natural vibration frequencies, mode shapes and damping ratio in operating conditions.

2.9.1 Before retrofitting works

Ambient vibration tests are carried out on the whole building. Three accelerometers per floor were positioned: two sensors, measuring along two orthogonal axes (transverse and longitudinal), were placed in the same point at a side of the building while the third, measuring along the transverse direction, was located in the opposite side of the building, far from the first two, to better catch the rotational component of the floor, as we can see from the figure:

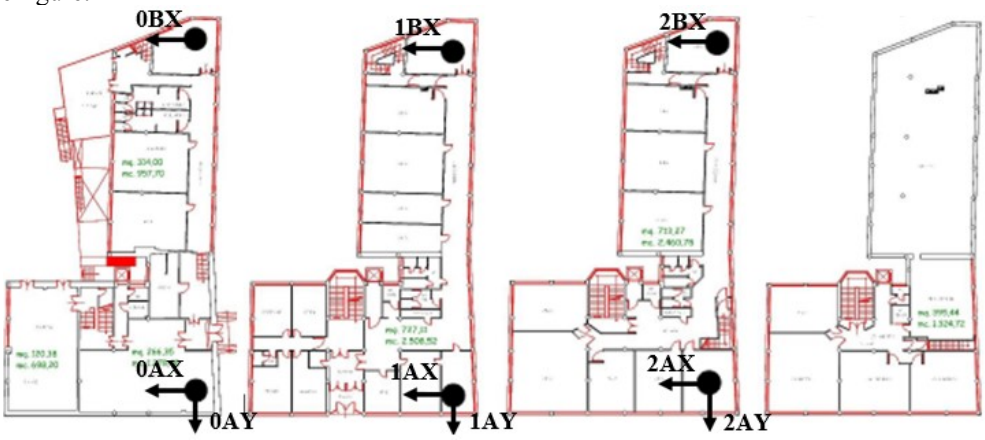

Figure 2-21: Accelerometers layout for each floor.

The modal parameters are extracted by means of the SSI-COV.

Table 2-2- Experimental resonance frequencies of the building.

Mode number	Mode type	Frequency [Hz]
1	1st transversal	3.61
2	1st torsional	3.70
3	1st longitudinal	4.00

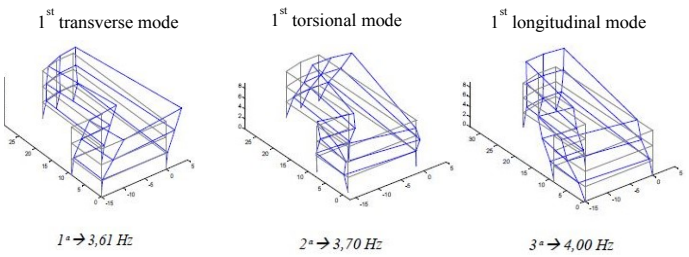

Figure 2-22: Experimental mode shapes of the building

The model on which the calibration was performed, as already anticipated, is the one closest to reality, consisting of internal and external infill walls modelled with shell elements characterized by dense mesh. However, the objective of the thesis, that is to perform non-linear analyzes to calculate the vulnerability risk index of the structure, involves a considerable computational burden. Therefore, the mesh size cannot be too small to allow the calculation program to run the analysis, so in this case the mesh is an integral part of the calibration process. In particular, a larger mesh adds stiffness to the system, therefore the calibration was carried out by iteratively decreasing the stiffness values of the elastic modules of the infill walls with respect to the starting ones taken from the C8A.2.1 of NTC 2008. The final values of the elastic modules that allowed the calibration of the model are listed in the table below.

Table 2-3: Elastic and dynamic modules of the modelled elements

Element	Material	Estatic [N/mmq]	Edynamic [N/mmq]
Beam and column	Concrete	25599	32255
slab	Concrete	23039,25	27647,1
stairway	Concrete	23039,25	27647,1
Ext. Infill	Masonry	4125	4950
Int. Infill	Masonry	2887,5	3465
Ground wall	Masonry	3024	3628,8

The analytical mode shapes considered for the comparison were identified taking into account the participating masses. Numerical resonance frequencies obtained from a classical modal analysis are compared with the experimental ones, resulting from the OMA (Table 2-4). Experimental and numerical values show a very good agreement.

Table 2-4: Experimental vs. analytical values of the building resonance frequencies

Mode	Experimental Frequency [Hz]	Analytical Frequency [Hz]	Percentage error [%]	Mode type
1	3,61	3,45	4,43%	1st transverse
2	3,70	3,69	0,27%	1st torsional
3	4,00	4,10	2,50%	1st longitudinal

The following is a comparison between the modal shapes obtained from the OMA procedures and those obtained from the f.e. model.

	Mode shapes	
	Experimental	Analytical
1	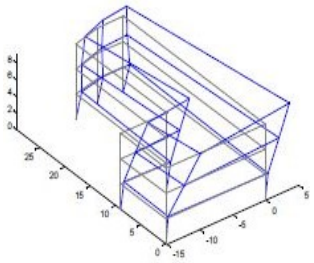	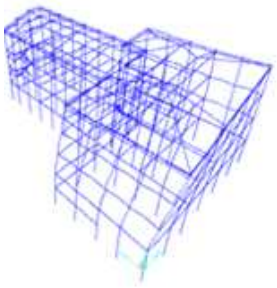
	3.61 Hz	3.45 Hz
2	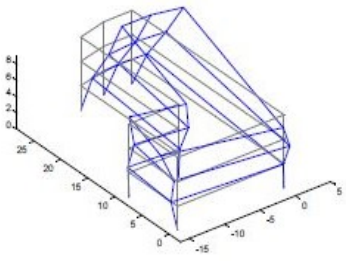	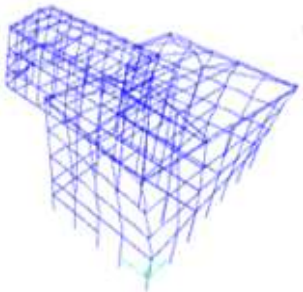
	3.70 Hz	3.69 Hz

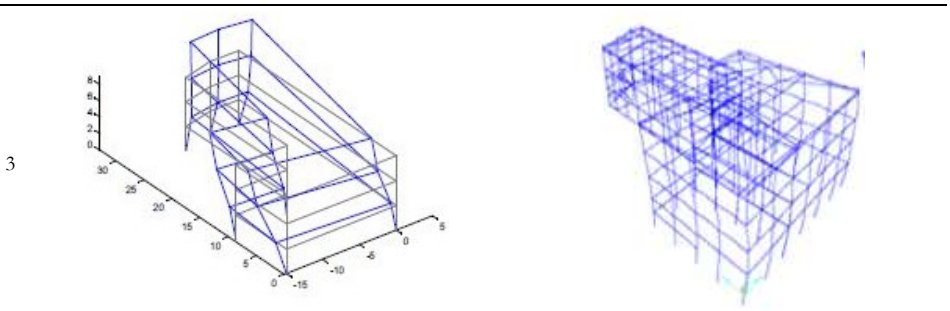

Figure 2-23: Experimental mode shapes vs. analytical mode shapes

The modal parameters thus obtained were compared with the experimental ones using the MAC formula described in the first chapter, in order to verify that the modal shapes are coherent.

3	0.0449	0.1409	**0.9799**
2	0.0365	**0.9856**	0.1730
1	**0.9384**	0.0077	0.1308
	1	2	3

Figure 2-24: Mac Matrix experimental vs. analytical displacements

2.9.2 After retrofitting works

After retrofitting works many different ambient vibration tests were carried out in order to assess the dissipative capacity of the new structural system at greater input energy level, and to catch the behaviour of the structure under seismic event. In this thesis only the measurement of 10/05/2013 are describe. Below are shown the modal parameters obtained by OMA procedures after retrofitting, and the accelerometers configurations.

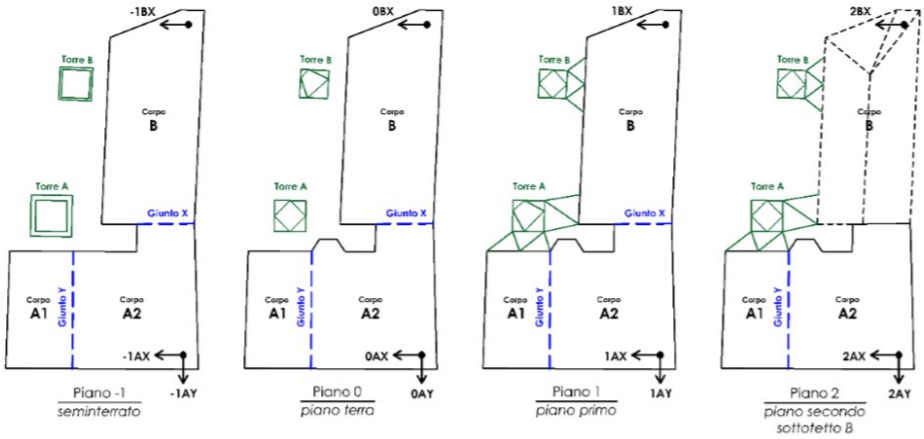

Figure 2-25: Accelerometers configuration for each floor.

Table 2-5- Experimental resonance frequencies of the building after retrofitting.

Mode number	Mode type	Frequency [Hz]
1	1st transverse	3.60
2	1st torsional	3.82
3	1st longitudinal	4.14

As we can see, there are no significant variations in the natural frequencies and in the modal shapes of the structure, proving that the dissipative towers do not modify the dynamic behaviour of the original building.

With reference to the calibration phase of the model, the geometry, the characteristics of the materials and any other data have been kept identical to the model before retrofitting, to which the structures of the dissipative towers have simply been added.

Table 2-6: Experimental vs. analytical values of the building resonance frequencies

Mode	Experimental Frequency [Hz]	Analytical Frequency [Hz]	Percentage error [%]	Mode type
1	3.60	3.47	3,61%	1st transverse
2	3.82	3.79	0,79%	1st torsional
3	4.14	4.18	0,97%	1st longitudinal

The following is a comparison between the modal shapes obtained from the OMA procedures and those obtained from the f.e. model.

Mode shapes		
	Experimental	**Analytical**
1	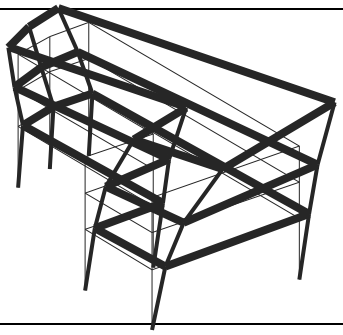	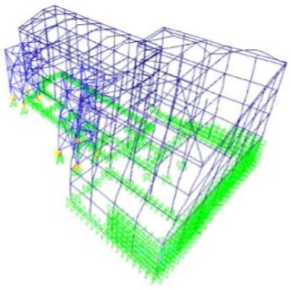
	3.60 Hz	3.47 Hz
2	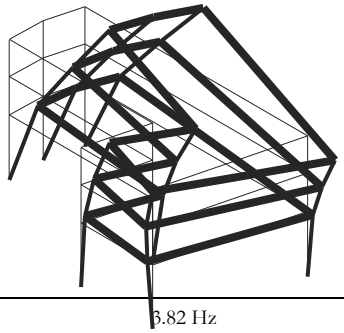	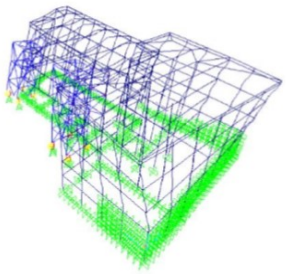
	3.82 Hz	3.79 Hz

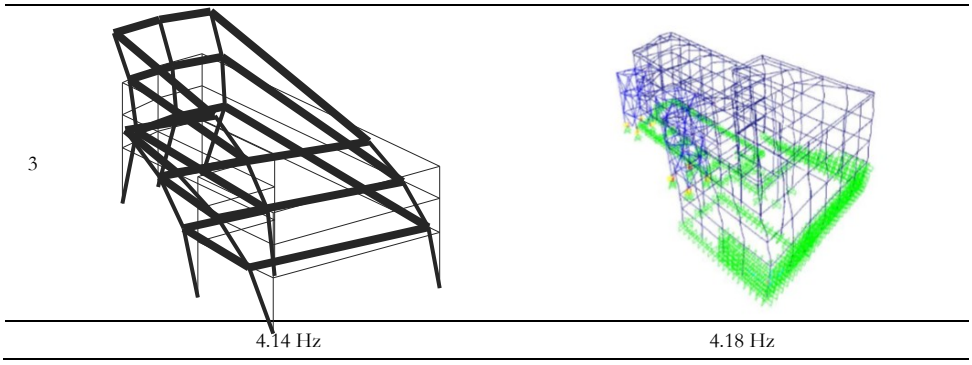

Figure 2-26: Experimental mode shapes vs. analytical mode shapes after retrofitting

The results of the Modal Assurance Criterion between experimental and analytical modal displacements are also shown.

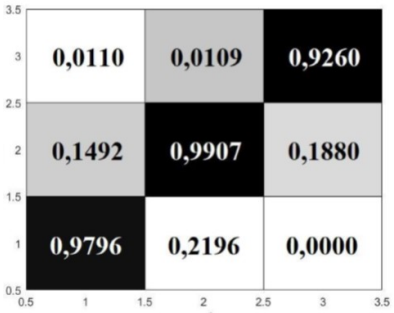

Figure 2-27: Mac Matrix experimental vs. analytical displacements

2.10 Vulnerability Index Before Retrofitting Works

As already mentioned in the introduction, the purpose of this thesis work is to evaluate how much the accuracy in finite element modelling affects the calculation of the seismic vulnerability index of the structures. For this purpose, three models have been implemented, characterized by increasing degree of accuracy:

Also in this second case study, 3 models are proposed:

- Model A: frame without non-structural elements
- Model B: frame with external infill walls modelled with equivalent rods according to literature
- Model C: frame with external and internal infill walls modelled with shell elements characterized by a wider mesh compared to the calibrated starting model in order to perform complex computational analyzes.

The modelling of external infill walls of model B, as anticipated, was carried out through the introduction of equivalent connecting rods according to the "Decanini" theory.

2.10.1 Non-linear Static Analysis – Pushover

Also in this case, the seismic vulnerability index was calculated through non-linear static analysis (Pushover Analysis). Non-linear Static Analysis – Distribution of forces

According to the NTC08 (NTC 2008 § 7.3.4.1) at least two distributions of the inertia forces must be considered, one in the main distributions (Group 1) and the other in the secondary distributions (Group 2) illustrated below.

Group 1 - Main distributions

- distribution proportional to the static forces (linear static analysis), applicable only if the fundamental vibration mode in the considered direction has a mass participation of not less than 75% and on condition of using the second distribution as the second one;
- distribution corresponding to a distribution of accelerations proportional to the vibration mode, applicable only if the fundamental vibration mode in the considered direction has a mass participation of not less than 75%;
- distribution corresponding to the distribution of the shear plan calculated in a linear dynamic analysis, applicable only if the fundamental period of the structure is greater than Tc.

Group 2 - Secondary distributions

a) uniform distribution of forces, to be understood as derived from a uniform distribution of accelerations along the height of the construction;

b) adaptive distribution, which changes as the displacement of the control point increases as a function of the plasticization of the structure.

As the Ordinance PCM 3431 (03.05.2005) suggests, generally two distributions of forces are considered:

- one proportional to the masses;
- one proportional to the product of the masses for the deformation corresponding to the first mode.

They are respectively equivalent to the first of Group 2 and the second of Group 1.

The analysis has as an initial condition of undeformed structure the case of non-linear static analysis "Grav" (only with gravitational loads).

In particular, in this work the "Grav" case is defined by the forces and coefficients shown in Figure 2-28.

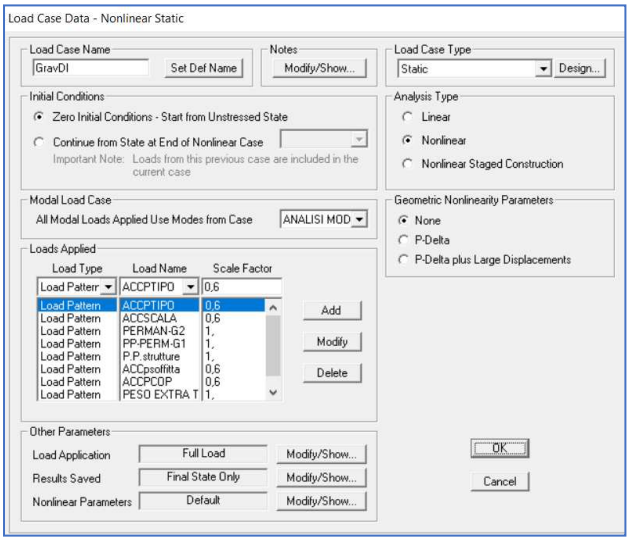

Figure 2-28: Load case “GRAV”

To take into account the spatial variability of the seismic motion, as well as any uncertainties in the location of the masses, at the center of mass an accidental eccentricity must be attributed to its position as it derives from the calculation.

For buildings only and in the absence of more accurate determinations accidental eccentricity in any direction cannot be considered inferior to 0.05 times the size of the building measured perpendicularly to the direction of application of the seismic action. This eccentricity is assumed to be constant, by entity and direction, on all the horizontal sections.

The cases to be evaluated are the following:

1. PushmassaX+TP
2. PushmassaX+TN
3. PushmassaX-TP
4. PushmassaX-TN
5. PushmassaY+TP
6. PushmassaY+TN
7. PushmassaY-TP
8. PushmassaY-TN
9. PushmodeX+TP
10. PushmodeX+TN
11. PushmodeX-TP
12. PushmodeX-TN
13. PushmodeY+TP
14. PushmodeY+TN
15. PushmodeY-TP
16. PushmodeY-TN

Where:

- Pushmassa: distribution of force proportional to the masses;
- Pushmode: force distribution proportional to the fundamental mode of vibration in the direction of analysis;
- +, -: push direction (in relation to the global reference system of the structural model);

- TP: torque associated with the horizontal thrust accidental positive (defined with reference to the axis z of the global structural model system).
- TN: torque associated with the horizontal thrust accidental negative (defined with reference to the axis z of the global structural model system).

In this case only four load cases are analysed: PushmassaX+, PushmodoX+, PushmassaY+, PushmodoY+.

BUILDING A

The load distribution inserted for load case "pushmassa" is shown in Table 1-18: Load distribution "Pushmassa"

Table 2-7: Load distribution "Pushmassa"

	Mass [kN*s²/m]	Force [kN]	PushMass
Floor 1	693.78	6805.98	1.38
Floor 2	496.74	4873.02	0.98
Floor 3	476.34	4672.90	0.94
Floor 4	504.36	4947.77	1.00

The load distribution inserted for load case "pushmodo" is shown in Table 1-19.

Table 2-8: Load distribution "Pushmodo"

	U1 [m]	U2 [m]	Mass [kN*s²/m]	U1*Mass	U2*Mass	Pushmodo X	Pushmodo Y
Floor 1	0.0004	0.0003	693.78	0,28	0,21	0.02	0.01
Floor 2	0.0143	0.0134	496.74	7,10	6,66	0.42	0.41
Floor 3	0.0263	0.0242	476.34	12,53	11,53	0.73	0.72
Floor 4	0.0338	0.0320	504.36	17,05	16,14	1.00	1.00

BUILDING B

The load distribution inserted for load case “pushmassa” is shown in Table 2-9.

Table 2-9: Load distribution “Pushmassa”

	Mass [kN*s²/m]	**Force [kN]**	**PushMass**
Floor 1	1162	11407	2.51
Floor 2	395	3881	0.85
Floor 3	389	3816	0.84
Floor 4	464	4552	1.00

The load distribution inserted for load case “pushmodo” is shown in Table 2-10.

Table 2-10: Load distribution “Pushmodo”

	U1 [m]	**U2 [m]**	**Mass [kN*s²/m]**	**U1*Mass**	**U2*Mass**	**Pushmodo X**	**Pushmodo Y**
Floor 1	0.0002	-0.0001	1162	0,23	-0,12	0.02	0.01
Floor 2	0.0127	-0.0146	395	5,02	-5,77	0.35	0.35
Floor 3	0.0245	-0.0264	389	9,53	-10,27	0.65	0.63
Floor 4	0.0315	-0.0353	464	14,62	-16,38	1.00	1.00

The seismic vulnerability index was calculated using the CSM (Capacity Spectrum Method) method and is presented for the three f.e. models previously described and characterized by increasing accuracy: model A, model B and model C. Also in this case, for the presence of short column in the staircase, two cases have been distinguished: fragile and ductile. In the first case, all types of plastic hinges presented are included, including those with brittle fractures, in the second case, instead, the possible fragile mechanisms are omitted assuming that these can be avoided through local interventions (FRP wrapping for short column in the staircase).

2.10.2 Model A: Seismic Vulnerability Index

As already mentioned, the A model, characterized by a lower level of accuracy, is composed only of structural components.

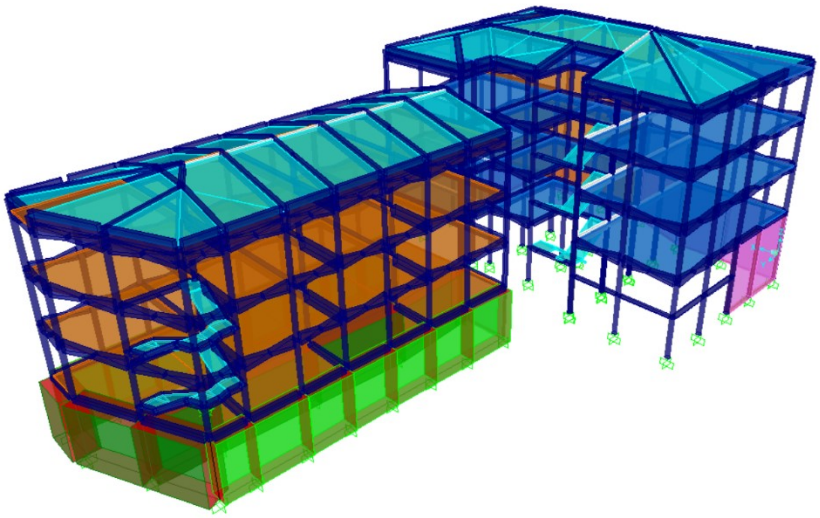

Figure 2-29: Extruded view of Model A

$$E_{conc} = 50\% E_{conc\ el}$$

The results obtained are divided for building A and building B.

BUILDING A

The results obtained for the four most important analysis cases are summarized in the table:

Table 2-11: Summarize of seismic vulnerability index for model A

	I_R SLD	I_R SLV BRITTLE	I_R SLV DUCTILE
Pushmass X+	0,320	0,530	0,530
Pushmodo X+	0,290	0,470	0,470
Pushmass Y+	0,620	0,260	0,510
Pushmodo Y+	0,560	0,240	0,510

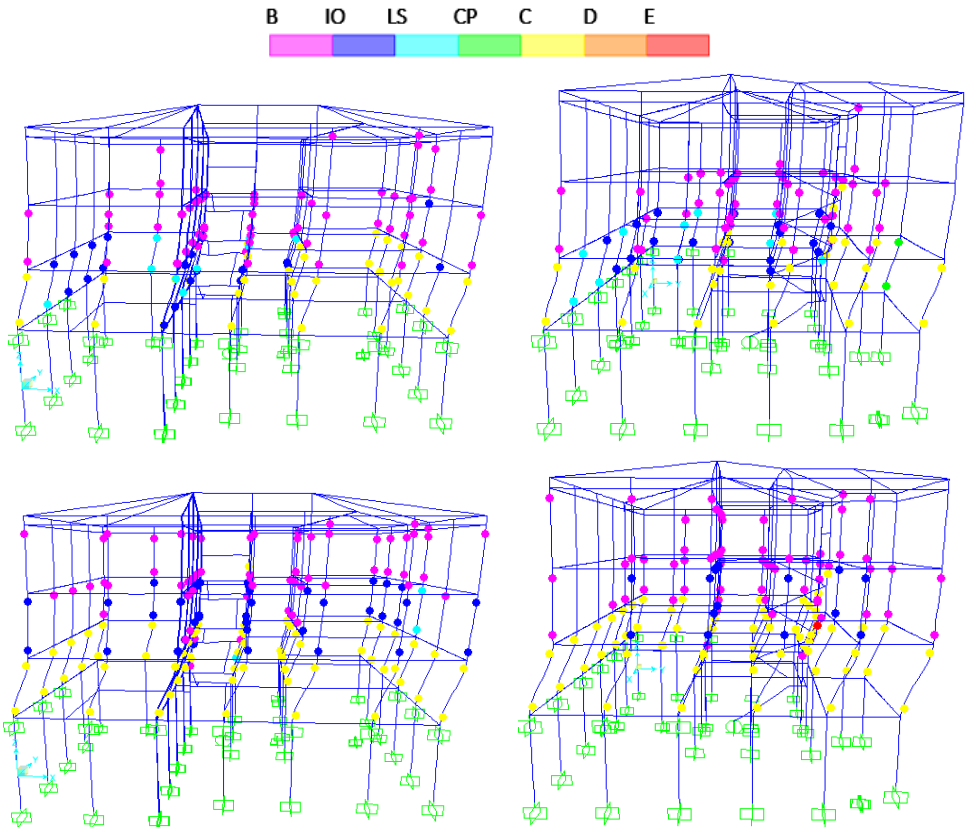

Figure 2-30: Last step of analysis for PushmassaX, PushmassaY, PushmodoX, PushmodoY

.

BUILDING B

The results obtained for the four most important analysis cases are summarized in the table:

Table 2-12: Summarize of seismic vulnerability index for model A

	I_R SLD	I_R SLV BRITTLE	I_R SLV DUCTILE
Pushmass X+	0,170	0,290	0,640
Pushmodo X+	0,170	0,230	0,500
Pushmass Y+	0,620	0,270	0,850
Pushmodo Y+	0,400	0,230	0,570

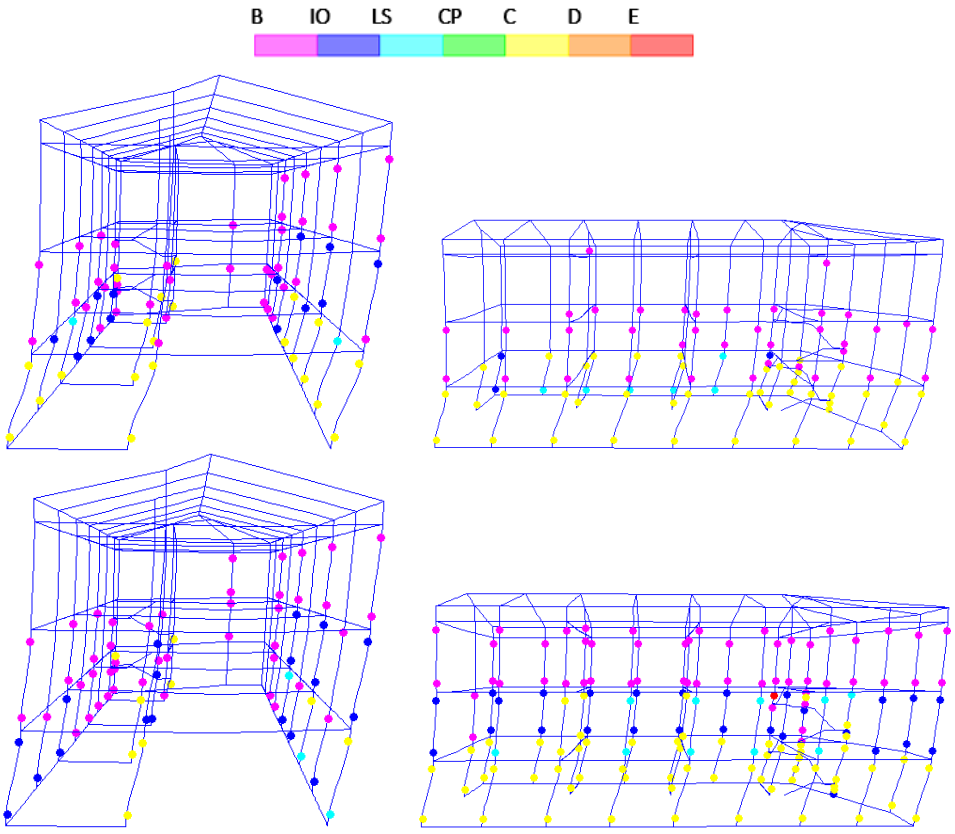

Figure 2-31: Last step of analysis for PushmassaX, PushmassaY, PushmodoX, PushmodoY

2.10.3 Model B: Seismic Vulnerability Index

Model B, characterized by an intermediate level of accuracy, is composed of external infill walls modelled as equivalent rods according to literature, in addition to the structural components.

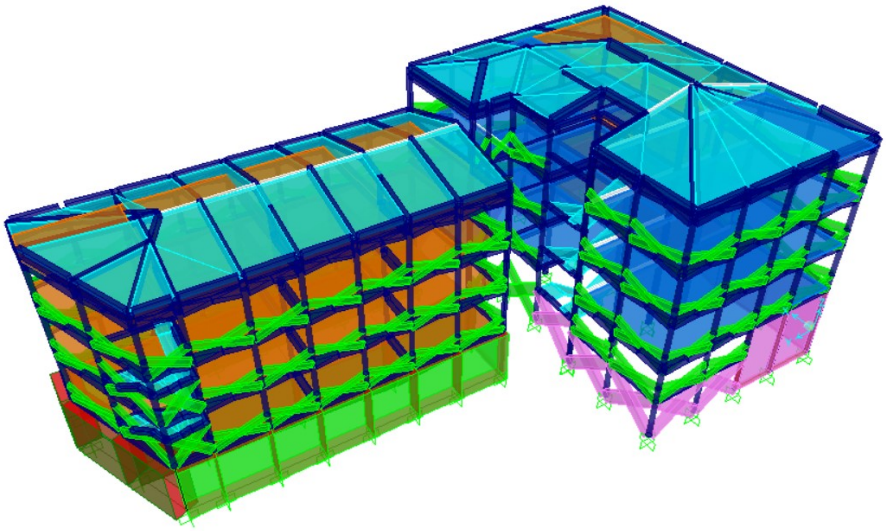

Figure 2-32: Extruded view of Model B

$$E_{conc} = 50\% E_{conc\ el}$$

The constitutive laws and the corresponding law of the plastic hinges inserted in the model are shown below:

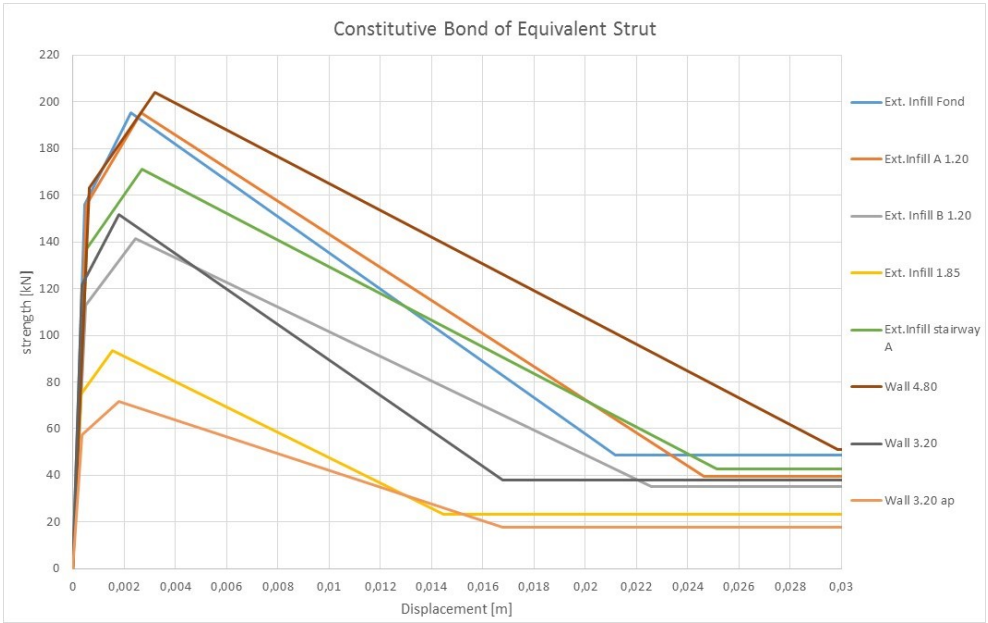

Figure 2-33: The constitutive laws of the equivalent strut

The results obtained are divided for building A and building B.

BUILDING A

The results obtained for the four most important analysis cases are summarized in the table:

Table 2-13: Summarize of seismic vulnerability index for model A

	I_R SLD	I_R SLV BRITTLE	I_R SLV DUCTILE
Pushmass X+	0,490	0,590	0,590
Pushmodo X+	0,400	0,530	0,530
Pushmass Y+	0,520	0,310	0,570
Pushmodo Y+	0,400	0,240	0,570

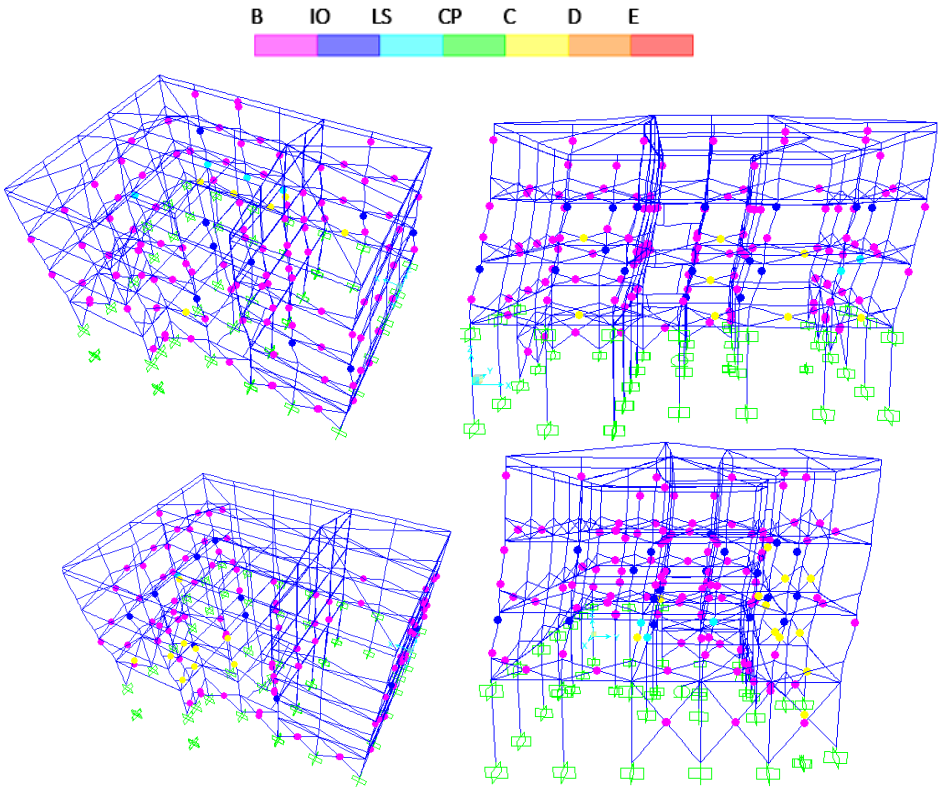

Figure 2-34: Last step of analysis for PushmassaX, PushmassaY, PushmodoX, PushmodoY

.

BUILDING B

The results obtained for the four most important analysis cases are summarized in the table:

Table 2-14: Summarize of seismic vulnerability index for model A

	I_R SLD	I_R SLV BRITTLE	I_R SLV DUCTILE
Pushmass X+	0,190	0,260	0,690
Pushmodo X+	0,140	0,190	0,580
Pushmass Y+	0,590	0,270	0,800
Pushmodo Y+	0,380	0,160	0,670

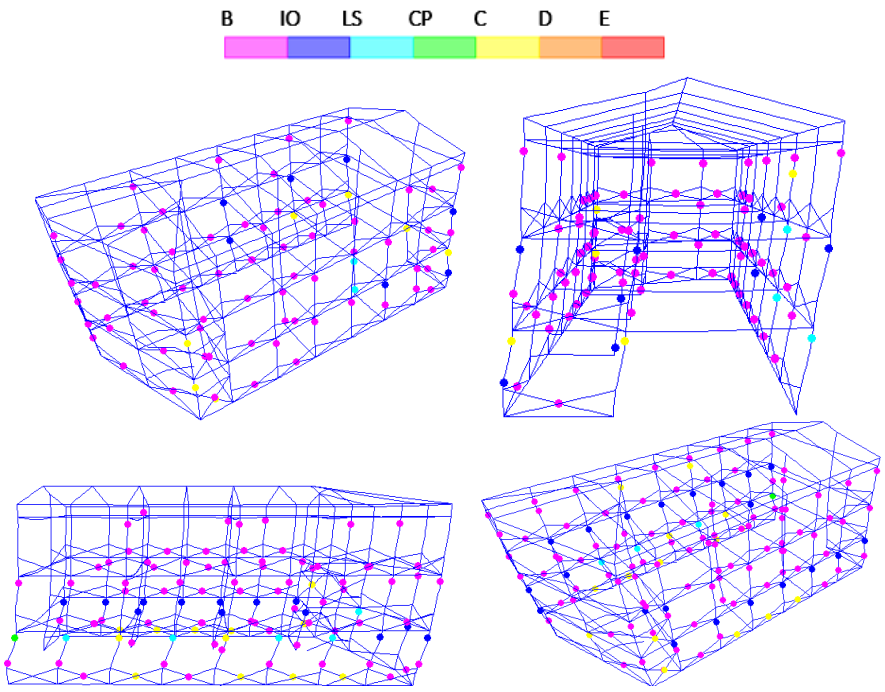

Figure 2-35: Last step of analysis for PushmassaX, PushmassaY, PushmodoX, PushmodoY

2.10.4 Model C: Seismic Vulnerability Index

Model C, characterized by a higher level of accuracy, is composed of external and internal infill walls, in addition to the structural components, modelled as non-linear shell element and calibrated through OMA procedures. The non-linear shell elements, unlike the equivalent struts introduced in the second model, do not allow, in the analysis phase, to evaluate which panels are breaking and which remain intact. In fact, based on what has been said, with this model it will not be possible to evaluate the resistant and dissipative contribution of the infilling elements with respect to lateral actions, while it will be possible to obtain a greater degree of detail in the response to the damage limit state as the information input on the stiffness transmitted to the structural elements is more realistic. In the following, only the mass proportional combinations (PushmassaX and PushmassaY) are illustrated as it was observed that the latter response, unlike the Pushmodo cases, resulted in the initial elastic investigation in accordance with the purely elastic-linear calibrated model.

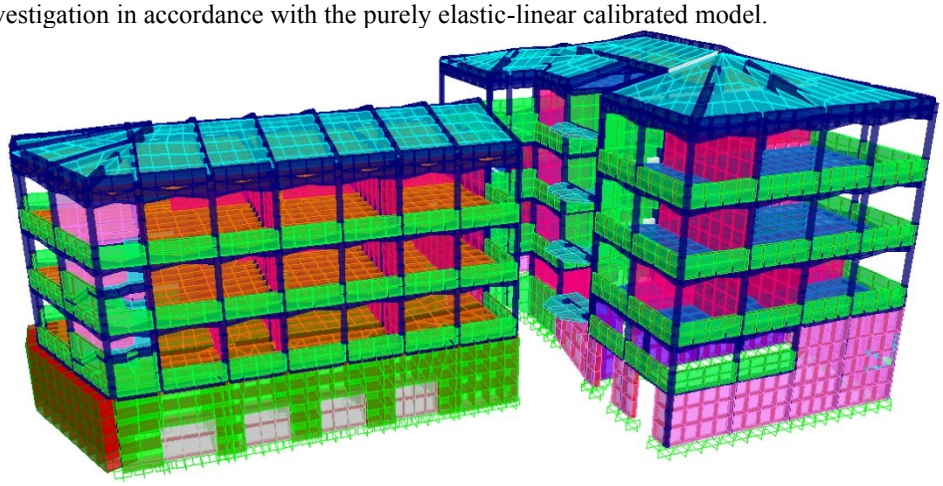

Figure 2-36: Extruded view of Model C

$$E_{conc} = 50\% E_{conc\ el}$$

The results obtained are divided for building A and building B.

BUILDING A

The results obtained for the four most important analysis cases are summarized in the table:

Table 2-15: Summarize of seismic vulnerability index for model A

	I_R SLD	I_R SLV BRITTLE
Pushmass X+	1.19	0,55
Pushmass Y+	1.89	1.42

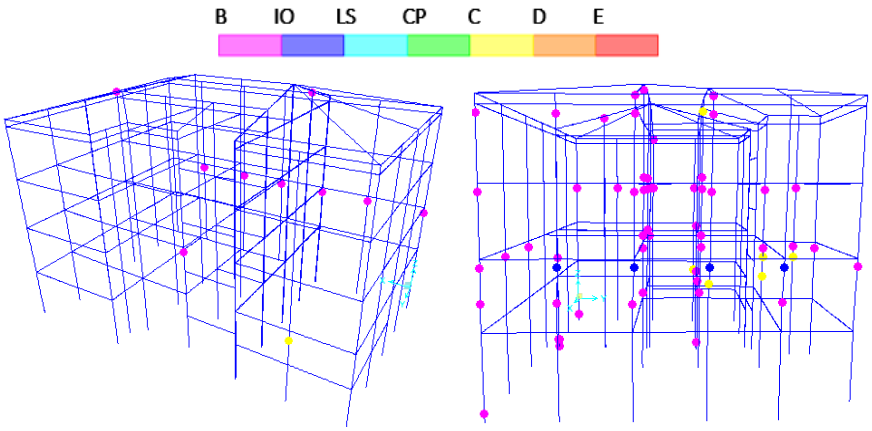

Figure 2-37: Last step of analysis for PushmassaX, PushmassaY,

It is noted that for this model the seismic vulnerability index values obtained are very high, exceeding the unit value corresponding to the seismic admissible situation. Therefore, as already anticipated, given the high uncertainty of the non-linear modelling of the two-dimensional elements, the aspects on which attention was focused concern rather the typology of the failure mechanisms established: it is in fact noted that the presence of the external panels in the frames perimetral determine the emergence of hinges characterized by shear failure mechanism, as already seen for the model with the diagonal struts for the simulation of the external infill.

BUILDING B

The results obtained for the four most important analysis cases are summarized in the table:

Table 2-16: Summarize of seismic vulnerability index for model A

	I_R SLD	I_R SLV BRITTLE
Pushmass X+	0,97	0,45
Pushmass Y+	0,90	0,42

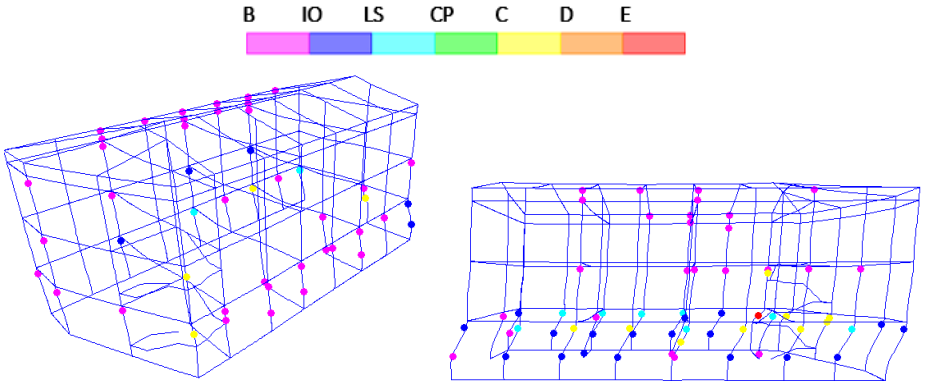

Figure 2-38: Last step of analysis for PushmassaX, PushmassaY,

2.10.5 Comparisons between models

Below, the SLV seismic vulnerability index of the structure for the combinations characterized by the most conservative results, is compared for the three models implemented, for the push direction.

BUILDING A

Table 2-17: Seismic vulnerability index obtained for the most severe load cases, for models containing brittle fracture mechanisms, based on the push direction

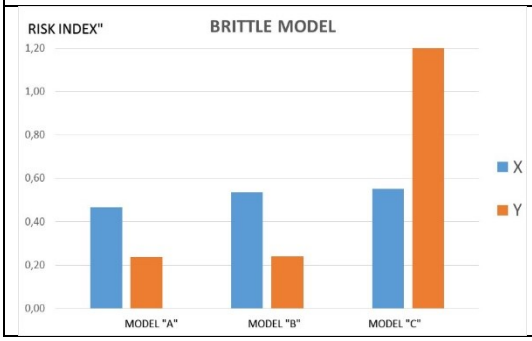

Table 2-18: Seismic vulnerability index obtained for the most severe load cases, for models without brittle fracture mechanisms, based on the push direction

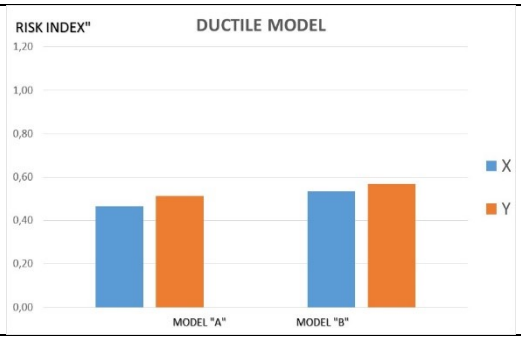

BUILDING B

Table 2-19: Seismic vulnerability index obtained for the most severe load cases, for models containing brittle fracture mechanisms, based on the push direction

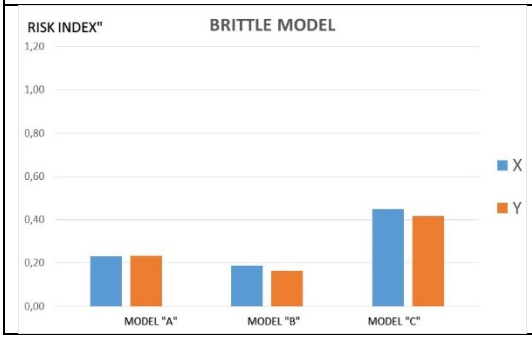

Table 2-20: Seismic vulnerability index obtained for the most severe load cases, for models without brittle fracture mechanisms, based on the push direction

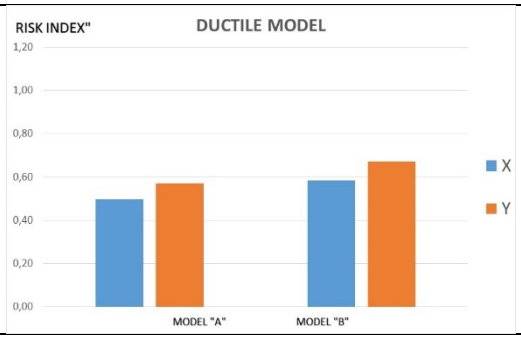

Transcending the contribution of the model c, whose reliability in the plastic field is uncertain due to the presence of shell elements with non-linear behavior, for the other models we can see how, in the x direction, there is an increase in the seismic vulnerability index to the SLV as the accuracy of the modelling increases, for building A, both in the fragile case and in the ductile case. While, for the building B, this increase of the seismic vulnerability

index with the increase of the precision in the modelling, is had only for the model that does not take into account the breakages of fragile type.

In addition, a comparison between different model is shown in terms of intensity level of the seismic action necessary to reach the SLD.

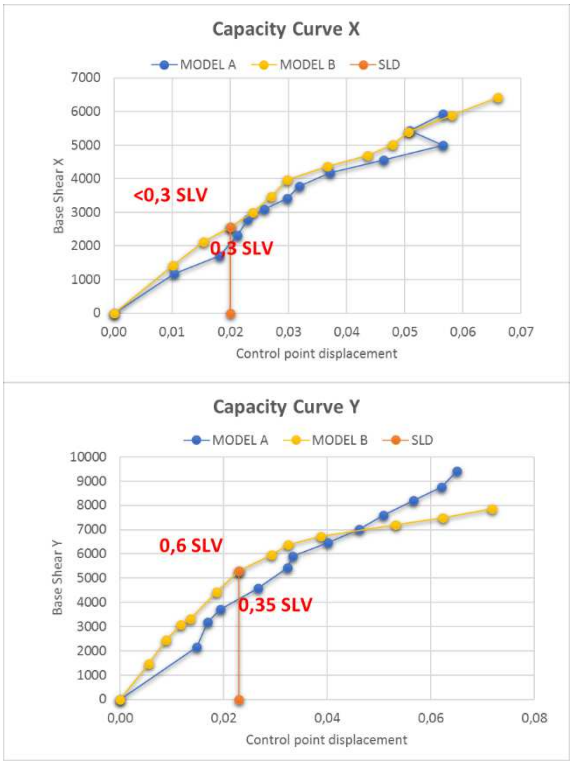

Figure 2-39: Comparison between different model in terms of intensity level of the seismic action necessary to reach the SLD

From the figures it has been noted that the level of seismic energy necessary to reach the SLD limit displacement increases as the degree of detail of the model increases in Y direction, where the presence of infill walls is significant. The level of seismic energy necessary to reach the SLD limit displacement in Y direction for model B is 0.6 SLV, compared to a level equal to 0.35 SLV necessary to reach the SLD for model A. However, with respect to previous case study, the results are less evident because the fundamental period of model A is related to a lower seismic acceleration than the model B. Therefore, the increase in stiffness of the model B with respect to the model A is accompanied by an increase in the seismic acceleration in input. This means that the results on the two models are closer to each other than in the previous case study.

2.10.6 Seismic classification

For the normative references related to the seismic classification of buildings, refer to paragraph 1.9.7 of the previous chapter.

Having obtained in the previous chapter the seismic vulnerability index for the various models, the various push cases, for the limit states SLD and SLV (ductile and fragile case) we proceed now reporting the final summary of the seismic classification for the worst load cases of each model, divided into two directions. Note that, for the cases which not take in to account the brittle breakages of the column in the stairway, the model C is not reported for the reasons already specified.

BUILDING A

Table 2-21:Seismic classification for brittle model	Table 2-22: Seismic classification for ductile model
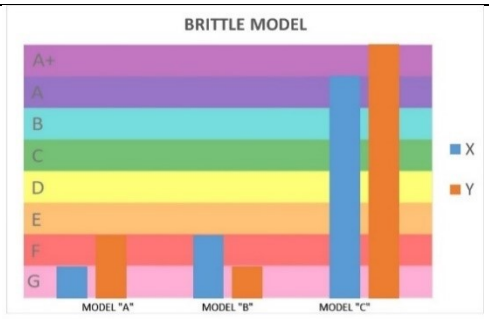	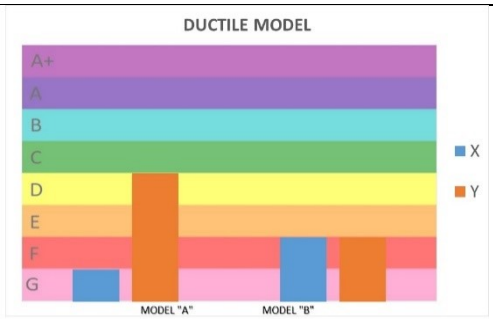

BUILDING B

Table 2-23: Seismic classification for brittle model	Table 2-24: Seismic classification for ductile model
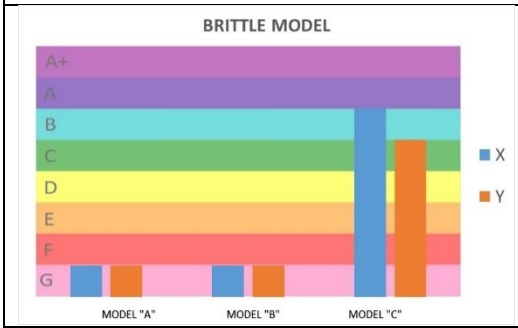	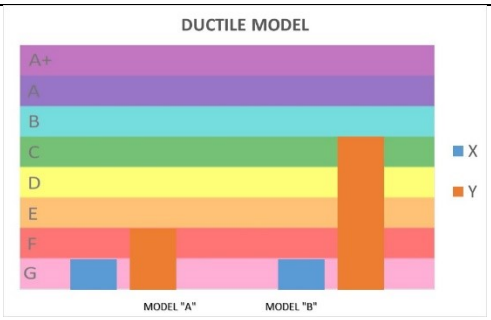

As the accuracy of the model in building A increases, an increase in the risk class from G to F is observed in X due to the positive contribution in terms of external infill stiffness, and a worsening in Y both for the ductile and fragile model, due to the fragile mechanisms.

In building B the results are unchanged in X due to the lack of collaborating infill walls, while in Y direction there is a significant improvement, even passing from F to C in the ductile case, due to the high quantity of panels.

2.11 Vulnerability Index After Retrofitting Works

As for the post-retrofitting, as already mentioned, the f.e. models are the same as pre-retrofitting with the addition of dissipative towers. Therefore, the geometrical and material characteristics and the degree of accuracy are the same as described in the previous chapter. However, in this case, the computational burden due to the non-linear dynamic analysis did not allow the implementation of the calibrated C model, with a high degree of accuracy; therefore, the models are:

- Model A: frame without non-structural elements
- Model B: frame with external infill walls modelled with equivalent rods according to literature

2.11.1 Incremental Dynamic Analysis – I.D.A

As already seen in the first case study presented, also in this case the seismic vulnerability index is evaluated with incremental dynamical analysis. For the theoretical references concerning the Incremental Dynamic Analysis, see paragraph 1.10.1 of the previous chapter.

2.11.2 Spectro-Compatible Accelerograms

The choice of a set of significant earthquakes was made by determining artificial spectrum-compatible accelerograms obtained as foreseen in par. 3.2.3.6 of the NTC'08. The program used to generate accelerograms compatible with assigned response spectra is the SIMQKE-1 (SIMulation of earthQuaKE ground motions). The program automatically calculates the response spectra according to the indications of the Technical Standards for Construction (Ministerial Decree 14-1-2008) and of the Order of the President of the Council of Ministers No. 3274 (OPCM 3274). Below, in Figure 1-50, the captured images of the program show the generated spectrum-compatible acceleration and its overlap with the elastic spectrum at the SLV.

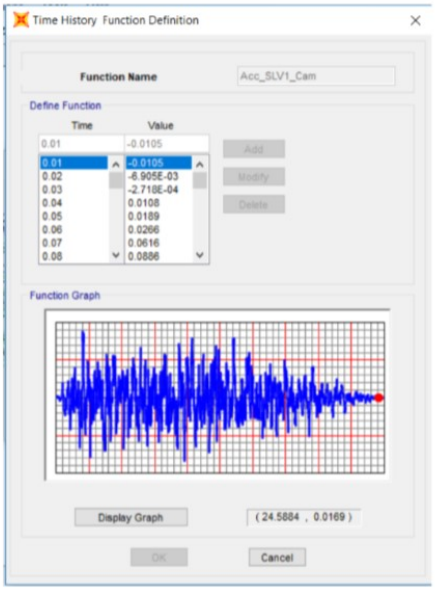

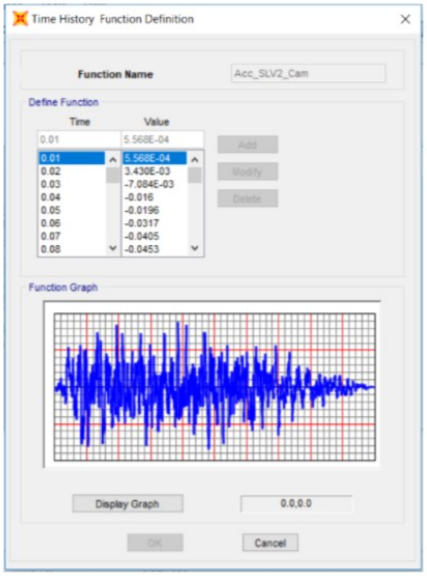

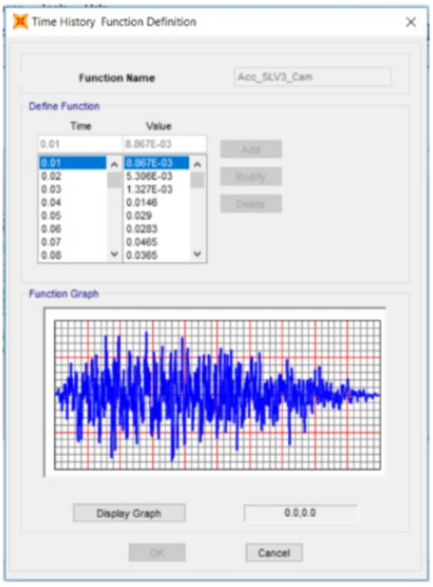

Figure 2-40: Spectro-compatible accelerograms SLV 1 - SLV 2 - SLV3

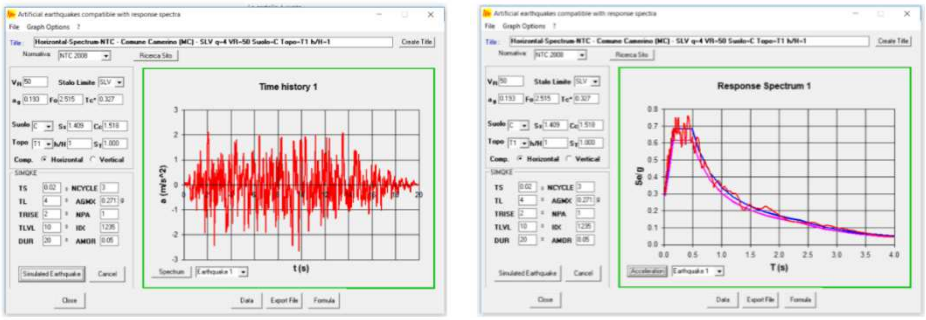

Figure 2-41: SIMQUAKE - superposition of the elastic spectrum with spectrum-compatible acceleration

In this study, due to the high computational burden, we chose to use only the SLV1 accelerogram in the analyzes, applying it in different models.

2.11.3 Evaluation of viscous damping

As already seen for the first case study, also in this case, the modal damping coefficient must be specified for two different frequencies, based on the coefficients a_0 and a_1. Assuming that the modal damping coefficient $\xi i = \xi j = \xi$, the Rayleigh damping coefficients have been defined by Chopra (2001), as:

$$a_0 = \xi \cdot \frac{2\omega_i \omega_j}{\omega_i + \omega_j}$$

$$a_1 = \xi \cdot \frac{2}{\omega_i + \omega_j}$$

Where ω_i and ω_j are the circular frequencies to which the damping coefficient is applied.

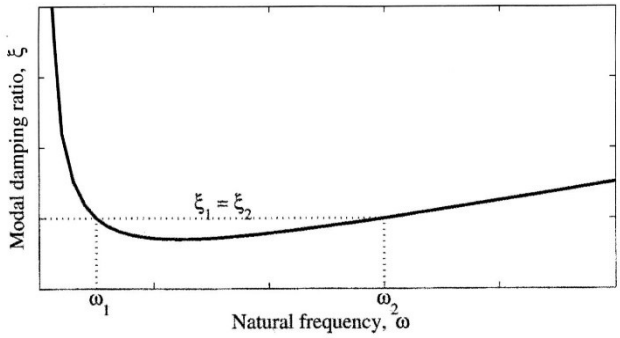

Figure 2-42: Modal damping coefficients for the Rayleigh model

In this thesis work, the values assumed to determine the viscous damping of the building in question are divided into two groups:

- I.D.A. pre retrofitting:

ω_i	ω_j	ξ	$a_{0=0,2285}$
0,2T	0,9T	0,05	$a_{1=1,042*10\text{^}-3}$

- I.D.A. post retrofitting:

ω_i	ω_j	ξ	$a_{0=0,5712}$
0,2T	0,9T	0,02	$a_{1=2,604*10\text{^}-3}$

2.11.4 Plastic Hinges and Takeda model

Also in this case, as in the previous case study, Takeda's hysteretic model (Takeda et al., 1970) is used to represent the non-linear behaviour of concrete structures, where non-linearity is modelled using concentrated plastic hinges. The model takes into account the yield, the cracking and therefore the degradation of the material.

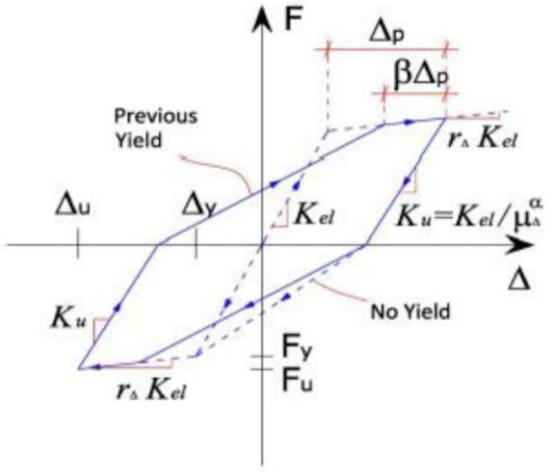

Figure 2-43: Takeda's hysteretic model

These laws are characterized by a lower discharge and reloading stiffness than the initial elastic one.

In the Takeda model the values of α are variable between 0 and 0.5; if α = 0 a drain is considered with a stiffness equal to the initial elastic. The reloading phase of the second and subsequent cycles does not lead directly to the point of maximum displacement reached in the previous cycle, but to a point distant from the latter of the quantity β Δp, along the plasticization direction with inclination $r_\Delta K_{el}$. For the beams in c.a., built with attention to detail, values considered appropriate are: α = 0.3 and β = 0.6.

In the SAP2000 v20 calculation program it is possible to select, in the characteristics of the plastic hinges, Takeda's hysteretic cycle and Figure 1-54 the scheme used by the program is shown. The definition of plastic hinges is the same as in the case of pre-retrofitting seen in the paragraph 1.9.1

Figure 2-44: Takeda's hysteretic model in SAP2000 V.20

Also in this case, the seismic vulnerability index was calculated using the CSM (Capacity Spectrum Method) method and is presented for the two f.e. models previously described and characterized by increasing accuracy: model A, model B. Compared to the pre-retrofitting case, in this case the analyses refer to the ductile model only; without plastic shear hinges. It should be noted that the capacity curves obtained by I.D.A analysis by discretizing the input accelograms must be converted to be compared, in the ADRS plan, with the demand. At this point the capacity curve should have been bilinearized, in order to find the performance point, however the aforementioned capacity curve of the structure do not, in any case, reach the SLV, thus always maintaining itself in the elastic range. Therefore, the aforementioned bilinearization would have had no meaning and therefore the comparison between capacity and demand takes place only in graphic terms, from which it is possible to see that the capacity is always higher than the demand, for each model and for each limit state.

2.11.5 Model A: Seismic Vulnerability Index

As already mentioned, the A model, characterized by a lower level of accuracy, is composed only of structural components.

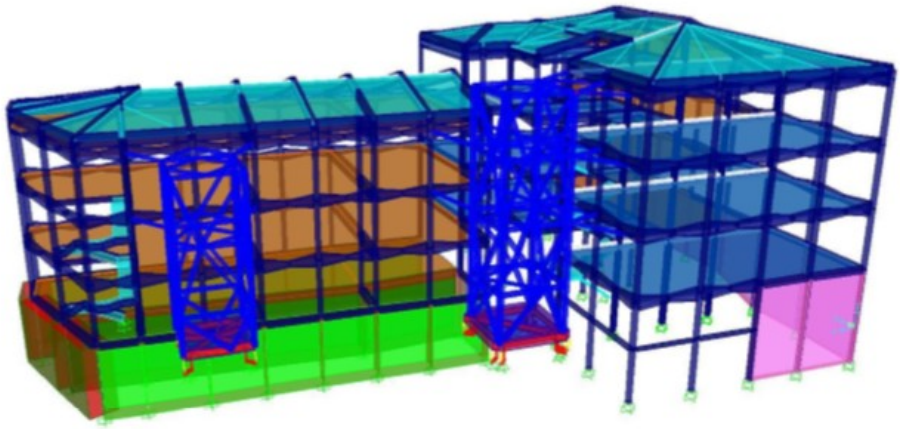

Figure 2-45: Extruded view of Model A

$$E_{conc} = 50\% E_{conc\ el}$$

The accelerogram used to determine the capacity curve is scaled in a range between 0.1 and 1.4 per step of 0.1.

The capacity curves obtained in the ADRS plane compared to the corresponding demand curves are shown from Figure 2-46 to Figure 2-49.

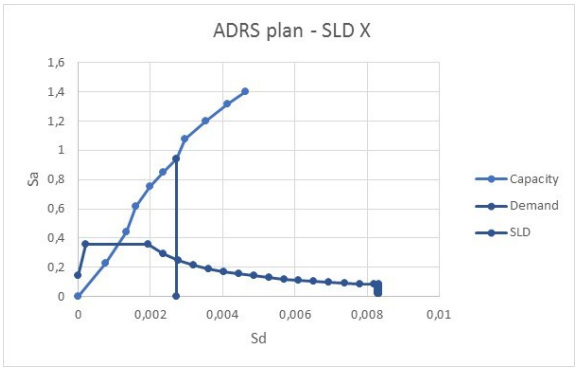

IRSLD > 1

Figure 2-46: SLD – X DIRECTION

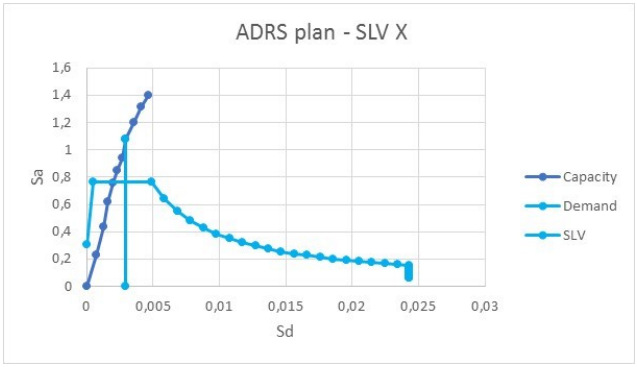

IRSLV > 1

Figure 2-47: SLV – X DIRECTION

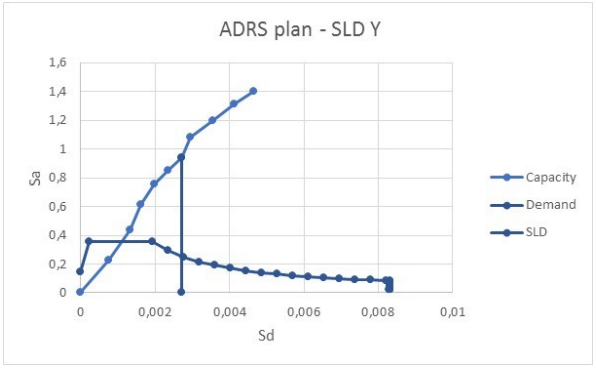

IRSLD > 1

Figure 2-48: SLD – Y DIRECTION

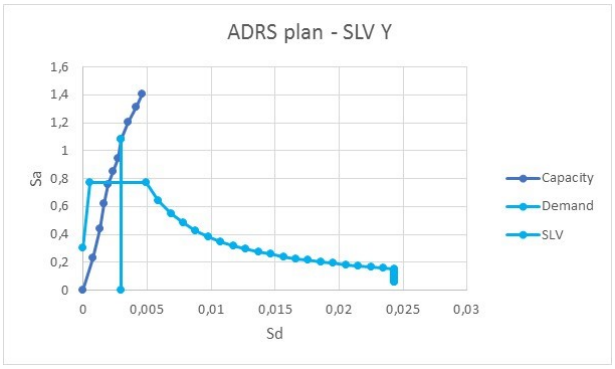

IRSLV > 1

Figure 2-49: SLV – Y DIRECTION

2.11.6 Model B: Seismic Vulnerability Index

Model B, characterized by an intermediate level of accuracy, is composed of external infill walls modelled as equivalent rods according to literature, in addition to the structural components.

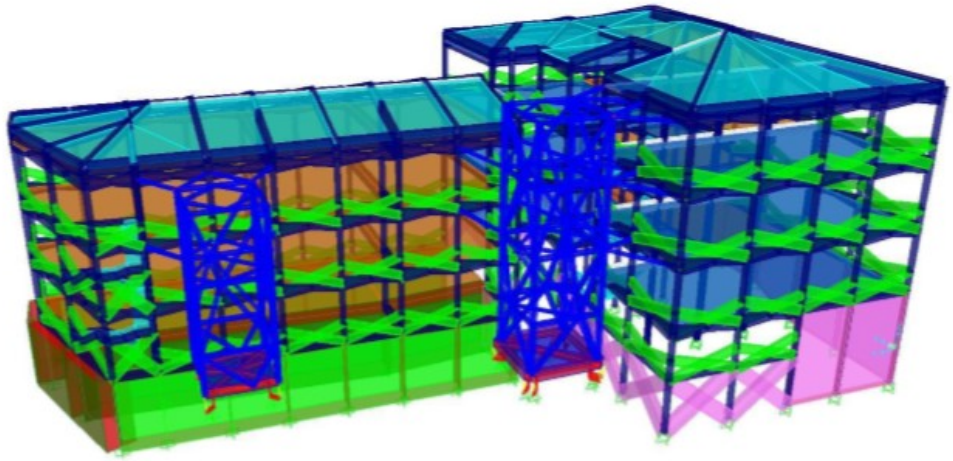

Figure 2-50: Extruded view of Model B

$$E_{conc} = 50\% E_{conc\ el}$$

The accelerogram used to determine the capacity curve is scaled in a range between 0.1 and 1.4 per step of 0.1. The capacity curves obtained in the ADRS plane compared to the corresponding demand curves are shown from Figure 2-51 to Figure 2-54.

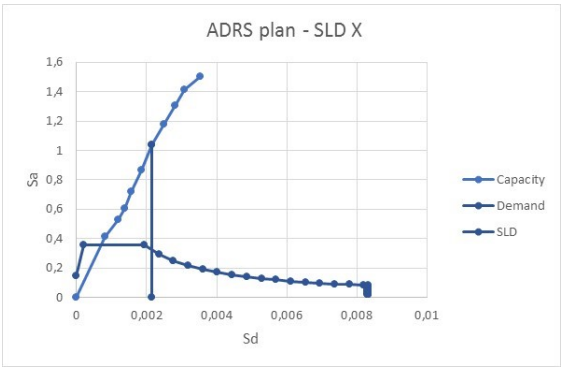

IRSLD > 1

Figure 2-51: SLD – X DIRECTION

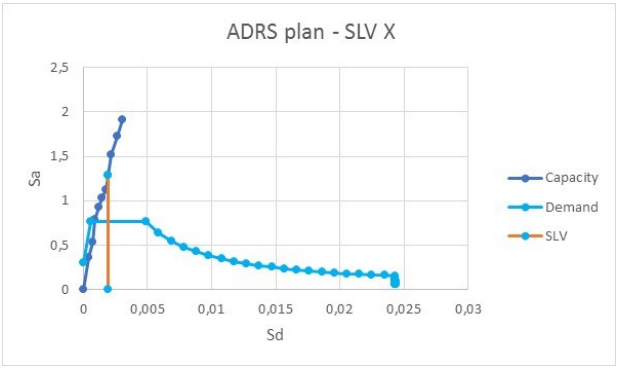

IRSLV > 1

Figure 2-52: SLV – X DIRECTION

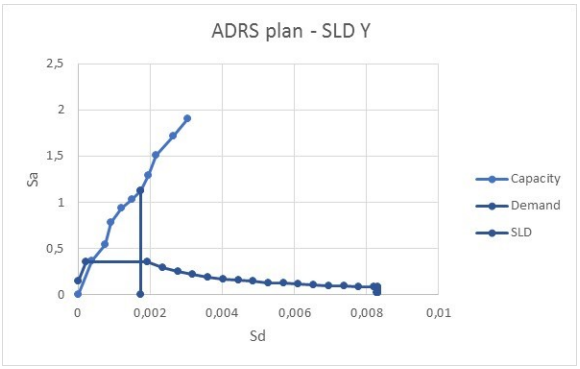

IRSLD > 1

Figure 2-53: SLD – Y DIRECTION

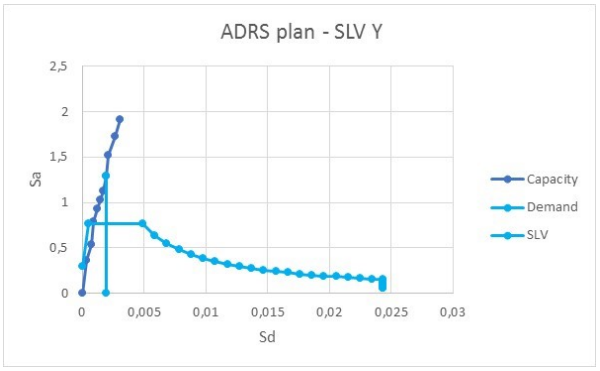

IRSLV > 1

Figure 2-54: SLV – Y DIRECTION

2.11.7 Comparisons between models

In order to evaluate the effectiveness of dissipative towers, IDA analyzes were also performed on pre-retrofitting models. Below are shown, in Figure 2-55, 2-56, the obtained capacity curves referred to each model with and without the presence of dissipative towers.

- Model A

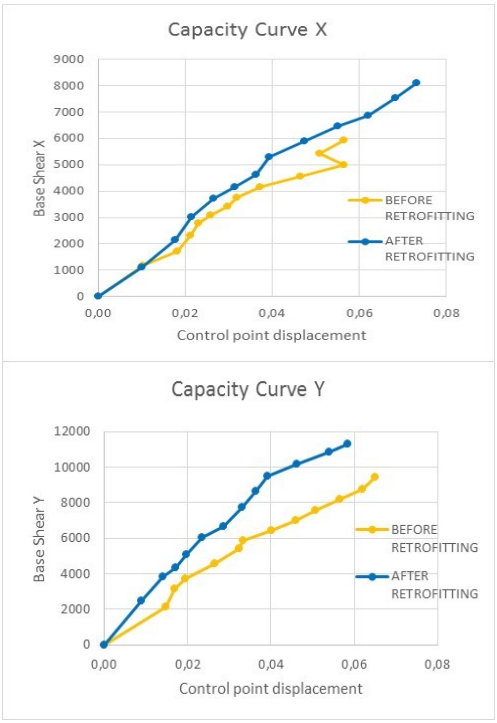

Figure 2-55: Comparison of pre and post retrofitting capacity curves for model A

- Model B

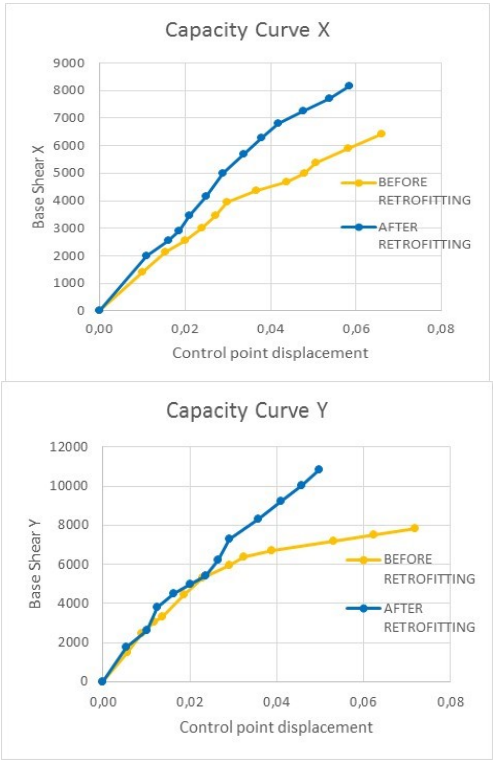

Figure 2-56: Comparison of pre and post retrofitting capacity curves for model B

Also in this case the results show how, following retrofitting works, an increase in the structural capacity was obtained both in terms of increase in shear base and reduction of the maximum displacements of the control point.

In addition, a comparison between different model is shown in terms of intensity level of the seismic action necessary to reach the SLD.

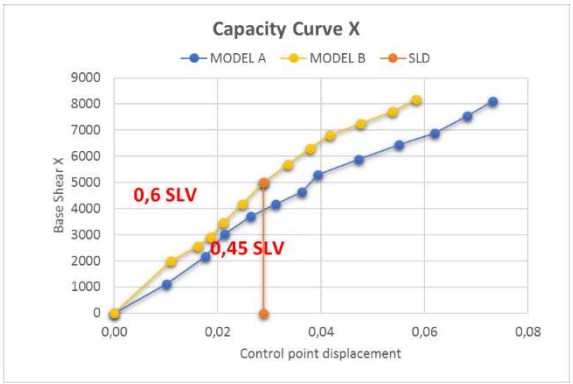

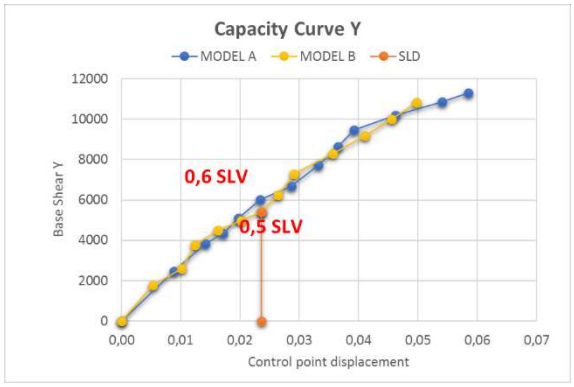

Figure 2-57: Comparison between different model in terms of intensity level of the seismic action necessary to reach the SLD – After retrofitting

Also in this case, it has been noted that the level of seismic energy necessary to reach the SLD limit displacement increases as the degree of detail of the model increases. However, less evident results were obtained in post-retrofitting, because the effectiveness of dissipative towers obscures the accuracy problem of the model.

Moreover, from the comparison between the situation before and after retrofitting it is noted that the shear on the columns does not change significatively because the predominant part of this increase is absorbed by the dissipative towers. This difference is shown through the figure below of shear related to two columns in the pre- and post-retrofitting works, respectively.

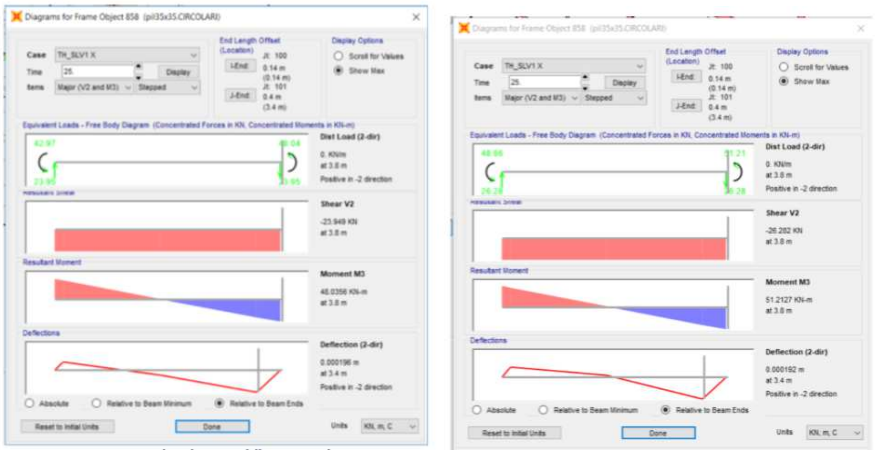

Figure 2-58: Comparison of shear on the Column pre and post-retrofitting respectively

There are also benevolent effects due to retrofitting in the plastic field. It is possible to see from the energy balances how the dissipation of energy by the structural elements has decreased.

Figure 1-75 shows the hysteresis cycles recorded on a type damper at the base of the towers in the analyzes with the SLV1 accelerograms. From the hysteresis loops of the damper it is possible to deduce the amplitude of the elongations and the maximum shortening of the damper, as well as the maximum work force.

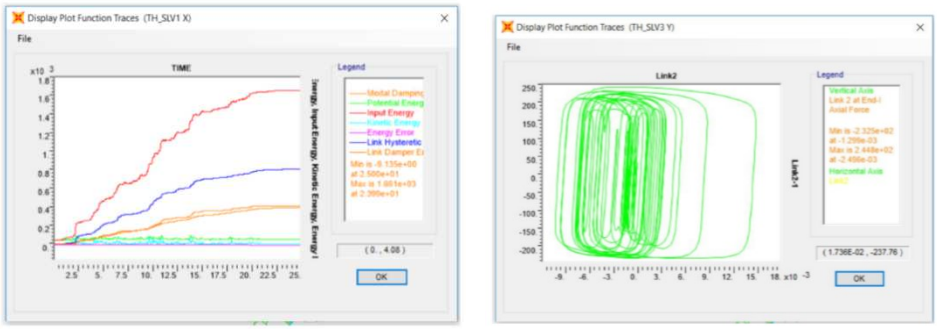

Figure 2-59: Energy balance and hysteretic cycles of damper

To further demonstrate the effectiveness of the dissipative system, the hysteretic cycles of two flexural hinges referring to the pre- and post-retrofitting situation are reported.

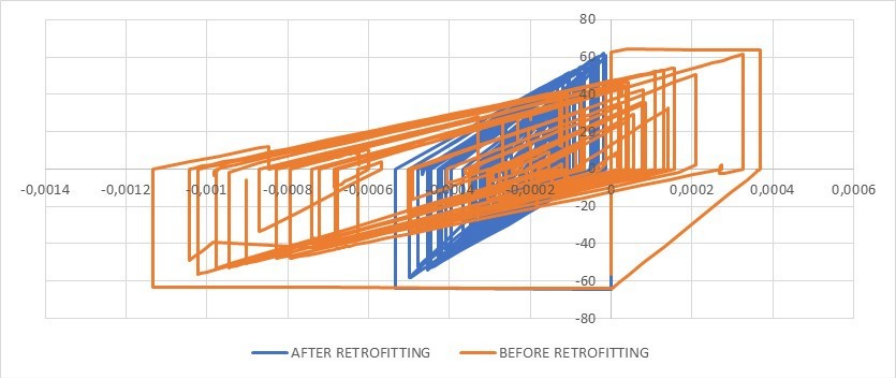

Figure 2-60: Hysteretic cycles of pre and post retrofitting flexural hinges

The graphs show that the area inside the cycle, which represents the energy dissipated, of the model without towers is greater than the area of the model cycle with towers. This proves that energy dissipation is entrusted to viscous devices and not only to the structural elements.

2.11.8 Seismic classification

For the theoretical discussion of the seismic classification, see the chapter 1.9.7.

Also in this case the seismic vulnerability index relative to various limit states and to the tested models is greater than the unit, therefore being all the analysis situations attributable to the same result it is reported univocally.

The calculation of the PAM parameter in the post retrofitting case leads to the value of:

$$PAM = 0{,}873$$

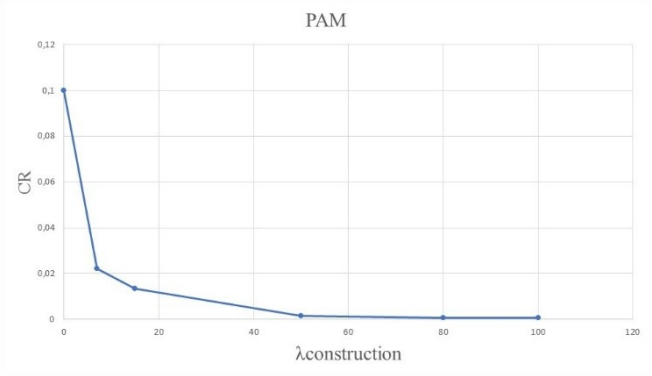

Figure 2-61: PAM

This value of the PAM parameter falls in the class A range. While the seismic vulnerability index greater than 1 falls in class A +; therefore the risk class is identified as the lower of the two.

CLASS A

2.11.9 Conclusion

Below is shown a summary table of the seismic risk classes obtained in the pre and post-retrofitting cases, for the three models implemented.

Table 2-25: Risk class for pre and post retrofitting case

	PRE-RETROFITTING		**POST-RETROFITTING**
	BUILDING A	**BUILDING B**	
MODEL A	CLASS G	CLASS G	CLASS A
MODEL B	CLASS F	CLASS G	CLASS A

Also in this case, as can be seen from the results obtained, the incidence of modelling is significant only in the pre retrofitting, as in the post retrofitting the improvement obtained through the inclusion of dissipative towers largely overcomes the problems related to f.e. modelling.

Chapter 3.

Conclusion and future developments

The purpose of this thesis work is to evaluate the incidence of modelling of non-structural elements in the assessment of seismic vulnerability index of strategic buildings, by calibrating their operating stiffness through vibrational measurements. To do this, two case studies were analysed before and after retrofitting intervention: High School Benedetto Croce in Avezzano and High School Varano in Camerino. For each of them, three finite-element models have been implemented, characterized by a growing accuracy level.

For what concerns the High School Benedetto Croce, three models were implemented before and after retrofitting works: model A with only structural components, model B with infill panels modelled as equivalent connecting strut according to literature, model C with external infill walls modelled as equivalent connecting struts and stiffness calibrated through the results of operational modal analysis and internal infill walls modelled as equivalent connecting struts and stiffness calibrated according to experimental modal analysis. Comparing modal parameters of the f.e. model C with those obtained from the in-situ dynamic tests after model calibration, a good agreement has been found both for natural frequencies and for modal shapes. Subsequently, seismic vulnerability index was calculated before and after retrofitting works. The results obtained show that there are significant differences between the different types of modelling; both for elastic (SLD) and plastic field (SLV). In particular, clear results were obtained for pre-retrofitting, less evident results were obtained in post-retrofitting, where the effectiveness of dissipative towers obscures the accuracy problem of the model. Therefore, for pre-retrofitting, in relation to the SLV it is possible to observe that, for ductile failure mechanisms, the seismic vulnerability index increases as the degree of detail of the model increases, since the introduction of stiffness consequent to modelling of the infill walls determines a reduction of displacements and therefore also of stresses on the structure. As regards the brittle failure mechanisms, on the other hand, in the Y direction where the presence of infill walls is significant, the modelling of non-structural elements accelerates the onset of the failure mechanisms determining a lowering of the seismic vulnerability index with increasing degree of model detail.

While, for what concerns elastic field, it has been noted that the level of seismic energy necessary to reach the SLD limit displacement increases as the degree of detail of the model increases. The level of seismic energy necessary to reach the SLD limit displacement in X direction for model C is greater than 1.5 SLV, compared to a level equal to 0.45 SLV necessary to reach the SLD for model A. However, the striking results obtained for SLD must be read carefully in the right perspective. The fundamental period of model A without infill walls, model B and model C with calibrated internal and external infill walls, fall between the fundamental periods of the spectrum: Tb and Tc, therefore correspond to the maximum seismic acceleration. Consequently, the striking difference found derives, in part, from the fact that the model C is characterized by a stiffness much greater than models A and B, despite having their same seismic acceleration. On the other hand, the common engineering practice leads to considering the results obtained as an overvalue of the elastic stiffness stretch of the infill walls. The choice of evaluate the elastic modulus of the infill panel through experimental modal analysis, characterized by very low level of dynamic input, can lead to the overvalue of this parameter in the assessment of seismic vulnerability index in linear field (SLD). Probably, the real elastic stretch of the infill walls stiffness lies between the one measured by experimental dynamic tests (calibrated on low input level, non-destructive test), and the one proposed in literature (calibrated on high input level, failure test), because the seismic energy level connected to the SLD is greater than the one related to the dynamic identification tests and less than the one associated with the breaking tests on infill panels present in the literature.

For what concerns the High School Varano, three model was implemented before and after retrofitting works: model A with only structural components, model B with external infill panels modelled as equivalent connecting struts according to literature, model C with external and internal infills modelled as non-linear shell element and stiffness calibrated through the results of operational modal analysis. Comparing modal parameters of the f.e. model C with those obtained from the in-situ dynamic tests, a good agreement has been found both for natural frequencies and for modal shapes. The model C was used only in the first part of the research work, for the calibration of the model and the comparison between analytical and experimental modal parameters, while for the second part, the impossibility of using the equivalent connecting struts to model the internal infill walls made necessary to use non-linear shell elements, whose computational burden in non-linear dynamic analysis prevented the conclusion of the study. Subsequently, seismic vulnerability index was calculated for model A and model B before and after retrofitting works. The results obtained show that there are significant differences between the different types of modelling; both for elastic (SLD) and plastic field (SLV). In particular, also in this case, clear results were obtained for pre-retrofitting, less evident results obtained in post-retrofitting, where the effectiveness of dissipative towers obscures the accuracy problem of the model. Therefore, for pre-retrofitting, in relation to the SLV it is possible to observe that, for brittle failure mechanisms in buildings A and B, especially in the Y direction where the presence of infill walls is significant, the modelling of non-structural elements increases the seismic vulnerability index due to the decrease of the displacements and, consequently, of the stresses on the structural elements, as a result of the increase in stiffness of the system.

While, for what concerns the elastic field, also in this case, it has been noted that the level of seismic energy necessary to reach the SLD limit displacement increases as the degree of detail of the model increases in Y direction, where the presence of infill walls is significant. The level of seismic energy necessary to reach the SLD limit displacement in Y direction for model B is 0.6 SLV, compared to a level equal to 0.35 SLV necessary to reach the SLD for model A. However, with respect to previous case study, the results are less evident because the fundamental period of model A is related to a lower seismic acceleration than the model B. Therefore, the increase in stiffness of the model B with respect to the model A is accompanied by an increase in the seismic acceleration in input. This means that the results on the two models are closer to each other than in the previous case study.
In conclusion, the present thesis study has shown that neglecting the modelling of non-structural elements can lead to significant differences in the calculation of the seismic vulnerability index.

It has been shown that the modelling of infill walls is essential in the evaluation of the current seismic vulnerability index for strategic buildings and also in the design of seismic retrofitting project, with special regard to retrofitting projects involving the introduction of seismic energy dissipation elements (damper). The calibration of the stiffness characteristics of the infill panels is fundamental in the evaluation of seismic vulnerability index of strategic construction because an incorrect estimate of this parameter can lead to very different results from the real ones. As regards the stiffening contribution of the infills walls, from the present research work it emerged that the dynamic experimental analysis can be a valid, effective and fast instrument for the calibration of f.e. models, but, however, tends to overestimate the stiffness of the elastic stretch for analysis aimed at evaluating the seismic vulnerability index in the linear field (SLD), with reference to the usual engineering practice. Therefore, we are still working to estimate the elastic modulus of the infill walls through laboratory tests, in particular, according to the latest analysis, the stiffness of the infill panels seems to depend on the amplitude of the vibration even in the absence of damage. New experiments are in progress to verify this consideration and find the constitutional law.

References

Albanesi, T., Bergami, A.V., Nuti, C., 2006. Comportamento sperimentale di tamponature leggere. Sperimentazione su materiali e strutture, Convegno nazionale, Venezia 6-7 Dicembre 2006, pp. 821-830.

Astroza R., Ebrahimian H., Conte J.P., Restrepo J.I., Hutchinson T.C. (2015) Influence of the construction process and nonstructural components on the modal properties of a five-story building. *Earthquake Engineering and Structural Dynamics*, DOI: 10.1002/eqe.

Bertoldi, S. H., Decanini, L. D., Gavarini, C., 1993. "Telai tamponati soggetti ad azione sismica, un modello semplificato: confronto sperimentale e numerico" (in Italian). Atti del 6 convegno nazionale ANIDIS. Perugia, Italy.

Biondi, S., Colangelo, F., Nuti, C., 2000. La risposta sismica dei telai con tamponature murarie. C.N.R. Gruppo Nazionale per la Difesa dai Terremoti, Roma.

Biondi, S., Candigliota, E., Nuti, C., 2002. Tests on different infilled specimens: a critical review of Code ultimate state criteria. 12th European Conference on Earthquake Engineering, London 2002, paper 748.

Brincker R., Zhang L. (2009) Frequency domain decomposition revisited. *Proc. of the International Operational Modal Analysis Conference* (*IOMAC'09*), 615-626.

Brincker R., Zhang L., Andersen P. (2000) Modal identification of output-only systems using frequency domain decomposition. *Smart Materials and Structures*, Vol.10, No.3, 441-445.

Calvi, G. M., Bolognini D., 1999. Seismic response of R.C. frames infilled with weakly reinforced hollow masonry panels. Università degli Studi di Pavia, Dipartimento di Meccanica Strutturale, Pavia, Italy.

Calvi G.M., Bolognini D., Penna A. (2004) Seismic performance of masonry – infilled r.c. frames – benefits of slight reinforcements. *Proc. of SISMICA, 6th Congresso National de Sismologia e Engenharia Sismica*, Portugal.

Camposeo G. (2016), Thesis title: Calibration of The Mechanical Parameters Of Secondary Structural Elements Of Reinforced Concrete Buildings Through Impulsive Tests.

Censori A. (2018), Thesis title: Seismic classification of school buildings with dissipative towers: High school "C.Varano" of Camerino (MC).

Circolare 2/2/2009 (2009) Istruzioni per l'applicazione delle "Nuove Norme Tecniche per le Costruzioni" di cui al D.M. 14/1/2008, G.U. n.47 del 26/2/2009, suppl. ord. n.27.

Crisafulli F.J. (1997) Seismic behavior of reinforced concrete structures with masonry infills. *PhD Thesis*, University of Canterbury, New Zeland.

Dhanasekar, M. 1985.The performance of brick masonry subjected to in plane loading. Dissertation No. 990. Newcastle: University of Newcastle, Australia.

Di Fabio R. (2017), Thesis title: Changes of modal parameters of r.c. school building due to the damages of infill walls induced by the Central Italy earthquake.

D.M.14.01.2008, Nuove Norme Tecniche per le Costruzioni, Ministero delle Infrastrutture, G.U. n.29, 04.02.2008 (in Italian).

F. Dunand, J.E. Rodgers, A.V. Acosta, M. Salsman, P.-Y. Bard, M. Çelebi [2004], "Ambient vibration and earthquake strong-motion data sets for selected USGS extensively instrumented buildings", Open-File Report 2004-1375.

FEMA 356. Prestandard and Commentary for the Seismic Rehabilitation of Buildings, *Federal Emergency Management Agency*, Washington (DC).

FEMA450. NEHRP Recommended Provisions for Seismic Regulations for New Buildings and Other Structures, *Federal Emergency Management Agency*, Washington (DC).

Gioiella L., Balducci A., Carbonari S., Gara F., Dezi L. (2017), An Innovative Seismic Protection System for Existing Buildings: External Dissipative Towers, WCEE.

James G.H., Carne T.G., Lauffer J.P. (1995) The natural excitation technique (NExT) for modal parameter extraction from operating structures. *The International Journal of Analytical and Experimental Modal Analysis*, Vol.10, No.4, 260-277.

Marcucci T. (2018), Thesis title: Seismic Classification of School Buildings with Dissipative Towers: High School "B. Croce" Of Avezzano.

MathWorks (2009), "MATLAB", version 7.9 (R2009b), The MathWorks Inc., Natick, Massachusetts.

Monterubbiano J. (2017), Thesis title: Seismic classification of a building in relation to the accuracy adopted during the modelling phase.

Morandi P., Hak S., Magenes G. (2011) Comportamento sismico delle tamponature in laterizio in telai in c.a.: definizione dei livelli prestazionali e calibrazione di un modello numerico. *Proc. of ANIDIS 2011*, Bari.

M. Turek, C. Ventura, S. Guerrero (2007), Ambient vibration testing and model updating of a 44-storey building in Vancouver, Canada, 25th International Modal Analysis Conference, Orlando FL, USA, Paper 250.

Nichols J.M., Totoev Y.Z., Experimental determination of the dynamic Modulus of Elasticity of masonry units.

Nicoletti V., Gara F., Regni M., Carbonari S., Dezi L. (2018), Dynamic in Situ Tests for the Calibration of an Infilled R.C. Building F.E. Model, EESMS.

Nicoletti V. (2017), PhD thesis title: Experimental Evaluation of Infill Masonry Walls Stiffness for the Modelling of Non-Structural Components in R.C. Frame Buildings.

Popovics J.S., Zemajtis J., Shkolnik I. (2008) A study of static and dynamic modulus of elasticity of concrete. *ACI-CRC Final report*, University of Illinois, Urbana, IL.

Reza Tabeshpour M., Azad A. (2012), Seismic Behavior and Retrofit of Infilled Frames. Earthquake-Resistant Structures – Design, Assessment and Rehabilitation (11), 280-301.

Roia D., Gara F., Balducci A., Dezi L. (2013), Dynamic tests on an existing R.C. school building retrofitted with “dissipative towers, ICOVP.

SAP2000 advanced (v14.1.0) Static and dynamic finite element analysis of structures, Berkeley, CSI Computer & Structures, Inc., 2009.

Speranza E., Gara F., Carbonari S., Balducci A., Dezi L. (2018), Dynamic Test Based Model Calibration of an Existing R.C. School Building, ASMM18.

Speranza E., Nicoletti V., Carbonari S., Gara F. (2019), Dynamic Test-Based Model Calibration Of An Existing Rc School Building Before The Seismic Retrofitting, SPONSE.

S.S. Ivanovic, M.D. Trifunac, M.I. Todorovska (2000), Ambient vibration tests of structures - A review. ISET J. Earthq. Tech., 37(4), 165-197.

Stafford Smith, B., 1966. "Behaviour of square infilled frames". Journal of the Structural Division, Vol. 92, No. 1, pp. 381 - 403.

Tassios, T.P., 1998. Meccanica delle murature, Liguori Editore, Napoli.

Zancocchia T. (2017), Thesis title: Influence of infill walls modelling on the seismic vulnerability assessment in r.c. buildings.

Zarri, F. 1994. Parametri di resistenza e di deformabilità meccanica di murature di laterizio. Costruire in Laterizio, anno 7, n. 41, pp. 452-455.